Republic of Iraq
Ministry of Higher Education
and Scientific Research
University of Babylon
College of Engineering

MODELING AND CONTROL OF PLANAR FLEXIBLE ROBOT ARM

A Thesis

Submitted to the College of Engineering of University of Babylon in Partial Fulfillment of the Requirements for the award of Degree of Master of Science in Mechanical Engineering (Applied Mechanics)

By

Mustafa Turkee Hussein

Al – Khafagi

(2005 B. Sc)

2007 A.M ***1428 A.H***

بسم الله الرحمن الرحيم

يرفع الله الذين آمنوا منكم والذين أوتوا العلمَ دَرَجاتٍ والله بما تعملونَ خبيرٌ

صدق الله العلي العظيم

سورة المجادلة ، الآية ﴿١١﴾

ABSTRACT

In this thesis the dynamic modeling, and trajectory control of single link flexible, and two link (rigid-flexible) manipulators are studied. An efficient assumed mode/lagrangian approach is deve1oped for dynamic modeling of manipulators with flexible link, For planar case, the nonlinear and coupled equations of motion of single link, and two link (rigid-flexible) manipulators are derived using minimum number of coordinates by considering joint or relative coordinates.

The dynamic inversion technique has been used to find trajectory control of single-link flexible manipulator. The proposed technique was used to find the joint torques required to move the end point from rest to rest along a specified path; a simple PD controller is used to gain some robustness to control system. The technique is complete and effective and can be used to find joint torques as feedforward controls in order to minimize the work of the feedback controllers.

In this work the effect of different parameters were studying such as B.C.'s ,number of flexible modes, modulus of elasticity and cross sectional area on the dynamic model and control system to show the influence on each them.

ACKNOWLEDGEMENT

Many people have given me help, guidance, and inspiration in my years in graduate study. To all of them I am very grateful. First of all, I wish to thank my supervisors, **Dr. Adel A. Alwan**, and **Dr. Baha'a I. Kazem**, since they introduced me to this challenging research area. Their comments and suggestions on most of the theoretical developments made in this thesis, and also on computational and practical aspects of real-time control which have been instrumental in the completion of this research. I appreciate their invaluable guidance, encouragement, and support which greatly changed my way of thinking in dealing with control engineering problems.

I am grateful to **Professor Jean-Claude P.**, the advisor in Sciences and Technologies to the Vice-President Sciences, Technologies and Programmers at the Canadian Space Agency, to my friend **Mr. Ali A. Jasim** mechatronic engineering, graduate student in the mechatronic engineering department in Baghdad University, and to the team of the **Thuraya Com.** for computers services.

I take this opportunity to express my deepest appreciation to my dear parents for their encouragement, support, and all they have given to me. I would also like to thank my brothers who made my life joyful and were always careful to provide a peaceful environment for my study.

Finally, my heartfelt thanks to my family for their wholehearted support and encouragement throughout this endeavor, special thanks to my uncles Hadi, Baqir, and Ahmed J. Sa'eed, and my uncle's wife Suha Abd Alhadi for their assistance.

This thesis is dedicated to:

My parents, all sisters, and brothers

All my teachers

LIST OF CONTENTS

Chapter 1 Introduction

Chapter 2 Literature Review

Chapter 3 Modeling of Flexible Robot Arm

Chapter 4 Trajectory Control of Flexible Robot Arm

Chapter 5 Results and Discussion

Chapter 6 Conclusions and Suggestions Future Work

NOMENCLATURE

Symbol	Description	Unit
A	Transformation matrix	---
Al	Aluminum	---
a	Cross sectional area of the link	m^2
c	normalized coefficient	---
E	Modulus of elasticity	N/m^2
F	Non-linear vector(coriolis and centrifugal vector)	---
I	Moment of inertia	m^4
J	Total mass moment of inertia of link	$kg.m^2$
J_h	Mass moment of inertia of hub	$kg.m^2$
K	Stiffness matrix	---
KE	Kinetic energy	N.m
k_v	derivative gain	$1/s$
k_P	Proportional gain	$1/s^2$
L	Lagrangain	---
l	Length of the link	m
M	Mass matrix	---
m	Mass of the link	kg
m_p	Payload mass	kg
m_h	Hub mass	kg
m	Vector related to the flexible coordinate	---
n	Number of flexible coordinates	---
N	Number of link	---

PE	Potential energy	N.m
p	Position vector	---
q	generalized coordinate	---
Q	generalized force	---
r	Position vector of link end point	---
S	Flexible transformation matrix	---
t	Time	sec
Ti	Titanium	---
W	Bending deformation	*m*
x	Position along the link	*m*
y	Tip position output	rad
z	Normalized position along the link	---

SUBSICRPT

Symbol	Description
d	Desired value
e	End point of the arm
h	Hub notation
i	Number of modes
l	Link notation
OL	Open-loop control
OL.PD	Open-loop proportional derivative controller
p	Payload notation
t	Total value

GREEK SYMBOLS

Symbol	Description	Unit
$\dot{\alpha}$	Absolute angular velocity	rad / sec
β	Eigen mode	---
δ	Flexible mode	m
θ	Hub angle (rigid mode)	rad
λ	Normalized eigen mode	---
ρ	Mass per unit length	kg / m
τ	Torque input	$N.m$
ϕ	Shape function	---
φ	The angle for point along the arm	rad
ω	Natural frequency	rad / sec

1

Chapter One

Introduction

INTRODUCTION

1.1. Prologue

Probably the first occurrence of mechanical arms was in the prosthetic devices to replace lost limbs. These arms were designed to grasp objects. The second field in which robot arms had found application was remote manipulation. The need to work with hazardous material or environment, led to the design of teleoperator systems. These devices permit to a user to perform simple manipulations from a safe distant place. Applications in space, nuclear, and underwater environments are the typical use of teleoperators. Also robots are now to be found in various applications such as spot welding, arc welding, material handling, and assembly. Mainly, they are uses to reduce labor cost and material wastage, to increase output rate, and to improve production quality [8].

Robots are so new that there is no standard definition for them. However, an industrial robot is defined by US Robot International Association (RIA) as: “a programmable, Multifunctional manipulator designed to move materials, parts, tools, or specified devices through variable programmed motions for the performance of a variety tasks “.

Industrial robots are built of the following basic systems:

1. The mechanical structure consisting of mechanical linkage and joints.
2. The control system.
3. The power input which can be hydraulic, pneumatic, electrical, or their combination.

Robots are very different from any other structures, Their structure consists of active linkages which differ from passive ones such as crank mechanisms. In active linkages each link has its own power supply, while in the passive linkages all the links receive motion from a single driving motor. As it was mentioned earlier, the load carrying capacity of most of the existing

industrial manipulators is very low. This low weight efficiency is mainly due to control design which is usually based on rigid body dynamics. The excessive mass of the arms limits their speed and increases the energy requirements and the size of actuators. Moreover, manipulator systems with large workspace volumes and large payloads, such as long-reach manipulators for nuclear waste remediation or the outer space arms with extreme penalty on the mass carried into orbit should be as light as possible. Therefore, many benefits can be received from manipulators with low payload to weight ratio and high stiffness. This is why a new generation of light robots which are able to handle heavy payloads is required to replace the inefficient and massive ones. Lighter manipulators need less energy and can operate at higher speeds. Therefore, they save manufacturing time and increase productivity. Due to the flexibility of the links, the assumption of rigid body dynamics and kinematics is no longer valid and the problem of position control resulting from link flexibility needs to be resolved.

1.2. Flexible Robot Overview

It goes without saying that accurate dynamic modeling is the first step for design and control of lightweight, heavy payload, and high speed manipulator systems. Due to the distributed flexibility of the links, they should be regarded as deformable bodies with an infinite number of degrees of freedom. These degrees of freedom are used to define the location of each point of the system. The rigid body or nominal motion of the system changes the geometry of the system. These results in varying system parameters which influence the elastic deformations of the link. In turn the elastic deformations influence the rigid body motion. In other words, since the interconnected bodies of the manipulator system undergo large translational and rotational displacement; the dynamic equations of the motion of the system are highly nonlinear and coupled the dynamic formulation of flexible robot systems leads to a set of partial differential equation.

In multibody systems, the motion of each body is constrained because of the mechanical joints which connect the adjacent bodies. The configuration of a multibody system can be described by vector quantities such as displacement and velocity. These quantities should be measured with respect to an appropriate coordinate system. In general, two kinds of coordinates are required. The first one is an inertial or global frame of reference which is fixed in time and the second one is a body reference coordinate for each component of the system. This reference frame translates and rotates with the body; therefore, its location and orientation change with time and with respect to the inertial frame. In rigid body analysis, the set of coordinates defining the location and orientation of the body references is enough for defining the location of an arbitrary point of the rigid body. However, the configuration of deformable bodies must be identified not only by a complete set of coordinates defining the location and orientation of a selected body reference, but also the elastic coordinates describing the deformation of the body with respect to the body reference [22].

Two main techniques were used to develop the dynamic equations of motion of flexible manipulator systems, namely: Newton-Euler approach, and Lagrangian approach, while vector quantities are used in Newtonian mechanics, scalar quantities such as kinetic energy, potential energy, and work are used in lagrangian dynamics which greatly simplify the problem. Another way for dynamic modeling of flexible manipulators is to find the dynamic response of the system directly with reference to a fixed global coordinate frame. This approach eliminates the nonlinear Coriolis and centrifugal terms from the dynamic equations; however, it requires the use of finite strains, large displacements, and large rotations. Therefore, this approach is somehow complicated and not suitable for the control design specify for chains of flexible links.

One of the major open problems related to flexible manipulators is controlling the position of their end-point. There are two types of control problems for such manipulators, namely, trajectory control and time-optimal

control (TOC). In the first one the position of the payload is given versus time, while in the second one the path and the joint torque constraints are known. Various feedback control strategies are proposed in the literature for trajectory control of flexible manipulators. Due to such control systems are non-collocated and position commands contain high frequency components, the feedback control may cause these systems to become unstable.

This why inverse dynamic methods have been recently proposed by many authors to determine the joint torques such that the end-point of the flexible manipulator follows a given trajectory. Due to the flexibility, a complete model consisting of the kinematic and dynamic equations should be solved simultaneously. The main difficulty is the noncausality of the inverse dynamics of flexible manipulators. Because the point for which the prescribed motion is specified and the application points of control torques are connected by elastic bodies.

1.3. Scope of the Present Work

The scope of this research can be summarized in the following stages:

1. Developing the dynamic modeling of flexible robot arm, deriving the equation of motion of single link and two link robot.
2. Developing the control of flexible robot arm, an inversion based control was used to solve the equation of motion of the system for flexible robot arm.
3. Study the effect of different parameters; such modulus of elasticity, cross section area, and payload on the dynamic model and performance of control system.

2

Chapter Two

Literature Review

LITRETURE REVIEW

The review of the literature related to the present work can be classified into the following categories:-

2.1. Dynamic Modeling of Flexible Robot

Book [1] utilized 4x4 Transformation matrices to model a spatial manipulator which was light and operated at low speed by neglecting the mass of the manipulator compared to the mass of the payload and assuming that the links bent in the first mode of vibration. He developed the linear equations of manipulator as two rigid masses connected by a chain of massless beam segments. In his method, it is necessary to approximate the physical system with distributed mass and elasticity as a system of rigid bodies connected with massless elements.

Sunada and Dubowsky [2] presented a general Lagrangian/finite element approach in the field of robotics to model industrial manipulators with elastic members; they utilized ***NASTRAN*** (a large general-purpose FE program) to generate the lumped mass and stiffness matrices of the individual links. In their method the effect of the system deformations on the kinematics of succeeding links was ignored. They used finite element method approaches which based on linear superposition theorem, in which elastic deformations were found by assuming known rigid body motion and later superposing the elastic deformations to the rigid body motion. Therefore, they did not consider the coupling effects between rigid body motion and elastic deformations.

Book [3] developed the assumed mode method for modeling the dynamics of flexible manipulator systems consisting of rotary joints that connect pairs of flexible links. In fact he extended the recursive Lagrangian dynamics to flexible manipulator systems by using the assumed mode method. In his model,

4x4 transformation matrices were used to describe the kinematics of both the rotary-joint motions and the link deformations. Therefore, hybrid coordinates including the joint motions and elastic deformations described by a series of vibration modes were employed to describe the system behavior, and then he used Lagrangian approach to formulate the dynamic equations of flexible multibody systems.

Usoro, et al [4] illustrated a finite element/lagrangian approach for modeling of lightweight flexible planar manipulators. They introduced a model in which the system configuration at any time is described by a combination of gross motion and elastic coordinates. The tangent coordinate systems, which were attached at the base of the links, and utilizing this model was based on small deformation theory and neglecting axial deformations. Although most of the coupling terms were taken into account, this model can not be easily used for manipulators with more than two Links due to its computational complexity. Even though most of the coupling terms were taken into consideration.

Naganathan and Soni [5] described a finite element/ Newton-Euler approach for Modeling of Flexible Manipulators. In their works they consider only rigid body motion and elastic motion coupling terms, therefore, their work neglected the effect of elastic motion on the rigid body motion, and this work included coupling effects and presented a nonlinear finite element based model for flexible manipulators.

Benati and Morro [6] proposed an analytical (assumed mode)/ Lagrangain approach for dynamic modeling of the chain of flexible links. They described the flexibility of each link by the first two eigenmodes of clamped beams. In their work the first two eigenmodes of the links were found by treating the mass of distal links as a lumped effect at the extremity of the link under consideration. This method of finding modes for links is only an approximation because the mode shapes of the links are configuration dependent especially when the effect of gravity is taken into account. The main drawback

in this method is the difficulty in finding modes for links with non-regular cross sections and for multi-link manipulators.

James and Ben-Li [7] derived the dynamic equations for a two-link flexible robot arm. The arm is moving in the vertical plane. The payload is simulated by attaching additional masses to the arm at any specific locations. Although the governing equations of the system and the measurements are nonlinear, they arc explicitly obtained. The control strategy and the general procedures to construct a linear observer and to formulate a control law are discussed.

Mehrdad M. [8] designed a flexible link manipulator. In his work inertial reference frame coordinates system are used to describe the motion of the manipulators, and the transformation matrix to describe the coupling between rigid body motion and elastic deformations. The dynamic model is derived using analytical (assumed mode) / lagrangain approach. In his work the link is formulated as a cantilever beam with payload at it's end. ***Symofros program*** *was used* to find the dynamic model of single and two link flexible manipulator, structural shape optimization is considered as means to improve the dynamic behavior. In this regard, an optimization index is introduced to achieve some desired features such as higher flexible mode natural frequencies and easier accessibility of flexible modes by the control inputs.

Mehrdad F. [9] showed a dynamic modeling, trajectory control, and time optimal control of planar multi-links flexible manipulators. First an efficient finite element/Lagrangian approach is deve1oped for dynamic modeling of planar and spatial manipulators with flexible links and joints, for planar case. The nonlinear and coupled equations of motion of multi-link manipulators are derived using minimum number of coordinates by considering joint or relative coordinates. In the case of spatial manipulators, the equations of motion are obtained using a mixed set of differential equations and algebraic constraints. Some cases are studied in his work such as effects of flexibility of

links, and joints on the over all motion of the manipulators. The dynamic model derived in his modeling work was used in control of flexible manipulator.

Jean-Claude P. [10] presented the modeling of serial manipulators with flexible links and joints. In his work the model of flexible link includes bending in two perpendicular directions and torsion around the longitudinal axis, second order strain-displacement relationships, coupled with the dynamic equations are exact to first order in terms of the generalized coordinates associated with the flexible links. The generalized coordinates and their first-time derivatives are assumed to be small (of first order). The model developed captures all the important phenomena, such as stiffening due to the angular speed or buckling due to the large payloads. The dynamic equations are developed recursively using Jourdain's principle to allow an efficient symbolic implementation. The equations associated with the flexible links are reformulated to enable off-line symbolic integration in control algorithm.

Victor O. Gamarra-Rosado [11] studied the dynamic modeling of a flexible robotic manipulator with two flexible links and two revolute joints, which rotates in the horizontal plane. The dynamic equation are derived using the Newton-Euler formulation and the finite element method, based on elementary beam theory, which is used to discretize the displacements such that the small motion represented in terms of nodal displacements. The dynamic model will completely describe motions of a manipulator with flexible links, including large motions, small motions, and their interactions. The robotic manipulator is modeled as being composed of two links attached to each other with the first link attached to a fixed base. Each link is assumed to be symmetrical about its longitudinal axis in the absence of deformation, a cubic shape function is assumed for a single beam element. Computer simulation results are presented to illustrate his study. The dynamic model becomes necessary for use in future design and control applications.

Ali and Farbod [12] improved method for deriving elastic generalized coordinates by using Kane's method. Then Kane's equations of motion for

multibody systems consisting of an arbitrary number of rigid and elastic bodies are presented. Their equations are in general form and are applicable for any desired holonomic system. Flexibility in choosing generalized speeds in terms of generalized coordinate derivatives in Kane's method is used. Their work showed that proper choice of a congruency transformation between generalized coordinate derivatives and generalized speeds leads to equations of motion for holonomic multibody systems consisting of an arbitrary number of rigid and elastic bodies. These equations are decoupled in first-order terms. In their work and in order to show the use of this method, a simple system consisting of a lumped mass, a spring and a clamped-free elastic beam is modeled. Finally, the numerical implementation of decoupling using congruency transformation is discussed and shown via simulation of a two-degrees-of-freedom flexible robot.

Somolinos, et al [13] described the design, dynamic modeling and experimental validation of a new three degrees of freedom flexible arm which is suitable for industrial applications. In his work the arm was designed on the assumption that all its mass was concentrated at the tip, in keeping with this, the arm was built with very lightweight links, and all the actuators were located at its base. From the dynamics point of view, this dynamic model also decouples the forces transmitted by the actuators to the tip of the arm, i.e. the torque generated by each actuator produces a tip force which is orthogonal to the forces produced by any of the other actuators. Because the assumption that all the mass is concentrated at the tip, a compliance matrix can be used to model the oscillations of the structure. Then, dynamics of the arm becomes very simple (a lumped single mass model instead of the usual distributed mass model), and its control system can be significantly simplified: minimum sensing effort is required (only motor and tip measurements are needed), and PID controllers combined with a dynamic inversion subsystem is used in his work. Experimental identification of the dynamics has confirmed the validity of the assumption of a single mass concentrated at the tip. A flexible manipulator of simplified

dynamics has been built and tested which is much lighter than equivalent standard industrial robots.

Mohamed S., et al [14] studied the Modal analysis of assumed-mode models of a flexible slewing beam. Their work compares the performances of different shape function-based models with respect to their ability to accurately represent the dynamic and the static behavior of a flexible rotating beam. Several assumed-modes are compared, namely, the eigenfunctions of a rotating beam, the eigenfunctions of a clamped-payload beam, the eigenfunctions of a clamped-free beam, the polynomial functions, the cubic splines and the cubic B-splines. A systematic and detailed comparison of the eigenvalues, the eigenmodes and their derivatives and the static deformations and their derivatives are performed on a slewing beam in the vertical plane. Load parameters are changed from their nominal values to test for the sensitivity of the shape functions based models.

2.2. Flexible robot Control System

Cannon and Schmitz [15] developed a specific linear mode1 for a single-link flexible manipulator moving on a horizontal plane. Gravity and Coriolis forces were neglected, with the linear model, collocated and non-collocated control systems were developed utilizing linear control theory. They recognized that a multi-link arm could not be controlled based on their approach because of nonlinearities in the dynamics of a multi-link arm. Their algorithm was used to suppress arm vibrations by measuring strains over the arm links.

Hasting and Book [16] utilized linear control theory, to control of flexible systems. Their works used one of the early studies to obtaine linear models from nonlinear equations of motion, and then they utilized linear control theory. They used joint and strain feedback to damp structural vibration of a flexible manipulator. However, their experiments showed overshoot and vibration to step position command. They were linearized the manipulator dynamics and using linear feedback control schemes. They neglected nonlinear

effects of Coriolis, centrifugal, and gravity forces, hence their model is not valid for many practical problems.

Bayo [17] developed a new approach to calculate the required torque from inverse dynamic to produce a desired end effector motion. Because of the non-causal solutions for inverse dynamic problems, he developed approach to calculate the required torque for a single-link arm by solving the inverse dynamic equation in the frequency-domain with inverse fast Fourier transform. This method took into consideration the non-causal nature of the inverse dynamics of flexible manipulators. Since the necessary torques is provided by the solution of the inverse dynamics, the reduction of vibration in positioning of the tip is no longer required for input shaping.

Khorrami and Ozguner [18] proposed singular perturbation approaches based on two-time scale model of the flexible arm to control flexible link manipulators. These approaches allowed the definition of a slow subsystem corresponding to the rigid body motion, and a fast subsystem describing the flexible motion. Then a composite control strategy was applied. First a slow control was designed for the slow subsystem as it would be done for an equivalent rigid arm, and then a fast control stabilized the fast subsystem. However, the separation of time scales between the rigid and flexible subsystem can not be realized for many systems.

De Luca and Siciliano [19] proposed the inverse dynamic methods to determine the joint torques such that the end-point of the flexible manipulator follows a given trajectory. In their work the trajectory-tracking control problem is considered for one-link flexible arm described by non-linear model. Two meaningful system outputs are chosen; the joint angle and the angular position of suitable point along the link. Their works were based on the input-output inversion algorithm, a state-feedback control law was designed. Joint based design is shown to be always stable, whereas in the link-point design the closed dynamics may become unstable depending on the location of the output along the link.

Mehrdad M. [8] designed two control strategies for the dynamic model derived by ***symofros program***. The first one is based on the concept of integral manifolds in singular perturbation theory, and the second is based on input-output decoupling in nonlinear systems theory. The practical implementation issues for the former require the inconvenient measurement of flexural rates. An observation strategy is proposed to circumvent this problem. Experimental evaluation of the control strategies are carried out on a setup constructed in the laboratory.

Mehrdad F. [9] studied the control of multi-link flexible manipulators. In his work proposed two types of control problems for such manipulators, namely, trajectory control and time-optimal control (TOC) problems. In the first one, the position of the payload is given versus time while in the second one the path and the joint torque constraints are known. Since feedback control systems are non-collocated and position commands contain high frequency components, they cause these systems to become unstable. He presented a technique based on numerical optimization to solve trajectory control and time optimal control of multi-link flexible manipulators. The "non-causality" of the inverse dynamics of such systems is taken into account.

Aoustin and Chevallereau [20] discussed the control of flexible robots. The flexible manipulator dynamic is derived on the basis of a finite-element type model. Nonlinear feedback control has been used with flexible arms. At most, the number of variables to be exactly linearized equal to the number of actuators. To overcome this drawback the singular perturbation strategy is used to give classic composite control. The slow subsystem can be shown to be the equivalent rigid-link robot. The computed torque method for slow control is selected. The fast control is designed to stabilize the fast subsystem around the equilibrium trajectory set up by the slow subsystem under the effect of the slow control. Results of this control method with one-and two-flexible-link robots are presented in their work.

Aria A. [21] showed the problem of force control of a flexible link manipulator in this research. The main objective is to design, simulate, and experimentally demonstrate a control scheme which provides good servo performance of this non-minimum phase system and simultaneously suppresses the effects of severe friction in the joint. A simplified pole/zero preserving methodology is suggested to obtain reliable models for the system in unconstrained and constrained (in contact with environment) motions. The impact phenomenon is addressed by modeling the transition process between the two states. The unknown parameters of the system are identified by off-line experiments.

Mohammad J. [22] designed and analyzed nonlinear H_∞ techniques applied to flexible-link manipulators. In his work due to purpose of robust control of an uncertain model of the flexible-link manipulator two types of modeling are studied. In the first type, uncertainty is due to parameter variations of the manipulator while performing a task or when its configuration is changing. In the second type of modeling, a new look at the notion of flexibility in robotic manipulators is presented. The approximate polynomial solution of the Hamilton-Jacobi-Isaacs (HJI) inequality for a general nonlinear system is derived for designing the nonlinear H_∞ controller.

Nurkan et al [23] studied the control possibilities of a flexible armed robot by Sliding Mode Control, because Flexible armed robots are usually used in material handling in remote dangerous environments and production line. In their work first, the mathematical model of the system is formulated, and then the Sliding Mode Control theory is applied. Special care is given to the nonlinear problem of classical Sliding Mode Controller. The nonlinear may have serious damaging effect on gear systems as well as motor drive systems. Hence, in their work the nonlinear character of classical Sliding Mode Control is overcome and new version of Sliding Mode Controller is applied on the flexible single-arm robot.

Reza Olfati-Saber [24] introduced a method that provides a nonlinear noncollocated output for trajectory tracking of a flexible one-link robot. in his work the link is modeled as a finite-order Lagrangian system obtained from truncated modal analysis, This noncollocated output is derived based on viewing a flexible link robot arm as an underactuated mechanical system and then applying an appropriate change of coordinates that transforms the system into a cascade nonlinear system with a minimum-phase zero dynamics. The output is the angle of rotation augmented with the (generalized) saturation of the weighted amplitudes of the deflection modes of the flexible link.

Min and Jean-Claude [25] presented a self-sensory robot arm to two basic sensing problems in control of flexible manipulators. In their works the two basic sensing problems: detection of the variations of position and orientation due to structural deformation and detection of the contact force of end-effector when manipulator interacts with its environment. The position and orientation of flexible arm are expressed as a function of curvature of the arm A relation between strain measurements and endpoint force of flexible arm is developed and the contact force of end-effector is then determined using a force propagation algorithm. The proposed technique and algorithm were implemented and evaluated in a laboratorial flexible arm. Experimental validations using a vision system and two force sensors have shown that the self-sensory flexible arm can provide accurate endpoint position and force in both static and dynamic loading situations.

Knani J. [26] designed robust control for a flexible arm via the deterministic approach. In his work the deterministic approach represents a new development in control theory and allows dealing with uncertain elements; which every dynamical system may contain, as well as with unknown or imperfectly known inputs and state measurement errors. The obtained controller will guarantee that all possible responses of the system behave in a desired fashion. The controllers, designed via this approach, are called ‘‘robust’’ or ‘‘deterministic’’. The deterministic or robust principle of control is successfully

applied to ***SIMO***. Two different controllers are designed, and the uncertain parameters appear here as a set of the natural frequencies of the system. The procedure for the design performed in his research, can also be applied (with some modification) to ***MIMO.***

De Luca A. [27] presented formulation of control problems of flexible link robot. In his work presents multi choice of the controlled output; Joint level angular output, tip level angular output, and output at a point along the link, he derived the transfer function for all cases, and use a traditional control algorithm with analysis; pole zero map, and Bode diagram (frequency response) analysis. On the other hand for tracking of a joint trajectory, tracking of an end-effector trajectory, and rest-to-rest motion in given time. An open loop control scheme is used based on inversion of the dynamic equation of motion, and a nominal feed forward is computed by forward integration of flexible dynamics which leads to a stable open-loop control. Accurate end-effector trajectory tracking is the toughest control problem for flexible robots direct extension of inversion strategies to end-effector output closed-loop instabilities.

Tso et al [28] designed, and experimental test Lyapunov-type controller based on the deflection feedback of flexible one link robot. In their work, an optical sensing system consisting of a laser diode and a position sensitive detector is introduced for the real-time measurement of the dynamic deflection. Utilizing a non-linear, coupled and measurement-based dynamic system model, a Lyapunov-type controller based on the deflection feedback is then proposed to damp out the tip oscillations and regulate the endpoint of the flexible robot. Experimental tests are conducted for a flexible one-link robot arm with a payload mass at the tip. The results demonstrate the effectiveness of the proposed measuring and control schemes.

Etxebarria et al [29] presented a robust control scheme for flexible link robotic manipulators, which is based on considering the flexible mechanical structure as a system with slow (rigid) and fast (flexible) modes that can be

controlled separately. The rigid dynamics is controlled by means of a robust sliding-mode approach with well-established stability properties while an LQR optimal design is adopted for the flexible dynamics. In their work Experimental results show that this composite approach achieves good closed loop tracking properties both for the rigid and the flexible dynamics.

2.3. Summary and Conclusion

It seems from the above review that there is two main techniques were used by researchers to develop the dynamic equations of motion of flexible multibody systems, namely: Newton-Euler approach, and Lagrangian approach, while vector quantities are used in Newtonian mechanics, scalar quantities such as kinetic energy, potential energy, and work are used in lagrangian dynamics which greatly simplify the problem, and eliminates the forces of constraints from the dynamic equations. Many approximate techniques were proposed to change the partial differential equations of motion to a set of ordinary differential equations, which are Lumped Method, Finite Element Method (FEM), and Assumed Mode Method (AMM). The solution of models based on assumed mode method (Book's method) especially for spatial manipulators which are computationally inefficient and time consuming, and the complexity of the Finite Element Method for control design is its main disadvantage.

As mentioned earlier the aforementioned authors have used linearized equations in control of motion of flexible manipulators. The linearized models can only work in the neighborhood of operating points about which linearization have been taken. Moreover, since control systems for flexible manipulator are non-collocated and position commands contain high frequency components, the feedback control may cause these systems to become unstable. The inverse dynamic problems was usually simplified by decoupling the kinematic, dynamic equations based on the concept of nominal joint motions, which are determined using the kinematic equations for the rigid link counterpart of a flexible link manipulator without neglecting the effect of Link deflections.

3

Chapter Three

Modeling of flexible Robot Arm

MODELING OF FLEXIBLE ROBOT ARM

3.1. Introduction

This chapter focuses on the presentation of method for generating dynamic models for flexible link of robots. In this chapter, a dynamic modeling of lightweight link was developed by using an analytical (assumed mode)/Lagrangian approach. Creating a dynamic model that accounts for link flexibility adds additional challenges beyond the standard rigid link robot dynamics. The dynamic elastic response of each flexible link was formulated relative to an inertial frame coordinate system. The link was modeled as a cantilever beam with or without payload at its end and the link is rotate and bends in horizontal plane. Both the rigid degrees of freedom and the elastic degrees of freedom of the system were treated as generalized coordinate. The most apparent complexity arises due to the additional degrees of freedom associated with link deformations. Although in theory this adds an infinite number of degrees of freedom, in practice only a finite number were used to generate a model that is sufficiently accurate for predictive simulation and control design. Then by using Lagrange's equation mass and stiffness matrices and load vector of the typical link are obtained. The effects of the payload and the revolute joints on the equations of motion of the system were included by using the kinetic and potential energies of the joints and the payload through applying Lagrange's equations. The dynamic model derived in this work takes into account the coupling effects between rigid body motions and elastic deformation. Axial deflections, shear deformations, and rotary inertia effects due to the elastic deformation are neglected, Bernoulli-Euler beam theory was used in the formulation.

3.2. Kinematics of Flexible Link

The distance between two points on a rigid body remains constant during the motion of the body. Therefore, there is no difference between the kinematics of the body and the kinematics of its reference coordinate. However, this is not the case when deformable bodies are considered. Consider the absolute coordinate system O-XY shown in figure (3-1), and frame O-xy which rotate with link. This coordinate system called body coordinate system is assigned to a flexible link whose origin is rigidly attached to point O. The manipulator system modeled in this chapter is a flexible link which is connected by revolute joint. The joint is rigid in the direction of rotation of the connecting link. The links are deformable due to bending during heavy payload operations and high speed motion. As it can be seen in figure (3-1) , O-XY is the inertial frame coordinate system and O-xy is the rotating frame associated with link of the manipulator. The axis O-x, of the rotating frame O-xy passes through the end point of the link whose transverse deflection $W(x,t)$ is expressed with respect to this rotating frame. The kinematics modeling was based on the following assumptions:

1) The manipulator is constrained to move in the horizontal plane O-XY, therefore, the effect of gravity is not taken into account.
2) Axial deflections are negligible and only transverse bending deflection $W(x,t)$ is taken in to account.
3) The link is so long and slender that shear deformation and rotary inertia effect can be neglected. Then Bernoulli-Euler beam theory can be used.

3.2.1. Position Vectors

Based on the aforementioned assumptions, the position vector of an arbitrary point i of link with respect to frame O-xy, as shown in figure (3-1) can be written in the following form [27]:

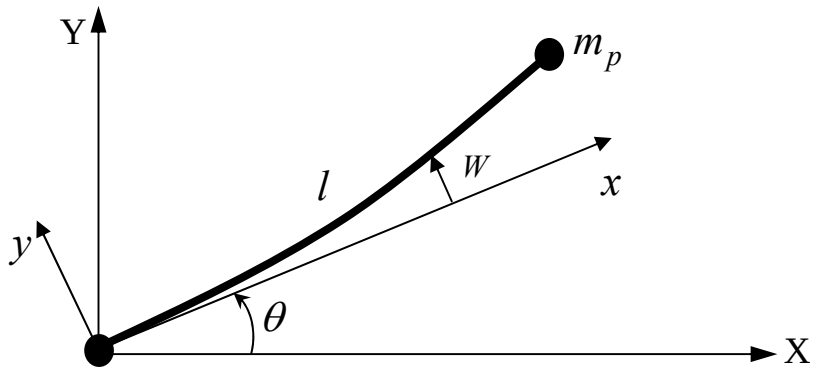

Figure (3-1) kinematics descriptions for a flexible one-link manipulator.

$$ {}^{i}\mathbf{p}_i(x) = \begin{bmatrix} x \\ W(x,t) \end{bmatrix} \quad \ldots\ldots\ldots (3.1)$$

While the position vector of tip of the link with respect to frame O-xy:

$$ {}^{i}\mathbf{r}_{i+1} = {}^{i}\mathbf{p}_i(l) \quad \ldots\ldots\ldots (3.2)$$

the position vector of an arbitrary point i of link with respect to inertial frame coordinate system O-XY:

$$ \mathbf{p}_i = \mathbf{r}_i + \mathbf{T}_i \, {}^{i}\mathbf{p}_i \quad \ldots\ldots\ldots (3.3)$$

Where:

$$ \mathbf{T}_i = \mathbf{T}_{i-1} S_{i-1} \mathbf{A}_i \quad , \quad \mathbf{r}_{i+1} = \mathbf{r}_i + \mathbf{T}_i \, {}^{i}\mathbf{r}_{i+1} $$

$$ \mathbf{A}_i = \begin{bmatrix} cos\,\theta_i & -sin\,\theta_i \\ sin\,\theta_i & cos\,\theta_i \end{bmatrix} \quad , \quad S_i = \begin{bmatrix} 1 & -W'_{ie} \\ W'_{ie} & 1 \end{bmatrix} \text{ , and } W'_{ie} = \left. \frac{\partial W_i}{\partial x_i} \right|_{x_i = l_i} $$

3.2.2. Differential Kinematics

Absolute angular velocity of frame O-XY was explained by [27]:

$$ \dot{\alpha}_i = \sum_{j=1}^{i} \dot{\theta}_i + \sum_{k=1}^{i-1} \dot{W}'_{ke} \quad \ldots\ldots\ldots (3.4)$$

Absolute linear velocity of a point on link:

$$ \dot{\mathbf{p}}_i = \dot{\mathbf{r}}_i + \dot{\mathbf{T}}_i \, {}^{i}\mathbf{p}_i + \mathbf{T}_i \, {}^{i}\dot{\mathbf{p}}_i \quad \ldots\ldots\ldots (3.5)$$

3.3. Flexible Link Analysis –Analytical Solution

Using Hamilton principle and calculus of variations, the bending deformation $W(x,t)$ and angle $\theta(t)$ satisfy the linear differential equations [27]:

$$EI\,W^{iv}(x,t)+\rho\left(\ddot{W}(x,t)+x\,\ddot{\theta}(t)\right)=0 \quad \ldots\ldots\ldots (3.6.a)$$

$$\tau(t)-J\,\ddot{\theta}(t)=0 \quad \ldots\ldots\ldots (3.6.b)$$

i.e., a PDE and an ODE (rigid motion), where $J=J_0+\left(\rho l^3\right)/3+m_p\,l^2$ and τ, $J_0, \rho, and\ m_p$ are torque input, actuator inertia, link mass per unit length and payload mass respectively. In the free evaluation $\tau(t)=0\Rightarrow\ddot{\theta}(t)=0$, the equation of motion for transverse vibration of Euler-Bernoulli beams is well known [27]. The boundary-value problem for a beam in flexure is defined by a fourth-order partial differential equation with two boundary conditions at each end. A brief review of dynamic beam analysis was provided to introduce key concepts, such a boundary conditions, natural frequencies, and mode shapes. The two-point boundary value problem [30] is:

$$EI\frac{\partial^4 W(x,t)}{\partial x^4}+\rho\frac{\partial^2 W(x,t)}{\partial t^2}=0 \quad \ldots\ldots\ldots (3.7)$$

Where boundary conditions are specified at $x=0$, and $x=l$. The cantilever beam (clamped-free) is a popular component to represent flexible links. The definitions for a beam with cantilever boundary conditions are illustrated in figure (3-2). At $x=0$, both the displacement and slope are zero. At the other end $x=l$, both the moment and shear are zero.

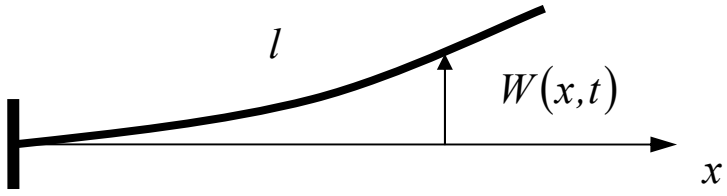

Figure (3-2) cantilever beam free vibration

The Euler-Bernoulli equation (equation 3.7) solved by separation of variables [31]:

$$W(x,t) = \phi(x)\ \delta(t) \qquad \ldots\ldots\ldots (3.8)$$

- **Time solution:**

$$\ddot{\delta}(t) = -\omega^2 \delta(t) \qquad \Rightarrow \quad \delta(t) = C_1 \sin\omega t + C_2 \cos\omega t \qquad \ldots\ldots\ldots (3.9)$$

With C_1, C_2 depending on the initial conditions $\delta(0)$ and $\dot{\delta}(0)$.

- **Space solution:**

$$\phi^{iv}(x) = \beta^4 \phi(x) \quad , \qquad \beta = \frac{\lambda}{l}$$

$$\Rightarrow \quad \phi(x) = A\sin\left(\lambda\frac{x}{l}\right) + B\cos\left(\lambda\frac{x}{l}\right) + C\ \sinh\left(\lambda\frac{x}{l}\right) + D\ \cosh\left(\lambda\frac{x}{l}\right)$$

…… (3.10)

3.4. Assumed Mode Shape

As stated earlier, there is no unique method for selecting the basis functions ϕ_i. Any set that satisfies the kinematics boundary conditions and linearly independent are acceptable. However, the quality of the approximate solution varies greatly with the choice of basis functions. One of the most important features of a mode shape (beyond the required conditions) is how well it approximates the true mode shape of analytical solution. For complicated systems, it may be difficult to assess whether the chosen mode shape resembles the true ones since the true mode shapes are not known analytically. At this point, engineering judgment is required in the analysis. Based on the assumed modes method the shape function given by [32]:

$$\phi_i(x) = c_i\left(cosh(\lambda_i x/l) - cos(\lambda_i x/l) - \gamma_i\left(sinh(\lambda_i x/l) - sin(\lambda_i x/l)\right)\right)$$

…… (3.11)

Where $\gamma_i = \dfrac{\left(cosh(\lambda_i) + cos(\lambda_i)\right)}{\left(sin(\lambda_i) + sinh(\lambda_i)\right)}$, If $z = \dfrac{x}{l}$

$$\phi_i(x) = c_i\left(cosh(\lambda_i z) - cos(\lambda_i z) - \gamma_i\left(sinh(\lambda_i z) - sin(\lambda_i z)\right)\right) \quad \ldots\ldots (3.12)$$

Where λ_i is calculated according to the boundary conditions (clam-free, and clamped- mass), i is the number of modes, and c_i is the normalized coefficient, which can be found by satisfying the relation:

$$\int_0^1 \phi_i^2 \, dz = 1. \quad \ldots\ldots\ldots (3.13)$$

A finite-dimensional approximation of the distributed bending deformation is obtained by truncation;

$$W(x,t) = \sum_{i=1}^{\infty} \phi_i(x)\delta_i(t) \approx \sum_{i=1}^{n_e} \phi_i(x)\delta_i(t) \quad \ldots\ldots\ldots (3.14)$$

Where n_e is the (arbitrary) number of the orthogonal modes that includes.

3.4.1. Clamped-Free Boundary Conditions

By using $W(x,t) = \phi(x)\delta(t)$ and $\ddot{\delta} = -\omega^2 \delta$, and holding the B.C.'s for any $\delta(t)$, these are rewritten in terms of $\phi(x)$ only:

$$\phi(0) = 0 \quad , \quad \phi'(0) = 0 \quad \ldots\ldots (3.15.a)$$

$$EI\,\phi''(l) = 0 \quad , \quad EI\phi'''(l) = 0 \quad \ldots\ldots (3.15.b)$$

Using the general solution $\phi(x)$, a system of linear homogenous equations follows:

$$\begin{bmatrix} \\ H(EI,l,\lambda) \\ \\ \end{bmatrix} \begin{bmatrix} A \\ B \\ C \\ D \end{bmatrix} = 0 \quad \ldots\ldots\ldots (3.16)$$

To exclude the trivial solution, the determinant of matrix H should be vanished (eigenvalue problem) [33], det $H(\lambda) = 0$ at infinite positive increasing roots λ_i of the transcendental characteristic equation:

$$1 + cos(\lambda_i)cosh(\lambda_i) = 0 \quad \ldots\ldots\ldots (3.17)$$

3.4.2. Clamped-Payload Boundary Conditions

As stated earlier the B.C.'s can be rewritten in terms of $\phi(x)$ only:

$$\phi(0)=0 \quad , \qquad \phi'(0)=0 \qquad \text{..... (3.18.a)}$$

$$EI\,\phi''(l)=0 \quad , \quad EI\phi'''(l)+m_p\,\omega^2\phi(l)=0 \qquad \text{..... (3.18.b)}$$

And a system of linear homogenous equations follows:

$$\begin{bmatrix} \\ H(EI,l,m_p,\lambda) \\ \\ \end{bmatrix}\begin{bmatrix} A \\ B \\ C \\ D \end{bmatrix}=0 \qquad \text{..... (3.19)}$$

And det $H(\lambda)=0$ gives:

$$1+cos(\lambda_i)cosh(\lambda_i)+\left(\frac{m_p}{m}\right)\lambda_i\left(sinh(\lambda_i)cos(\lambda_i)-cosh(\lambda_i)sin(\lambda_i)\right)=0$$

..... (3.20)

This is the transcendental characteristic equation for the clamped-payload B.C.'s.

3.5. Dynamic Modeling of Flexible Robot

The equations of motion of the system can be found by using the standard Lagrangian approach. This can be done by computing the kinetic energy, and the potential energy. Then the dynamic mode1 is obtained by satisfying the Lagrange's equations which was presented by [34] as:

$$L=KE_t-PE_t=L\left(\left\{\theta_i(t),\delta_{ij}(t),\dot{\theta}_i(t),\dot{\delta}_{ij}(t)\right\}\right) \qquad \text{..... (3.21)}$$

$$\frac{\partial}{\partial t}\left(\frac{\partial L}{\partial \dot{q}_i}\right)-\frac{\partial L}{\partial q_i}=Q_i \qquad i=1,2,.....n \qquad \text{..... (3.22)}$$

Where $q_i, Q_i, and\ n$ represent generalized coordinates, generalized forces, and the number of degrees of freedom of the system respectively. And

$L = KE_t - PE_t$ which represent the lagrangain where KE_t and PE_t are total kinetic, potential energies respectively. The total kinetic energy and total potential energy of the system can be found by summing those of various components of the system as:

$$KE_t = KE_h + KE_l + KE_P \quad \text{..... (3.23.a)}$$

$$PE_t = PE_l \quad \text{..... (3.23.b)}$$

Where $KE_h, KE_l, KE_P, and\ PE_l$ represent the kinetic energy of hub, link, payload, and elastic energy of link respectively.

3.5.1. Kinetic and Potential Energies

The kinetic and potential energies of link, hub, and payload can be written as showed by [34]:

1) Kinetic energy of link:

$$KE_l = \frac{1}{2}\int_0^l \rho\, \dot{p}(x)^T\, \dot{p}(x)\, dx \quad \text{..... (3.24)}$$

2) Elastic energy of link:

$$PE_l = \frac{1}{2}\int_0^l (EI)\left(\frac{d^2W(x)}{dx^2}\right)^2 dx \quad \text{..... (3.25)}$$

3) Kinetic energy of payload:

$$KE_p = \frac{1}{2} m_p\, \dot{r}_2^T\, \dot{r}_2 \quad \text{..... (3.26)}$$

4) Kinetic energy of hub:

$$KE_h = \frac{1}{2} m_h\, \dot{r}_1^T \dot{r}_1 + \frac{1}{2} J_h\, \dot{\alpha}_1^2 \quad \text{..... (3.27)}$$

Where $\rho, E, I, m_p, m_h, and\ J_h$ represent mass per unit length of link, modulus of elasticity of material, moment of inertia about z-axis, payload mass, hub mass, and hub inertia respectively.

3.5.2. Mass, Stiffness Matrices and Load Vector

Having the kinetic and potential energies of a typical element of an arbitrary link mass and stiffness matrices and load vector of the flexible link can be found by applying Lagrange's equations.

$$\frac{\partial}{\partial t}\left(\frac{\partial L}{\partial \dot{\theta}_i}\right)-\frac{\partial L}{\partial \dot{\theta}_i}=\tau_i \qquad i=1,\ldots,N \qquad \ldots\ldots\ldots (3.28)$$

$$\frac{\partial}{\partial t}\left(\frac{\partial L}{\partial \dot{\delta}_{ij}}\right)-\frac{\partial L}{\partial \dot{\delta}_{ij}}=0 \qquad j=1,\ldots,n_{ei} \quad i=1,\ldots,N \qquad \ldots\ldots\ldots (3.29)$$

N is the number of link, and n_{ei} is the number of flexible modes includes. For a flexible one link manipulator the dynamic equation of motion is formulated by using equations (3.29) and (3.30) as:

$$\begin{bmatrix} m_{\theta\theta}(\theta,\delta) & \mathbf{m}_{\theta\delta}(\theta,\delta) \\ \mathbf{m}^T{}_{\theta\delta}(\theta,\delta) & \mathbf{M}_{\delta\delta}(\theta,\delta) \end{bmatrix}\begin{bmatrix} \ddot{\theta} \\ \ddot{\delta} \end{bmatrix}+\begin{bmatrix} F_\theta(\theta,\delta,\dot{\theta},\dot{\delta}) \\ F_\delta(\theta,\delta,\dot{\theta},\dot{\delta}) \end{bmatrix}+\begin{bmatrix} 0 & \mathbf{0} \\ \mathbf{0}^T & \mathbf{K} \end{bmatrix}\begin{bmatrix} \theta \\ \delta_i \end{bmatrix}=\begin{bmatrix} \tau \\ 0 \end{bmatrix}$$

…… (3.30)

$$\mathbf{M}(q)\,\ddot{q}+F(q,\dot{q})+\begin{bmatrix} 0 \\ \mathbf{K}\delta_i \end{bmatrix}=[\tau] \qquad \ldots\ldots (3.31)$$

Where $m_{\theta\delta}(\theta,\delta)=[m_{11}\ \ m_{12}\ \ \cdots\cdots m_{1n}]$

Where $\mathbf{M}(q),\mathbf{K},\mathbf{F}(q,\dot{q}),\tau$ are the mass, stiffness matrix, coriolis and centrifugal vector, and load vector respectively.

The components of mass matrix $\mathbf{M}(q)$, stiffness matrix $\mathbf{K}$, and load vector are functions of elastic deformations, elastic velocities, and nonlinear terms including rigid body degrees of freedom and their time derivatives. Therefore, the dynamic equations of motion of one-link flexible manipulators are nonlinear.

3.5.3. Dynamic Model for Two Links (Rigid-Flexible) Manipulator

In order to achieve a typical work, master-slave type operation system was used in extreme environments, for example, outer space, nuclear power plants and the deep sea etc. In this system, human beings operate a slave manipulator by using a master manipulator in a safe place. consider using master-slave system in outer space, a slave arm will be long and lightweight arm. Then, the elastic vibration of a slave arm can lead to not only the deterioration of manipulability but also the instability of the closed-loop system [35]. Consider the two-link planar manipulator shown in figure (3-3), the first link is rigid and the second link is assumed to be flexible.

3.5.3.1. Kinematics Description

The kinematics description of this type of manipulator was derived by using equations (3.1) to (3.5)

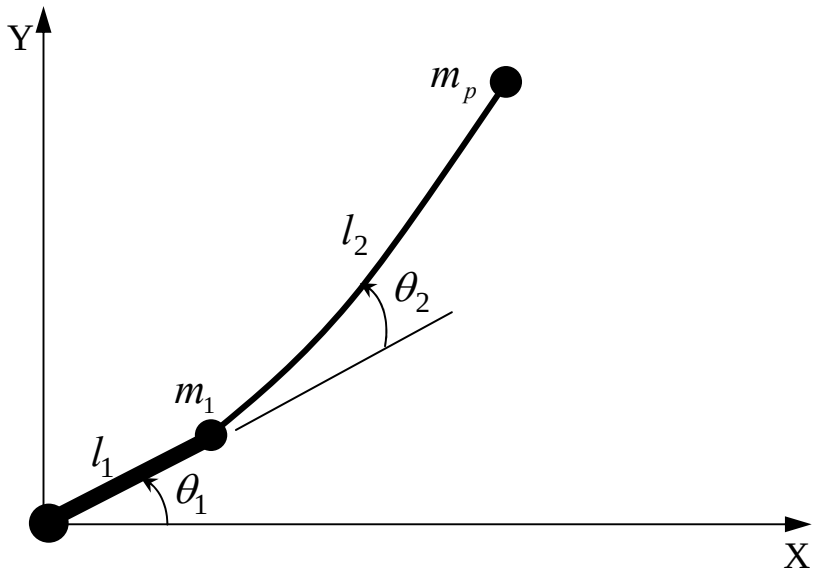

Figure (3-3) kinematics description of two links (rigid-flexible) manipulator.

1) Rigid Link:

$$ {}^{0}\mathbf{p}_1 = {}^{0}\mathbf{T}_1 \times {}^{1}\mathbf{p}_1 \quad , \quad {}^{1}\mathbf{p}_1 = \begin{bmatrix} x_1 \\ 0 \end{bmatrix} \qquad \ldots\ldots (3.32.a) $$

$$ {}^{0}\mathbf{T}_1 = \mathbf{T}_1 = \begin{bmatrix} c_1 & -s_1 \\ s_1 & c_1 \end{bmatrix} \qquad \ldots\ldots (3.32.b) $$

$$ {}^{0}\mathbf{p}_1 = \begin{bmatrix} c_1 & -s_1 \\ s_1 & c_1 \end{bmatrix} \begin{bmatrix} x_1 \\ 0 \end{bmatrix} \quad , \quad {}^{0}\mathbf{r}_1 = \begin{bmatrix} 0 \\ 0 \end{bmatrix} \quad , \quad \dot{\alpha}_1 = \dot{\theta}_1 \qquad \ldots\ldots (3.32.c) $$

2) Flexible Link:

$$ {}^{1}\mathbf{r}_2 = {}^{1}\mathbf{p}_1(l_1) = \begin{bmatrix} l_1 \\ 0 \end{bmatrix} \ , \ {}^{0}\mathbf{r}_2 = \begin{bmatrix} c_1 & -s_1 \\ s_1 & c_1 \end{bmatrix} \begin{bmatrix} l_1 \\ 0 \end{bmatrix} \qquad \ldots\ldots (3.33.a) $$

$$ \mathbf{T}_2 = \begin{bmatrix} c_1 & -s_1 \\ s_1 & c_1 \end{bmatrix} \begin{bmatrix} 1 & 0 \\ 0 & 1 \end{bmatrix} \begin{bmatrix} c_2 & -s_2 \\ s_2 & c_2 \end{bmatrix}, \ \mathbf{T}_2 = \begin{bmatrix} c_{12} & -s_{12} \\ s_{12} & c_{12} \end{bmatrix} \ldots (3.33.b) $$

Where $c_1 = cos\,\theta_1, s_1 = sin\,\theta_1, c_2 = cos\,\theta_2, s_2 = sin\,\theta_2,$

$$ s_{12} = sin(\theta_1 + \theta_2), c_{12} = cos(\theta_1 + \theta_2). $$

$$ {}^{0}\mathbf{p}_2 = l_1 \begin{bmatrix} c_1 \\ s_1 \end{bmatrix} + \begin{bmatrix} c_{12} & -s_{12} \\ s_{12} & c_{12} \end{bmatrix} \begin{bmatrix} x_2 \\ W_2(x_2, t) \end{bmatrix}, \dot{\alpha}_2 = \dot{\theta}_1 + \dot{\theta}_2 \ldots\ldots (3.33.c) $$

$$ \dot{\mathbf{p}}_2 = \begin{bmatrix} -l_1 s_1 \dot{\theta}_1 - (\dot{\theta}_1 + \dot{\theta}_2)(s_{12}\, x_2 + c_{12} W_2(x_2, t)) - s_{12} \dot{W}_2(x_2, t) \\ l_1 c_1 \dot{\theta}_1 + (\dot{\theta}_1 + \dot{\theta}_2)(c_{12}\, x_2 - s_{12} W_2(x_2, t)) + c_{12} \dot{W}_2(x_2, t) \end{bmatrix} $$

$\ldots\ldots$ (3.33.d)

3) Payload:

$$ {}^{2}\mathbf{r}_3 = \begin{bmatrix} l_2 \\ W_2(l_2, t) \end{bmatrix} \qquad \ldots\ldots (3.34.a) $$

$$ \mathbf{T}_3 = \begin{bmatrix} c_{12} & -s_{12} \\ s_{12} & c_{12} \end{bmatrix} \begin{bmatrix} 1 & -W'_{2e} \\ W'_{2e} & 1 \end{bmatrix} \begin{bmatrix} 1 & 0 \\ 0 & 1 \end{bmatrix} \qquad \ldots\ldots (3.34.b) $$

$$ {}^0\mathbf{r}_3 = l_1\begin{bmatrix} c_1 \\ s_1 \end{bmatrix} + \begin{bmatrix} c_{12} & -s_{12} \\ s_{12} & c_{12} \end{bmatrix}\begin{bmatrix} 1 & -W'_{2e} \\ W'_{2e} & 1 \end{bmatrix}\begin{bmatrix} l_2 \\ W_2(l_2,t) \end{bmatrix} \quad \text{..... (3.34.c)} $$

$$ {}^0\dot{\mathbf{r}}_3 = \begin{bmatrix} -l_1 s_1\dot{\theta}_1 + (\dot{\theta}_1+\dot{\theta}_2)(l_2 R_1 - R_2 W_2(l_2,t)) - \dot{W}'_{2e}(s_{12}\, l_2 + c_{12} W_2(l_2,t)) \\ l_1 c_1\dot{\theta}_1 + (\dot{\theta}_1+\dot{\theta}_2)(l_2 R_2 + R_1 W_2(l_2,t)) + \dot{W}'_{2e}(c_{12}\, l_2 - s_{12} W_2(l_2,t)) \\ + R_1\dot{W}_2(l_2,t) \\ + R_2\dot{W}_2(l_2,t) \end{bmatrix} \quad \text{.....}(3.34.d) $$

Where $R_1 = -(s_{12} + c_{12}\, W'_{2e}), R_2 = c_{12} - s_{12} W'_{2e}$.

3.5.3.2. Kinetic and Potential Energies

$$ KE_{h_1} = \frac{1}{2} J_{h_1}\, \dot{\theta}_1^2 \quad \text{..... (3.35.a)} $$

$$ KE_{l_1} = \frac{1}{2} m_1\, l_1^2\, \dot{\theta}_1^2 + \frac{1}{2} J_{G1}\, \dot{\theta}_1^2 \quad \text{..... (3.35.b)} $$

$$ KE_{h_2} = \frac{1}{2} J_{h_2}\, \dot{\theta}_2^2 \quad \text{..... (3.36.a)} $$

$$ KE_{l_2} = \frac{1}{2} \rho_2 \int_0^{l_2} {}^0\dot{p}_2 \times {}^0\dot{p}_2\, dx \quad \text{..... (3.36.b)} $$

$$ KE_P = \frac{1}{2} m_p\, {}^0\dot{r}_3 \times {}^0\dot{r}_3 \quad \text{..... (3.37)} $$

$$ PE_{l_2} = \frac{1}{2} EI \int_0^{l_2} \left(\frac{d^2\phi}{dx^2} \right) dx \quad \text{..... (3.38)} $$

$$ KE_t = KE_{h_1} + KE_{l_1} + KE_{h_2} + KE_{l_2} + KE_P \;, PE_t = PE_{l_2} \quad \text{.....(3.39)} $$

3.5.3.3. Mass, Stiffness Matrices and Load Vector

Having the kinetic and potential energies for the each link of the manipulator mass, stiffness matrices and load vector of Rigid-Flexible manipulator can be found by applying Lagrange's equations (3.28) and (3.29).

$$ \mathbf{M} = \begin{bmatrix} \mathbf{M}_{\theta\theta} & \mathbf{M}_{\theta\delta} \\ \mathbf{M}_{\theta\delta} & \mathbf{M}_{\delta\delta} \end{bmatrix} \quad \text{..... (3.40)} $$

$$\mathbf{M}_{\theta\theta}=\begin{bmatrix} m & m_1(\delta) \\ m_1(\delta) & m_2(\delta) \end{bmatrix},\ \mathbf{M}_{\theta\delta}=\begin{bmatrix} m_{11} & m_{12}\ldots\ldots & m_{1n} \\ m_{21} & m_{22} & \ldots\ldots\ m_{2n} \end{bmatrix}$$

…… (3.41)

$$\mathbf{M}_{\delta\delta}=\begin{bmatrix} m_{\delta 11} & m_{\delta 12}\ldots & m_{\delta 1n} \\ m_{\delta 21} & m_{\delta 22} & \ldots\ m_{\delta 2n} \\ \vdots & \vdots & \ddots \quad \vdots \\ m_{\delta n1} & m_{\delta n2} & \cdots\ m_{\delta nn} \end{bmatrix} \quad \ldots\ldots (3.42)$$

$$\mathbf{K}=\begin{bmatrix} k_1 & 0 & 0 & \cdots & 0 \\ 0 & k_2 & 0 & \cdots & 0 \\ \vdots & \vdots & \ddots & & \vdots \\ 0 & 0 & 0 & \cdots & k_n \end{bmatrix},\ \mathbf{F}^T=\begin{bmatrix} 0 & F_1 & F_2 & F_3 & F_{n+1} \end{bmatrix} \ldots\ldots (3.43)$$

The dynamic equation of motion can be written in the form:

$$\begin{bmatrix} \mathbf{M}_{\theta\theta} & \mathbf{M}_{\theta\delta} \\ \mathbf{M}_{\theta\delta} & \mathbf{M}_{\delta\delta} \end{bmatrix}\begin{bmatrix} \ddot{\theta}_1 \\ \ddot{\theta}_2 \\ \ddot{\delta} \end{bmatrix}+\begin{bmatrix} 0 \\ F_\theta\left(\theta_1,\theta_2,\delta,\dot{\theta}_1,\dot{\theta}_2,\dot{\delta}\right) \\ F_\delta\left(\theta_1,\theta_2,\delta,\dot{\theta}_1,\dot{\theta}_2,\dot{\delta}\right) \end{bmatrix}+\begin{bmatrix} 0 & 0 & \mathbf{0} \\ 0 & 0 & \mathbf{0}^* \\ \mathbf{0}^T & \mathbf{0}^{*T} & \mathbf{K} \end{bmatrix}\begin{bmatrix} \theta_1 \\ \theta_2 \\ \delta_i \end{bmatrix}=\begin{bmatrix} \tau_1 \\ \tau_2 \\ 0 \end{bmatrix}$$

…… (3.44)

Where $\mathbf{M},\mathbf{K},\mathbf{F},n$ are the mass and stiffness matrices, nonlinear vector, and number of including flexible coordinates respectively, and $\mathbf{0}^*=\begin{bmatrix}0_1\cdots 0_{n-1}\end{bmatrix}$.

3.6. Computer Programming for Analytical Solution

In this work all the calculation; solving equation, integration, and time simulation was done with ***MatLab 6.5*** software. This software used to generate ***M.file*** [36] to solve the equation, plotting the curves, and provides good ability for time simulation. The transcendental characteristic equation was solved by using three functions as described in [37] which is solved the equation by iterations until the program given an acceptable value for error .New functions were built in ***MatLab*** to used in calculations, while the programming can not be done without using these functions. There are two types for using these

functions; the first one is the traditionally for using any program, while the second which gives the equations symbolically. The second type of using these functions is very important especially for finding integration and differentiation of some equation in the modeling. Many ***M.files*** were built in this work to provide the solution for all equations in the modeling, and these ***M.files*** shown in appendix (B). The new three functions which were give the flexibility of the link based on the assumed mode method are:

1-Function ϕ (shape function): This function gives the mode shapes of the flexible link; the software of this function is based on the equation (3.11). This function was built and then linked with the ***MatLab 6.5*** program; it can be used numerically or symbolically. This function is very important due to use approximately in the all calculation in modeling of flexible arm, and there is another Function called ϕ_z which gives the same results but it works with dimensionless analysis equation (3.12), figure (3-4) shows the flowchart of this function .

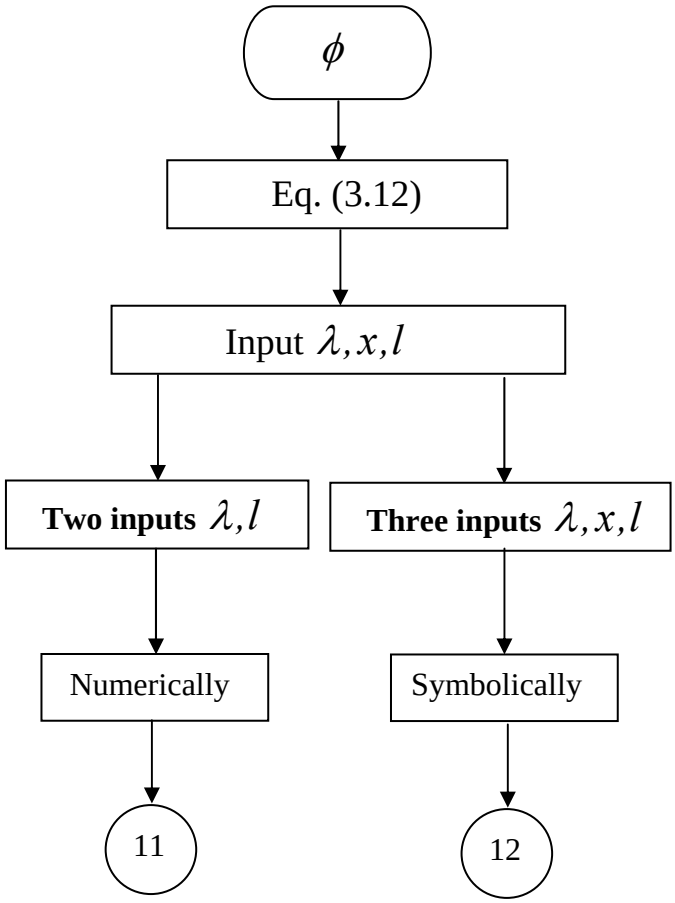

Figure (3-4) simple flowchart of Function ϕ

2-Function δ (flexible coordinates): This function presented the time solution of the Euler-Bernoulli equation based on the equation (3.9); it was used in time simulation of the deflection of link. This function is deal with the natural frequency of the system and the initial conditions. It works with the function ϕ to present the time simulation for the deflection of flexible robot arm. There are also two types of function δ numerically and symbolically, were used in calculation as shown in figure (3-5).

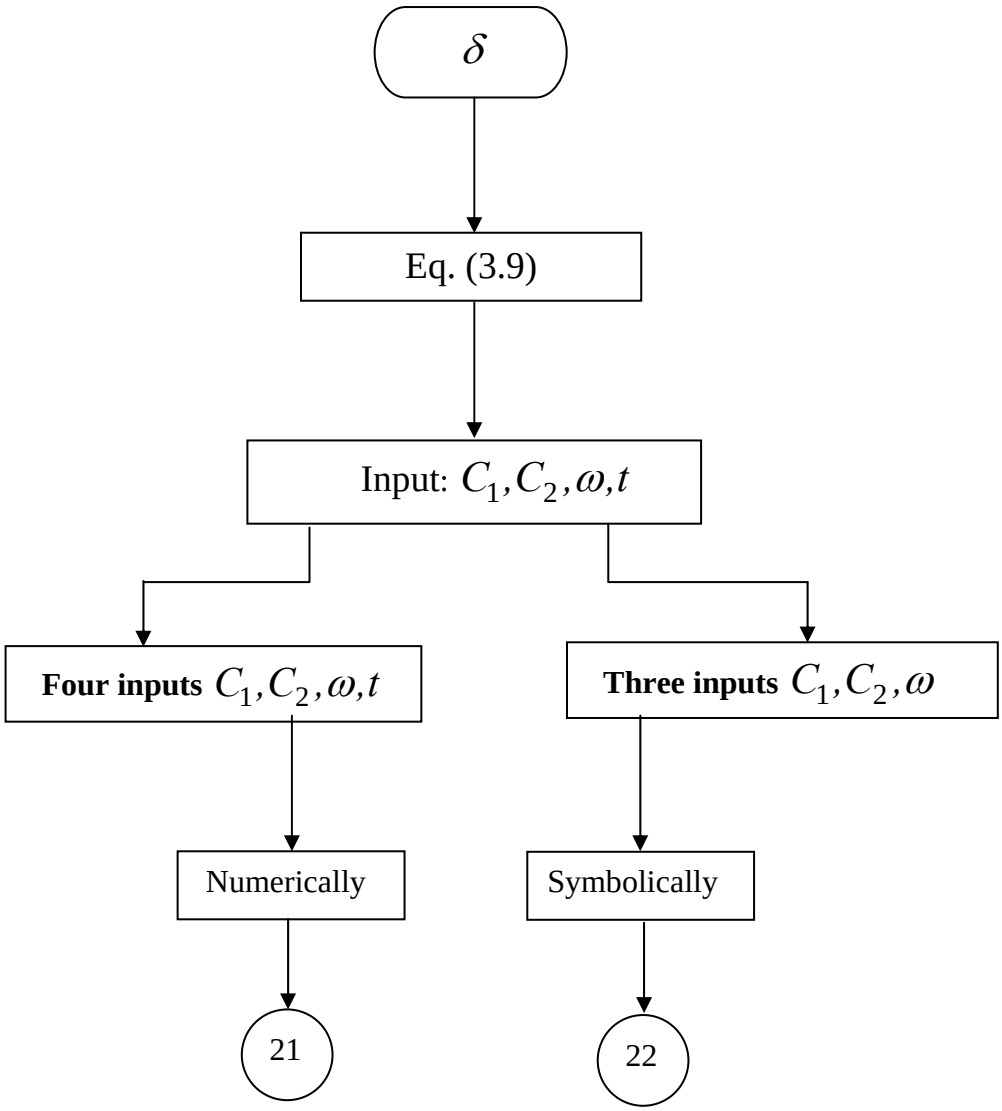

Figure (3-5) simple flowchart of Function δ

3- Function *W*(bending deformation): this function is the sum of the earlier two functions; this function was based on the equation (3.14). Moreover the function ***W*** can not be used in ***MatLab 6.5*** without the earlier two functions because they link in program and function ***W*** call them when it's done. This function was used also in two ways, depending on the application, finally a aforementioned functions is very important for use in inverse dynamics in chapter 4, and below there is simple flow chart for this function figure (3-6).

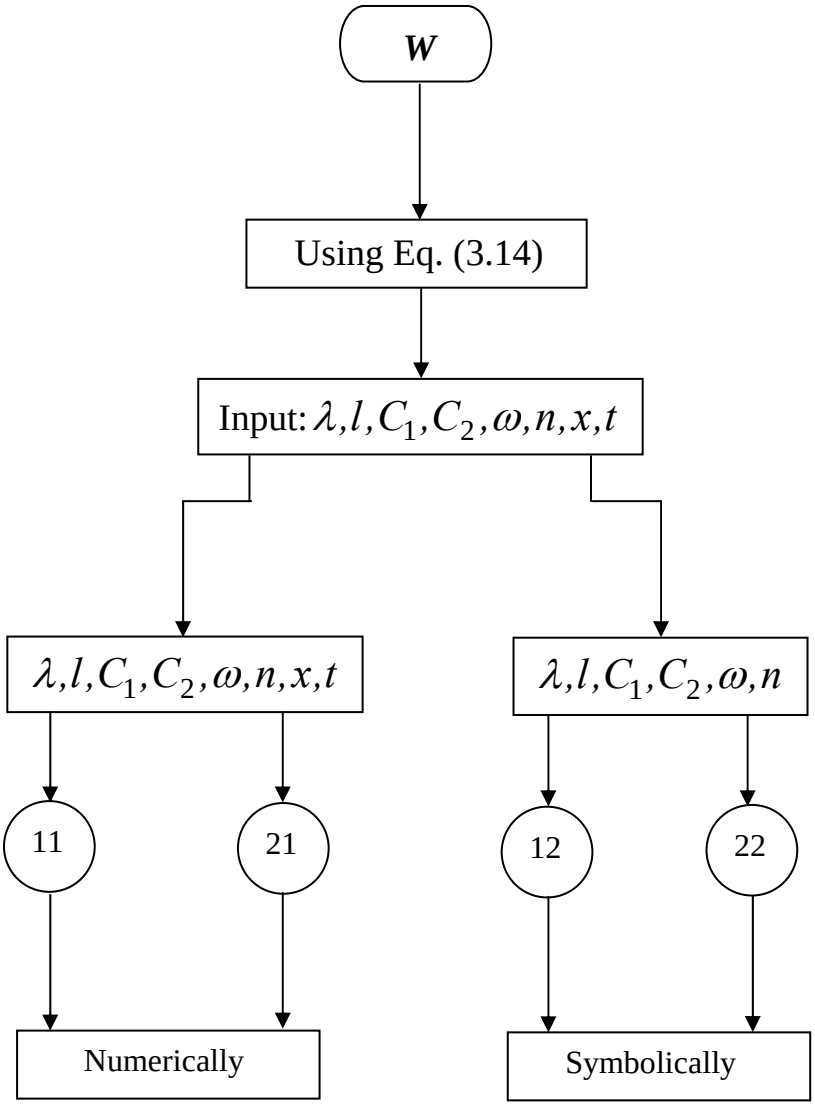

Figure (3-6) simple flowchart of Function ***W***

3.7. Dynamic model verification

The dynamic modeling of this work has been verified by comparing it with the model derived by using ***symofros*** package which is used with ***maple***

software. Moreover the model is tested experimentally to find the natural frequency in the present work by Mehrdad [8]. The matrices of the dynamic model are shown below and the difference between the two models it can be clearly shown.

Link data:

Parameter		Value	unit
Beam material		Steel	
Density	ρ^*	7980	$\left(kg/m^3\right)$
Modulus of elasticity	E	190×10^9	$\left(N/m^2\right)$
Length	l	0.6	m
Cross section area	a	0.88×50	mm^2
Hub moment of inertia	J_h	0.002	$\left(kg.m^2\right)$

- The model presented by Mehrdad M. [8]:

$$\mathbf{M}(q,\delta)=\begin{bmatrix} m(\delta) & 0.1863 & 0.0208 \\ 0.1863 & 0.2655 & -7.1518\times10^{-5} \\ 0.0208 & -7.1518\times10^{-5} & 0.2162 \end{bmatrix} \quad \text{.....(3.45)}$$

$$m(\delta) = 0.1334 + 0.2654\,\delta_1^2 + 0.2149\,\delta_2^2 \quad \text{..... (3.46)}$$

$$\mathbf{K}=\begin{bmatrix} 7.534 & 0 \\ 0 & 755.5287 \end{bmatrix} \quad \text{..... (3.47)}$$

Where the natural frequencies are calculated from the matrices above as presented also by Mehrdad M. [8]:

$$\left[\omega_1\ \omega_2 \cdots \omega_n\right]=\frac{1}{2\pi}\sqrt{eig\left(\mathbf{IM}_{nn0}\times\mathbf{K}\right)} \quad \text{..... (3.48)}$$

$$IM_{nn0}=M_{\delta\delta}^{-1} \quad at \quad t=0\Rightarrow\delta(0) \quad \text{..... (3.49)}$$

$\omega_1 = 5.2059\,Hz$, $\omega_2 = 21.7267\ Hz$.

And experimentally as:

$\omega_{1e} = 5.5\ Hz$,$\omega_{2e} = 20\ Hz$

$$\mathbf{F}\left(q,\dot{q},\delta,\dot{\delta}\right) = \begin{bmatrix} \dot{q}\dot{\delta}_1\left(0.2667\delta_1 + 4.2261\times10^{-4}\delta_2\right) + \dot{q}\dot{\delta}_2\left(0.5308\delta_2 + 4.2261\times10^{-4}\delta_1\right) \\ -0.5\dot{q}^2\left(0.2667\delta_1 + 4.2261\times10^{-4}\delta_2\right) \\ -0.5\dot{q}^2\left(0.5308\delta_2 + 4.2261\times10^{-4}\delta_1\right) \end{bmatrix} \quad \ldots\ldots\ldots (3.50)$$

- The model derived in this work

$$\mathbf{M} = \begin{bmatrix} m(\delta) & 0.1864 & 0.0205 \\ 0.1864 & 0.2654 & 0 \\ 0.0205 & 0 & 0.2161 \end{bmatrix} \quad \ldots\ldots\ldots (3.51)$$

$$m(\delta) = 0.1332 + 0.2654\,\delta_1^2 + 0.2162\,\delta_2^2 \quad \ldots\ldots\ldots (3.52)$$

$$\mathbf{K} = \begin{bmatrix} 7.228 & 0 \\ 0 & 724.528 \end{bmatrix} \quad \ldots\ldots\ldots (3.53)$$

The natural frequencies are:

$$\omega_1 = 32.7889\frac{rad}{sec} = 5.2185\ Hz,\ \omega_2 = 144.8686\frac{rad}{sec} = 23.0565\ Hz$$

$$\mathbf{F}\left(q,\dot{q},\delta,\dot{\delta}\right) = \begin{bmatrix} 0.2482\delta_1\dot{\delta}_1\,\dot{q} + 0.5633\delta_2\dot{\delta}_2\,\dot{q} \\ -0.5\dot{q}^2 \times 0.2482\delta_1 \\ -0.5\dot{q}^2 \times 0.5633\delta_2 \end{bmatrix} \quad \ldots\ldots\ldots (3.54)$$

3.8. Summary and conclusion

In this chapter a general overview on dynamic modeling of flexible manipulator systems was presented. An assumed mode/lagrangian approach for dynamic modeling of lightweight robots with flexible link has been developed. The dynamic elastic response of flexible link was formulated relative to an inertial frame clamped-free or clamped-mass coordinate system, the kinetic and potential energies of the flexible link, actuated joint and, payload were calculated. The equation of motion of the system has been found by using Lagrange's equations. The dynamic mode1 derived in this study is free from assumption of a nominal motion and takes into accounts the coupling effects between the rigid body motion and the elastic deformation. Due to the aforementioned couplings as well the variation in the effective inertia of the system as its configuration is changing with time, the model is highly nonlinear and coupled. The validity of the model is showed by compared case example with another work presented the dynamic model with ***symofros*** package and tested the same model experimentally and the model presented in this work can be used with three modes successfully. Also the dynamic model derived in this chapter is used to design control system to show the flexibility of the link on the control algorithm.

4

Chapter Four

Trajectory Control of Flexible Robot Arm

TRAJECTORY CONTROL OF FLEXIBLE ROBOT ARM

4.1. Introduction

Most of the researches in the area of flexible-link robot control have been applied to the case of a single flexible arm. However there is one major critique in this regard, in the multi-link case, the mass matrix contains joint position variables, which introduce considerable nonlinearities in the dynamic equations. For a single flexible link the mass matrix is only a function of deflection variables, which are quadratic type nonlinearities. Thus a single link may well approximate a linear system, while this is not true in the multi-link case. In spite of this fact, the experiments conducted with a single link case provide a basis for multi-link investigations, since both cases suffer from the undesirable non-minimum phase property [38].

This property shows up when the controlled output is the end-effector position. A case a critical situation was encountered when one tries to apply standard inversion techniques for exact trajectory tracking. Any attempt to achieve exact tracking via inversion results in unbounded state trajectories and unstable closed-loop system. The less difficult problem of end-point stabilization may also become troublesome, although not impossible, because of the non-minimum phase nature. On the other hand, the tracking of joint trajectories can always be obtained in a stable fashion in the presence of link flexibilities. This may of course yield unacceptable tip position errors.

In the trajectory control problems, the desired position of the end point of the manipulator is given versus time. Therefore, the required joint torques or forces should be applied to move the end point along the given trajectory. This type of problem is one of the major open problems related to the flexible manipulators. Various feedback control strategies are proposed in the literature for suppressing vibration of the flexible-link manipulators [15, and 16]. But due to

the non-collocated nature of the control system of flexible manipulators as well as the existence of high frequency components in the position commands, the feedback control may cause these systems to be unstable. To avoid this problem, many authors have recently proposed inverse dynamic methods. These methods simultaneously solve the equations of motion and the kinematics equations in order to determine the required joint torques or forces. But the main difficulty is that the numerical solution of the inverse dynamic problem of flexible manipulators normally diverges. This is not because of failure of the numerical analysis, but due to the nature of the problem which is noncausal.

4.2. Trajectory Generation

Trajectory was referred to a time history of position, velocity, and acceleration for each degree of freedom. This problem includes the human interface problem of how specify a trajectory or path through space. In order to make the description of manipulator motion easy for human user of a robot system, the user should not be required to write down complicated functions of space and time to specify the task. Rather, the user must allow the capability of specifying trajectories with simple descriptions of the desired motion, and let the system figure put the details. The user may just specify the desired goal position and orientation of the end-effector point, and leave it to the system to decide on the exact shape of the path to get there, the duration, the velocity profile, and other details. The desired output trajectory used this work is a higher order polynomials are some times used for path segments, this polynomial is quintic polynomial [39]:

$$\theta(t) = a_0 + a_1 t + a_2 t^2 + a_3 t^3 + a_4 t^4 + a_5 t^5 \quad \ldots\ldots\ldots (4.1)$$

Where the constraints are given as:

$$\theta_i = a_0$$
$$\theta_f = a_0 + a_1 t_f + a_2 t_f^2 + a_3 t_f^3 + a_4 t_f^4 + a_5 t_f^5 \quad \ldots\ldots\ldots (4.2.a)$$

$$\dot{\theta}_i = a_1$$
$$\dot{\theta}_f = a_1 + 2a_2 t_f + 3a_3 t_f^2 + 4a_4 t_f^3 + 5a_5 t_f^4 \quad \text{..... (4.2.b)}$$

$$\ddot{\theta}_0 = 2a_2$$
$$\ddot{\theta}_f = 2a_2 + 6a_3 t_f + 12a_4 t_f^2 + 20a_5 t_f^3 \quad \text{..... (4.2.c)}$$

These constraints specify a linear set of six equations with six unknowns solved by using ***MatLab 6.5***. The solution is provided from robot toolbox [40]. Function ***Jtraj*** in this toolbox gives the position, velocities, and acceleration of the rigid degree of freedom of the robot arm. The rigid joint trajectory is used in the inverse dynamic control strategy. In this work Function ***Jtraj*** gives the desired trajectory $\theta_d, \dot{\theta}_d, and, \ddot{\theta}_d$, to find the open-loop torque for the flexible link followed the desired trajectory.

4.3. The Non-minimum Phase Characteristic

To illustrate the non-minimum phase characteristic in flexible-link systems, consider a single-link flexible arm as shown in figure (4-1). A linearized dynamic model of this arm found by using the method of assumed modes and Lagrangian formulation. When a single flexural mode was used the following dynamics result [8] as:

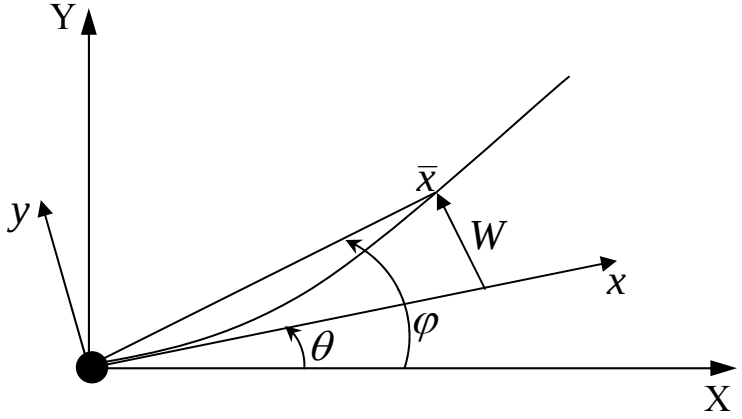

Figure (4-1) single flexible arm

$$m_{11}\ddot{\theta} + m_{12}\ddot{\delta} = \tau \quad \text{..... (4.3.a)}$$
$$m_{12}\ddot{\theta} + m_{22}\ddot{\delta} + k\delta = 0 \quad \text{..... (4.3.b)}$$

Where $m_{ij}, i, j \in \{1,2\}$, are components of the mass matrix given, for zero payload, by [8]:

$$m_{11} = \frac{\rho l^3}{3} + J_h,\ m_{12} = \int_0^l \phi(x)\, x\, \rho\ dx,\ m_{22} = \rho a \qquad \ldots\ldots\ldots (4.4)$$

Where a is the link's cross sectional area, ρ is its mass per unit length, $\phi(x)$ is the modal shape function, and k is the stiffness coefficient of the beam and is given by [8]:

$$k = EI \int_0^1 \left(\frac{d^2\phi}{dx^2} \right)^2 dx \qquad \ldots\ldots\ldots (4.5)$$

In equation (4.5), E is the link modulus of elasticity and I is the second moment of area. Also in equation (4.3), τ is the input torque. Defining the output y' as the tip position and $\phi_e = \phi(l)$, then:

$$y' = \theta + \phi_{ie}\, \delta_i \qquad \ldots\ldots\ldots (4.6)$$

Where $\phi_e = \phi(l)$. The zero-dynamics can be found by setting y' identically zero, which yields:

$$\tau = (m_{12} - m_{11}\phi_e)\ddot{\delta} \qquad \ldots\ldots\ldots (4.7)$$

$$0 = (m_{22} - m_{12}\,\phi_e)\ddot{\delta} + k\delta \qquad \ldots\ldots\ldots (4.8)$$

The zero dynamics represented by equation (4.8) are generally unstable since $m_{12} - m_{11}\phi_e < 0$. Note that by using equation (4.4) the latter term is given by:

$\rho\left(1 - \phi_e \int_0^1 x\,\phi(x)\,dx\right)$. Now, assuming a clamped-free mode shape it can be concluded from $\phi(x) < \phi_e$ that $\phi_e \int_0^1 x\,\phi(x)\,dx < \frac{\phi_e^2\, l^2}{2}$.

Therefore, if l is large enough the first coefficient in equation (4.8) is negative, i.e., unstable zero-dynamics. The non-minimum phase condition in this

case is a result of the non-collocated sensor and actuator positions. The system is under-actuated, and the input torque affects the tip position through flexural variable δ and rigid body mode θ.

From the control point of view, the zero-dynamics addresses an important question: Is there any control input that can identically regulate y to zero? The unstable zero-dynamics given by equation (4.8) implies that the internal states $\delta, and\ \dot{\delta}$ will be unbounded if the initial states are different from zero. This will require an unbounded input from equation (4.7) which is not desirable. However, relaxing the control goal of identically zeroing the output, it is possible to have sufficiently small bounded output while the internal states are bounded, even when the system is non-minimum phase.

4.4. Inverse Dynamics of Flexible Robot Arm

Consider a single-flexible manipulator shown in figure (4-2). The purpose of this analysis is to find the required joint torques $\tau(t)$ to cause the desired motion of the payload, which is a rest to rest motion tracking a specified path $\theta(t)$, from point A to point B in a given time interval. The inverse dynamics of the flexible manipulator is redundant due to its flexibility. Therefore, a complete model consisting of the kinematics and dynamic equations of the system should be solved simultaneously.

Using the dynamic model equations from chapter three, it has been written the equation of motion of the system in the following form:

$$\begin{bmatrix} m_{\theta\theta}(\theta,\delta) & \mathbf{m}_{\theta\delta}(\theta,\delta) \\ \mathbf{m}^{T}{}_{\theta\delta}(\theta,\delta) & \mathbf{M}_{\delta\delta}(\theta,\delta) \end{bmatrix} \begin{bmatrix} \ddot{\theta} \\ \ddot{\delta}_i \end{bmatrix} + \begin{bmatrix} F_{\theta}(\theta,\delta,\dot{\theta},\dot{\delta}) \\ \mathbf{F}_{\delta}(\theta,\delta,\dot{\theta},\dot{\delta}) \end{bmatrix} + \begin{bmatrix} 0 \\ \mathbf{K}\delta_i \end{bmatrix} = \begin{bmatrix} \tau \\ 0 \end{bmatrix}$$

…… (4.9)

Where $\theta, and\ \delta_i$, are the vectors of joint and elastic coordinates of the link. These variables all together present the degrees of freedom of the system.

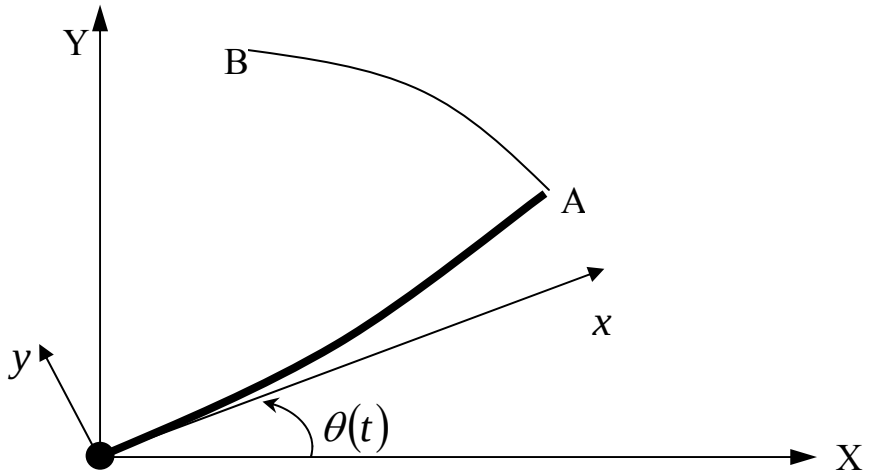

Figure (4-2) rest to rest motion of a flexible one-link manipulator.

From second set of n equations in the dynamic model, solve for $\ddot{\delta}$:

$$\ddot{\delta}_i = -\mathbf{M}_{\delta\delta}^{-1}\left(\mathbf{F}_\delta\left(\dot{\theta},\delta\right)+\mathbf{K}\,\delta_i+\mathbf{m}_{\theta\delta}^{T}\,\ddot{\theta}\right) \quad \ldots\ldots\ldots (4.10)$$

And plug in first set of $n+1$ equations $\Rightarrow$ effects of flexible dynamics onto rigid dynamics:

$$\left(m_{\theta\theta}-\mathbf{m}_{\theta\delta}\,\mathbf{M}_{\delta\delta}^{-1}\,\mathbf{m}_{\theta\delta}^{T}\right)\ddot{\theta}+F_\theta\left(\dot{\theta},\delta,\dot{\delta}\right)-\mathbf{m}_{\theta\delta}\,M_{\delta\delta}^{-1}\left(\mathbf{F}_\delta\left(\dot{\theta},\delta\right)+\mathbf{K}\,\delta\right)=\tau$$

$\ldots\ldots\ldots$ (4.11)

In the above equation. Solving for τ gives:

$$\begin{aligned}\tau &= \left(m_{\theta\theta}-\mathbf{m}_{\theta\delta}\,\mathbf{M}_{\delta\delta}^{-1}\,\mathbf{m}_{\theta\delta}^{T}\right)\ddot{\theta}+F_\theta\left(\dot{\theta},\delta,\dot{\delta}\right)-\mathbf{m}_{\theta\delta}\,M_{\delta\delta}^{-1}\left(\mathbf{F}_\delta\left(\dot{\theta},\delta\right)+\mathbf{K}\,\delta\right)\\ &= \tau^{*}\left(\ddot{\theta},\dot{\theta},\delta,\dot{\delta}\right)\end{aligned} \quad \ldots\ldots\ldots (4.12)$$

The input torque τ^{*} is the one that 'stiffens;' the motion of the flexible arm at the joint location, ensuring the tracking of any desired output trajectory.

4.5. Open-Loop Control

To avoid the aforementioned prob1ems of instabilities for closed-loop system , inverse dynamic with open-loop methods have been used to determine the joint torques such that the end-point of the flexible manipulator follows a given trajectory,

In this scheme set

$$\dot{\theta}(t)=\dot{\theta}_d(t), and\ \ddot{\theta}(t)=\ddot{\theta}_d(t) \quad \ldots\ldots (4.13)$$

The control τ^* is not completely specified by these identities, since knowledge of $\delta(t)$ and $\dot{\delta}(t)$ is still needed. This is essentially different from the case of rigid arms. The assigning of the behavior to the joint variables uniquely was determined the required torque inputs. Here, a dynamic generators to be set up to recover the time evaluation of the elastic coordinates δ. plugging the expressions for τ^* in to the dynamic equations and replacing the joint variables by their desired values gives:

$$\ddot{\delta} = -\mathbf{M}_{\delta\delta}^{-1}\left(\mathbf{F}_{\delta}\left(\dot{\theta}_d,\delta\right)+\mathbf{K}\,\delta+\mathbf{m}_{\theta\delta}^{T}\,\ddot{\theta}_d\right) \quad \ldots\ldots (4.14)$$

The off-line integration of the n second-order differential equations, starting from $\left(\delta(0),\dot{\delta}(0)\right)$, yields the desired time evaluation $\left(\delta_d(t),\dot{\delta}_d(t)\right)$ the resulting from open-loop torque to be applied at the joint then:

$$\tau_{OL} = \tau^*\left(\ddot{\theta}_d,\dot{\theta}_d,\delta_d,\dot{\delta}_d\right) \quad \ldots\ldots (4.15)$$

To gain some robustness at law expense, a linear feedback can be used in addition to this reference torque signal. A proportional derivative (PD) controller on the joint trajectory error is properly designed as [19]:

$$\tau_{OL.PD} = \tau^*\left(\ddot{\theta}_d,\dot{\theta}_d,\delta_d,\dot{\delta}_d\right)+\left(m_{\theta\theta}-\mathbf{m}_{\theta\delta}\,\mathbf{M}_{\delta\delta}^{-1}\,\mathbf{m}_{\theta\delta}^{T}\right)\left[k_p\left(\theta_d-\theta\right)+k_v\left(\dot{\theta}_d-\dot{\theta}\right)\right] \quad \ldots\ldots (4.16)$$

Where k_p and k_v are proportional and derivative gains.

Increasing gains in the above equation leads to faster response and lower steady-state error, and the natural frequency limit the magnitude of gains [39], the gains can be chosen according to the relation:

$$k_p = \omega_n^2\ ,\ k_v = 2\times\sqrt{k_p} \quad \ldots\ldots (4.17)$$

4.6. Inversion Control for a Point along the Arm

Necessitated by moving towards end-point trajectory tracking, inversion control is investigated next for stiffening the motion of the suitable point along the arm. In fact, there may exist a continuous range of points along the structure, other than just the joint location, for which a smooth trajectory can be exactly reproduced in stable way [19].

The angle φ formed by a generic point along the arm with the reference frame can be expressed in a parametric form with respect to x as (figure (4-1)).

$$\varphi(x) = \theta + arctg\left(\frac{W(x)}{x}\right) \quad \ldots\ldots\ldots (4.18)$$

For small deflections, the output can be defined as a linearized version of φ, i.e.

$$\varphi(x) = \theta + \frac{W(x)}{x} = \theta + \frac{\phi^T(z)\delta}{x} \quad , \; z = \frac{x}{l} \quad \ldots\ldots\ldots (4.19)$$

It was worth noting that this parameterization is convenient one, since for $x = 0$ the clamped boundary conditions

$$\lim_{x \to 0} \frac{W(x)}{x} = 0 \quad \ldots\ldots\ldots (4.20)$$

Conversely, for $x = l$, a true end-point strategy is obtained.

Inertia matrix with $M_{\delta\delta}$ of order $n \times n$, accordingly, [19] showed that the inverse can be written as:

$$\mathbf{D}(\delta) = M^{-1} = \begin{bmatrix} d_{11}(\delta) & \mathbf{d}_{12}(\delta) \\ \mathbf{d}_{12}^T(\delta) & \mathbf{D}_{22}(\delta) \end{bmatrix} \quad \ldots\ldots. (4.21.a)$$

$$d_{11}(\delta) = \frac{1}{m_{\theta\theta} - \mathbf{m}_{\theta\delta}\mathbf{M}_{\delta\delta}^{-1}\mathbf{m}_{\theta\delta}^T} \quad \ldots\ldots. (4.21.b)$$

$$\mathbf{d}_{12}(\delta) = -\frac{\Delta^{-1}(\delta)\mathbf{m}_{\theta\delta}^T}{m_{\theta\theta}} \; , \; \mathbf{D}_{22}(\delta) = \Delta^{-1}(\delta) \quad \ldots\ldots. (4.21.c)$$

$$\Delta(\delta) = \mathbf{M}_{\delta\delta} - \frac{\mathbf{m}_{\theta\delta}^T \mathbf{m}_{\theta\delta}}{m_{\theta\theta}} \quad \ldots\ldots (4.21.d)$$

Applying the inversion algorithm with output $y(x)$ and following the same steps as in the section (4.4) gives:

$$\ddot{y} = \left[d_{11}(\delta) + \frac{\phi^T(z)}{x} \mathbf{d}_{12}^T(\delta) \right] \left[\tau - \mathbf{F}_\theta(\dot{\theta}, \delta, \dot{\delta}) \right] \left[\mathbf{d}_{12}(\delta) + \frac{\phi^T(z)}{x} \mathbf{D}_{22}(\delta) \right] \left[\mathbf{F}_\delta(\dot{\theta}, \delta) + \mathbf{K}\, \delta_i \right] \quad \ldots\ldots (4.22)$$

The input-output linearizing control was computed [19] as:

$$\tau = \mathbf{F}_\theta(\dot{\theta}, \delta, \dot{\delta}) + \frac{1}{d_{11}(\delta) + \frac{\phi^T(z)}{x} \mathbf{d}_{12}^T(\delta)} \times \left[\ddot{\theta} + \left(\mathbf{d}_{12}(\delta) + \frac{\phi^T(z)}{x} \mathbf{D}_{22}(\delta) \right) \left(\mathbf{F}_\delta(\dot{\theta}, \delta) + \mathbf{K}\, \delta_i \right) \right] = \tau^* \left(\ddot{\theta}, \dot{\theta}, \delta, \dot{\delta} \right)$$

…… (4.23)

Under the above control law, the system equations in the new coordinates (y, δ) become, [19] illustrated as:

$$\ddot{\delta} = -\frac{\mathbf{M}_{\delta\delta}^{-1}}{\mathbf{\Gamma}(x)} \left[\mathbf{m}_{\theta\delta}^T \ddot{\theta} + \mathbf{F}_\delta(\dot{\theta}, \delta) + \mathbf{K}\, \delta_i \right] \quad \ldots\ldots (4.23)$$

$$\mathbf{\Gamma}(x) = 1 - \frac{\phi^T(z)}{x} \mathbf{M}_{\delta\delta}^{-1} \mathbf{m}_{\theta\delta}^T \quad \ldots\ldots (4.24)$$

The stability of the sink, i.e. of the flexible equations, has to be investigated with respect to the parameter $\bar{x} \in [0, l]$. This eventually determines the range along the link that's dynamic behaviour can be stiffened. Restricting the study to a local analysis around a given arm configuration, the zero dynamics was described by the relation [19]:

$$\ddot{\delta} = -\frac{M_{\delta\delta}^T}{\mathbf{\Gamma}(x)} \left[K\, \delta_i \right] \quad \ldots\ldots (4.25)$$

The sign of the scalar function $\Gamma(x)$ plays a crucial role in the evaluation of the stability properties. Note that $\Gamma(0)=1$, from which the stability of the join-based design is again implied. This suggests seeking that the value $\bar{x}$ at which Γ vanishes for the first time. Then, choosing as output a point on the arm at a location x in the range $[0,\bar{x})$ guarantees a stable tracking design.

4.7. Computer Programming of Control System

As state earlier, the programming was done with ***MatLab 6.5.*** The function ***Jtraj*** which was presented by [40], provides the time history of position, velocity, and acceleration for rigid motion of arm. This function is flexible to find the desired trajectory. In the first step in the control algorithm as shown in figure (4-3), the availability of using many initial conditions to cover all the cases of motion of robot arm with any time distribution. The functions δ,ϕ were called to find flexible coordinates acceleration, and use this acceleration to find the desired flexible modes, and to find the open loop torque as shown in figure (4-4). The simulation is done after the torque input was calculated to find the joint error, and the (PD) controller is shown in figure (4-5).

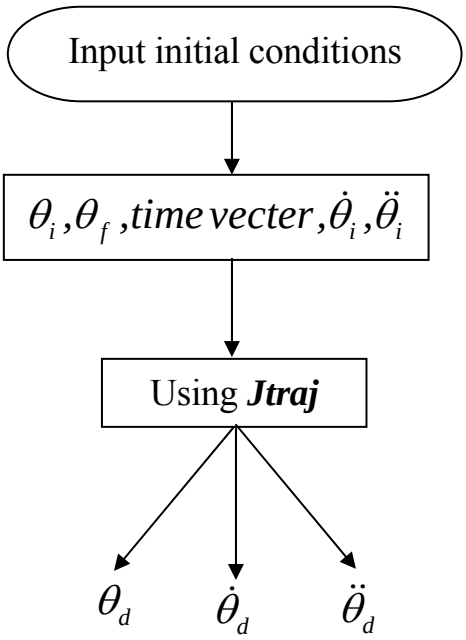

Figure (4-3) using function ***Jtraj*** .

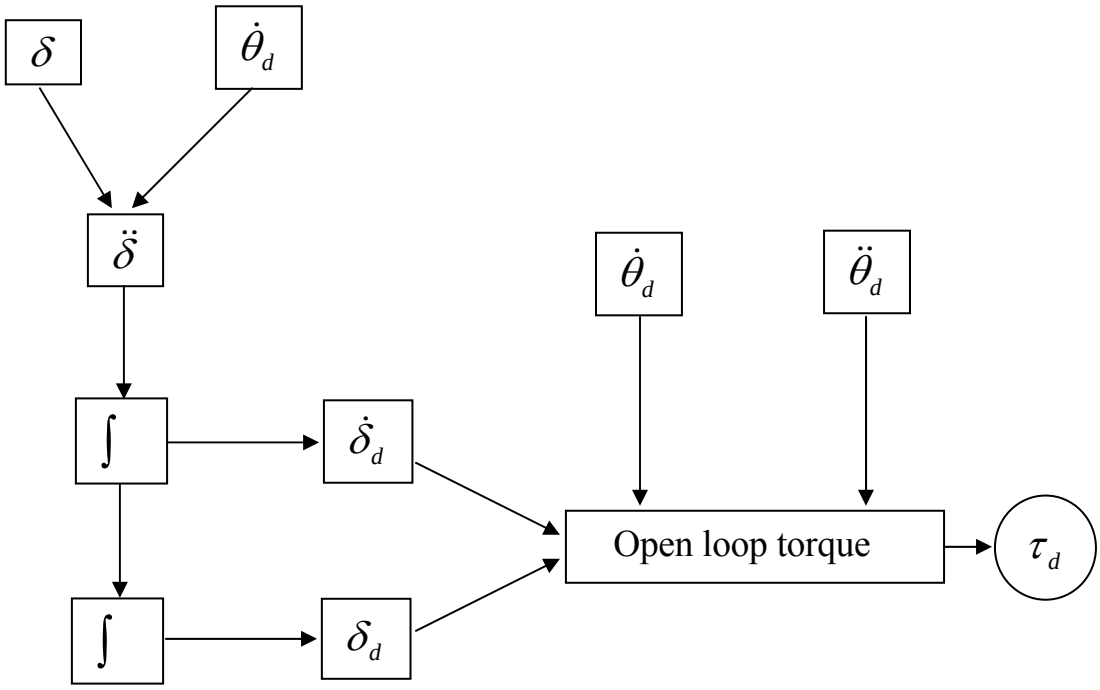

Figure (4-4) find open loop torque.

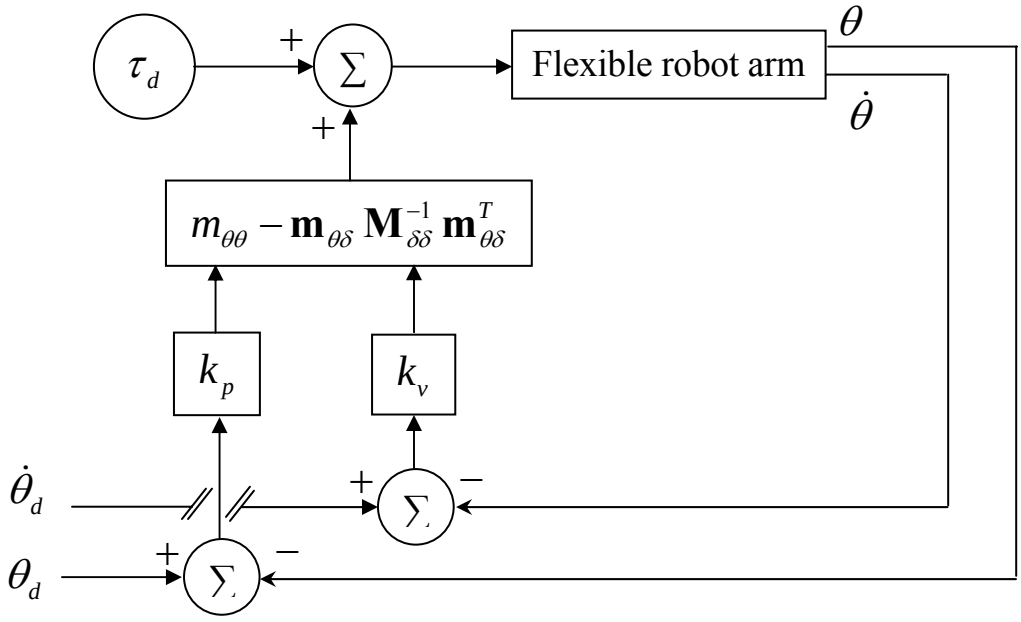

Figure (4-5) (PD) controller.

4.8. Verification Case Study

The dynamic model which is in the verification of the modeling in chapter three was also used in this chapter to verify the control algorithm for flexible robot arm, the experimental results presented work by Mehrdad M. [8] was also based on inversion control with (PD)controller, the results obtained is shown below :

(a) (b)

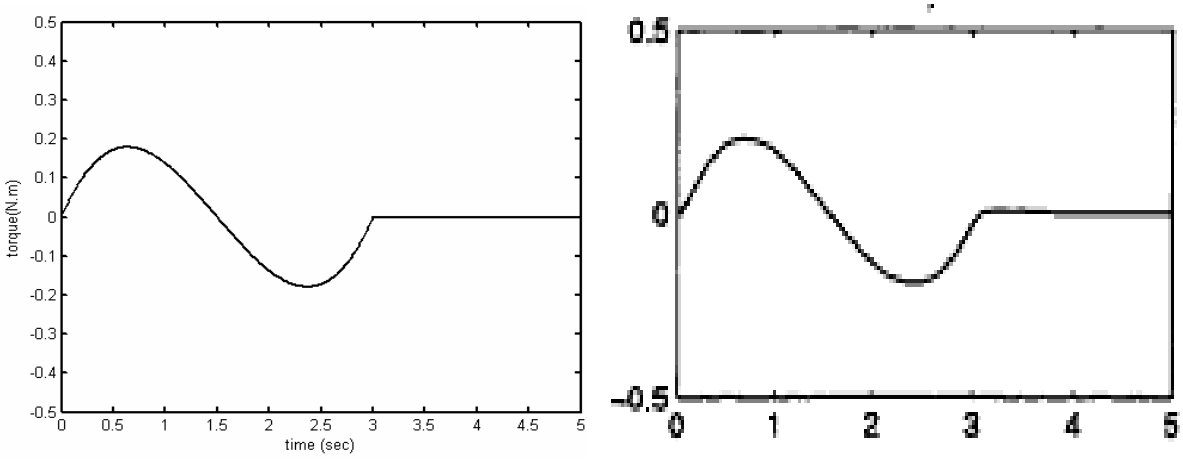

Figure (4-3) torque input:

(a) Present work, (b) Presented by Mehrdad M. [8].

(a) (b)

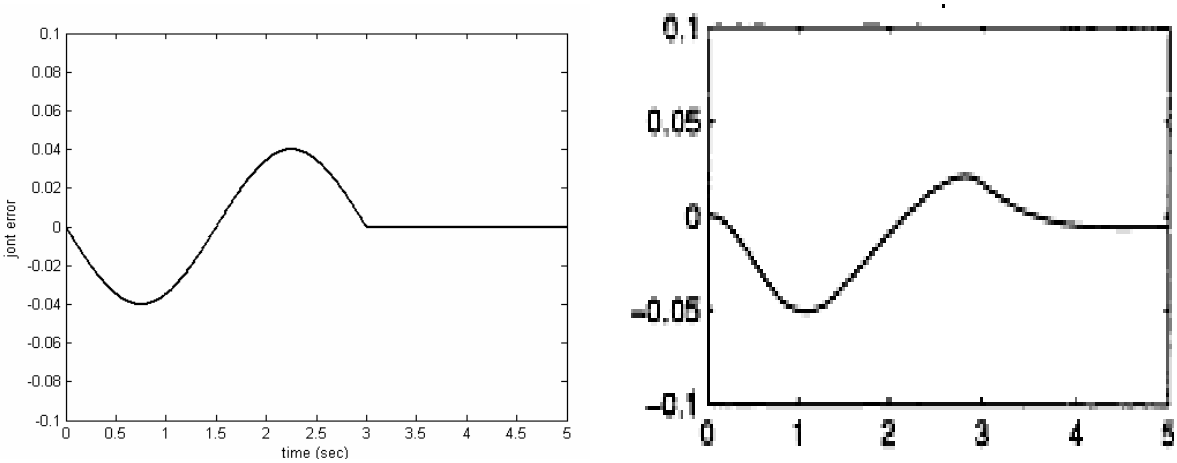

Figure (4-4) joint error:

(a) Present work, (b) Presented by Mehrdad M. [8].

Good agreement had been shown for torque input and joint error for the specified robot.

4.9. Summary and Conclusion

A technique based on inverse dynamics has been used to find the joint torques required to move the end point of flexible link through specified trajectories. The proposed approach takes into account the non-causality of such systems in the solution procedure. Results illustrate the non-causal nature of the inverse dynamic of flexible robot arm. It was shown that by applying the computed joint torques obtained from the proposed approach, the tracking errors were reduced significantly. The technique used in this work can be used to find the input torques for complicated flexible robot (multi-link flexible manipulator).The control system was compared with another work to check the validity of this system. Also the system works with the point along the link to investigate for stiffening the motion of the suitable point along the arm. The computed joint torques can be used as feedforward controls which minimize the work of the feedback controller needed to compensate modeling errors.

5

Chapter Five

Results and Discussion

RESULTS AND DISCUSSION

The results obtained in this work represent the effects of different parameters on the dynamic model and trajectory control of flexible arm for many cases. The dynamic model and the control algorithm which were verified in chapters three and four will be to show the effect of changing some parameters of link on the dynamic modeling and trajectory control of flexible robot. A single-link flexible manipulator and two links (rigid-flexible) manipulator are discussed in this chapter; the data of links and the parameters of all cases are shown in appendix (A).

5.1. Modeling of Flexible Robot Arm

The results of dynamic modeling of flexible robot arm were discussed, and it presented in two topics; single flexible link with clamped-free B.C.'s and clamped-mass B.C.'s as follows

5.1.1. Clamped-Free Boundary Conditions

The mode shapes for this type of link are shown in figure (5-1), where the basis functions $\phi_i(x)$ are specified in advance, therefore only the generalized coordinates are time varying. This basis functions the kinematics B.C.'s, from linearly independent set, and resemble the actual mode shapes. Two cases for this B.C.'s are derived to show the effects of the cross sectional area (rectangular or triangular) on flexibility of the flexible link, and three types of material are chosen to show the modulus of elasticity effect. Moreover the elastic degrees of freedom chosen are highly effective on the behavior of the flexible link with different number of flexible coordinates.

Result of natural frequency of case 1was presented in appendix A. These results appeared the effect of modulus of elasticity and the type of cross section.

The natural frequency is increased due to the change the cross section area from rectangular to triangular shape. The percentage of increasing is about 63.3 %, and this is the same for case 2. This percentage is the same for all the types of materials (different value of E). On the other side the natural frequencies have extrusive relation with the modulus of elasticity, the percentage for increasing natural frequencies with modulus of elasticity shown in table (5-1) were the percentage is chosen w.r.t. E_{Al}.

Table (5-1) percentage relation between (ω, E).

E %	46.7 %	160 %
ω_1 %	2.4 %	9.8 %
ω_2 %	6.3 %	24.6 %
ω_3 %	2.46 %	4.54 %

The tip-deflection of the link is very important property, it is clear that the most robots are doing their works by end-effector point, especially for the accurate applications. This deflection must be estimating, here was calculated by using the function $\boldsymbol{W}$ which is described in chapter three, the tip-deflection of the case 1, which is classified according to the type of material, the tip-deflection of the Flexible link with (Al) material shown in figure (5-2). For flexible link with (Ti) material is shown in figure (5-3), and for flexible link with steel material is shown in figure (5-4). The tip-deflection of the case 2, which is also classified according to the type of material, the tip-deflection of the Flexible link with (Al) shown in figure (5-5), for flexible link with (Ti) material is shown in figure (5-6), for flexible link with steel material is shown in figure (5-7). All figures are presented with two modes (a), and three modes (b) approximation. Max tip-deflection is shown in figures (5-8), is estimated for two cases with steel material, and by using two and three modes approximation.

This tip-deflection was estimated in the time which is chosen to service the operation of robots and it's chosen as two seconds because link is lightweight.

From figures (5-2) to (5-7), it is clear that the tip-deflection is highly nonlinear and the magnitude of it is changed in small time range hence the tip-deflection is estimating in very little time step (0.001sec) to find all the changes of tip-deflection in the time of motion, the difference between two and three modes approximation showed that the tip-deflection with two modes is greater than with three modes approximation, this is due to the coupling between modes which is for two modes produced tip-deflection greater from three modes. On the other hand the tip-deflection of the link with rectangular cross section is greater than from the link with triangular cross section, and this due to the flexibility of the link with rectangular cross section is greater than triangular.

Figure (5-8) shows the max tip-deflection; from this figure max deflection have inverse proportional with the dimension of cross sectional area, and the moment of inertia. The percentage change in E is shown in these figures (5-8a) and (5-8b) and the some percentage change for max tip-deflection is shown in table (5-2) below. The shape of tip-deflection with time is produced from the coupling between the two or three flexible modes (different natural frequency); also it is shown that in the present of link flexibility the tip points of the links oscillate undesirably which causes difficulties in control of flexible manipulators.

Table (5-2) percentage change (E, max Tip-deflection).

E %	-10 %	-30 %
Case 1, Rec. 2 modes	6.9 %	20.69 %
Case 1, Rec. 3 modes	1.56 %	17.97 %
Case 2, Tri. 2 modes	4.56 %	16.28 %
Case 2, Tri. 3 modes	7.94 %	19.5 %

5.1.2. Clamped-Mass Boundary conditions

Because the effect of the payload on the B.C.'s the solutions of the transcendental characteristic equation is changed with any change in the value of

payload added to the end of the flexible link. The changing in the mode shapes of the flexible link with various value of payload is shown in figures (5-9) to (5-11). Where the figure (5-9) present the comparison between free end and different values of payload on the first mode shape, figure (5-10) present the comparison between free end and different values of payload on the second mode shape ,and figure (5-11) presents the comparison between free end and different values of payload on the third mode shape. From aforementioned figures it is clear that the value of mode shapes decreasing especially in the tip-point of the link $\phi_i(l)$ with increase the payload, and this result from the decreases of the eigen modes λ_i which is calculated from the transcendental characteristic equation. This due to constraining which it comes from the addition of payload at the end point of link. Table (5-3) shows the effect of doubling m_p payload on the eigen modes λ, and in this table the value of eigen modes are compared with the free end beam in order to show the effect of payload, then eigen modes have inverse proportional with the payload.

Table (5-3) effect of payload on eigen modes values.

$m_p\ (kg)$	0.05	0.15
λ_1	-9.87%	-20.9%
λ_2	-7.24%	-11.53%
λ_3	-5.75%	-8.07%

The tip-deflection of the flexible link with various values of payload is shown in figures (5-12) to (5-14), the tip-deflection is also presented with two modes (a) and three modes (b) approximation. From these figures (5-12), (5-13), and (5-14), it is clear that the tip-deflection have an extrusive proportion with payload. The shape of this deflection was due to constrained motion of the flexible link. The payload cause the natural frequencies of the flexible link decreased due to increasing in the kinetic energy of the manipulator. The time of

estimating tip-deflection was chosen to be as (3 sec), to decrease the velocity of motion of the link for any application, decreasing velocity is very important due to avoid the resonance because the natural frequencies of the system is small.

Figure (5-15) shows max tip-deflection of the link with various values of payload. This figure shows that the values of max tip-deflection have an extrusive proportion with payload. The percentage of increasing max tip-deflection by doubling payload shown in table (5-4); this percentage was chosen with respect to the payload (0.05 kg):

Table (5-4) percentage change for max tip-Def. with payload.

max tip-Def.	Rec. 2 modes	Rec. 3 modes	Tri. 2 modes	Tri. 3 modes
0.1 kg	38.5 %	25 %	35.3 %	21.2 %
0.15 kg	70.3 %	44.2 %	61.7 %	39.4 %

5.2. Trajectory Control of Flexible Robot Arm

The inversion control law has been simulated using the single-link flexible, and two links (rigid-flexible) manipulator. The control law was verified in chapter four, by comparison the results with an experimental results presented by Mehrdad [8]. The control law was used with the dynamic models which were discussed in the previous section.

5.2.1. Single Link Flexible Robot

The desired trajectory specifies an angular motion from initial to final position and this trajectory was found by using function (***Jtraj***) [40]. The angular position, velocity, and acceleration profile $\theta_d, \dot{\theta}_d, \ddot{\theta}_d$ are shown in figures (5-16) to (5-21), where figure (5-16)(a), show the angular position profile for time two seconds, and figure (5-16)(b) show the angular position profile for time three seconds. The angular velocity profile shown in figure (5-17)(a) with two seconds, and in figure (5-17) (b) for three seconds. And the angular acceleration distribution had shown in figure (5-18) (a), and (5-18) (b). The simulations run for

two and three seconds due to the run time for flexible link with payload is greater than time without payload, and the sampling time of one millisecond. This sampling time is estimated to be long enough to perform in real-time the computations required by the complex of the control law.

The conventional PD joint controller was used first with clamped-free flexible arm from case 1; was tested for all types of material, and with two and three modes. Figure (5-19) shows the simulated and desired trajectories for the clamped–free link with (Al) material and was classified in two parts (a) and (b) to show difference between the using, two and three modes in the simulation. Figure (5-20) shows the desired and simulated velocity for this case (case 1(Al)), and figure (5-21) shows the open loop and corrected torques for this case also. The same results were illustrated in figures (5-22) to (5-24) but for the case 1 with (Ti) material, and also the figures (5-22) to (5-27) for the case 1 with steel material. From the figures (5-19) to (5-27) which mentioned earlier it is clear that; there is a steady-state error in the position command produced from using the PD controller and these error produce an error in the velocity profile for the cases, and the torque input is different for these three cases, and the change for each of these cases due to the effect of the mass per unit length on the PD controller which was affected with the dynamic equation (especially with mass matrix) which is configure the value and the shape of the torque input. The classification of the results in clam-free case in two and three modes, to show the effect of coupling between the flexible modes on the behavior of the control system and this important due to the increasing flexible modes increase the validity of the control system.

Figure (5-28) shows the simulation results for case 3, with $m_p = 0.05\,kg$, figure (5-28a) shows the input torque which is produced from the applying of PD controller, (5-28b) shows the joint trajectory error with (0.0015 rad as max. error) with remarkable improvement in the steady state, (5-28c) shows the simulated and desired trajectory, and (5-28d) shows the desired and simulated

velocity profile for this case. Figure (5-29) shows the simulation results for case 3, with $m_p = 0.1kg$ where figure (5-29a) shows the input torque, (5-29b) show the joint trajectory error with (0.0018 rad as max. error),and (5-29c) show the simulated and desired velocity profile, and (5-29d) shows the desired and simulated trajectory for this case . Figure (5-30) also present the same results illustrated in figures (27, and 28) but with payload $m_p = 0.15kg$. From figures (5-28),(5-29), and (5-30) aforementioned earlier , the important features from these figures that the inversion control law have been simulated using two mode models of one-link flexible arm. The doubling value of the load parameter (m_p), some ripples are present in the position joint error. But the achieved result indicates the robustness of the control scheme with respect to these variations. Also the value of the torque input is changing with increasing payload due to the effect on the dynamic model (PD controller). The max joint error was very affected with payload; and the value of it was changed percent as 2 % by double the payload from (0.05 to 0.1) kg, and by 3% when increase the payload to 0.15 kg; and these results shown that the effect of payload on joint error is decreased with increasing the value of payload.

5.2.2. Two Links (Rigid-Flexible) Manipulator

Figure (5-31) show the motion of the two-link (rigid-flexible) robot with time, the two-link is rotate under the conditions (a) $\theta_{1i} = 0, \theta_{2i} = 0, \theta_{1f} = 60^\circ$, $\theta_{2f} = 30^\circ$, and (b) $\theta_{1i} = 0, \theta_{2i} = 0, \theta_{1f} = 60^\circ, \theta_{2f} = 60^\circ$. The simulation of flexible motion is run under the time sampling as (0.1 sec) to approximate the motion of robot, and the simulation was used an active linkages hence the two links move and arrive to the desired point in the same time. Figures (5-32), and (5-33) show the effect of the flexibility of the second link in the (rigid-flexible) manipulator on the X, and Y components for $\theta_{1f} = 60^\circ, \theta_{2f} = 30^\circ$, these figures was drawing using equation (3.33). These figures shows that the end-effector

point vibrate undesirably during the motion of the manipulator. In figure (5-32) the shape of deflection in X component show that the link starting vibrate small and then increased, while in the figure (5-33) the deflection is starting high and then terminate in the final position and these due to the variations of the trajectory of the two link. Figures (5-34) and (5-35) show the effect of the flexibility of the second link in the (rigid-flexible) manipulator of the X, and Y component of the end-effector positions for conditions $\theta_{f1} = 60^{\circ}, \theta_{2f} = 60^{\circ}$, from these figures it is clear that the variations in the X, and Y component varies with the position of the end-effector.

Figure (5-36) shows the simulation results for two-link (rigid-flexible) manipulator with $\theta_{f1} = 60^{\circ}, \theta_{2f} = 30^{\circ}$, conditions and the flexible link under clam-free B.C.'s. The open-loop τ_{OL-PD} control has been evaluated for this case. Figure (5-37) shows the same results with different conditions $\theta_{1f} = 60^{\circ}$, $\theta_{2f} = 60^{\circ}$; by a comparison between figures (5-36) and (5-37) was made in order to see the difference between the two cases. The first max torque input was increased by 49.4 %, and the second max torque input by 96 %. Figure (5-38) shows the simulation results of the two-link robot, for the second link under clam-mass B.C.'s. The torques input for the two links was shown in the figure, and these torques increased when comparison with clam-free B.C.'s due to constraining of the system (addition of the payload); where the first max torque input is increased by 159.3 %, and the second max torque input by 115.4 %.

Figure (5-39) show the torque input for the PD controller for a point along the clam-free arm which is from case 1 (steel), in order to implement the inversion-based control for point along the arm, there are essential in determining the range of points that leads to stable design, the torque is determining at the value of the $x = 0.72\ \mathrm{m}$ zeroing the $\mathbf{\Gamma}(x)$ equation (4.24). On the basis of the previous analysis the torque input is chosen as $x = 0.87\ \mathrm{m}$, the figure (5-40)

show this torque input for the case 3,with $m_p = 0.05kg$, and the evidence of the control effort after time =3 sec necessary to maintain the output at the final target.

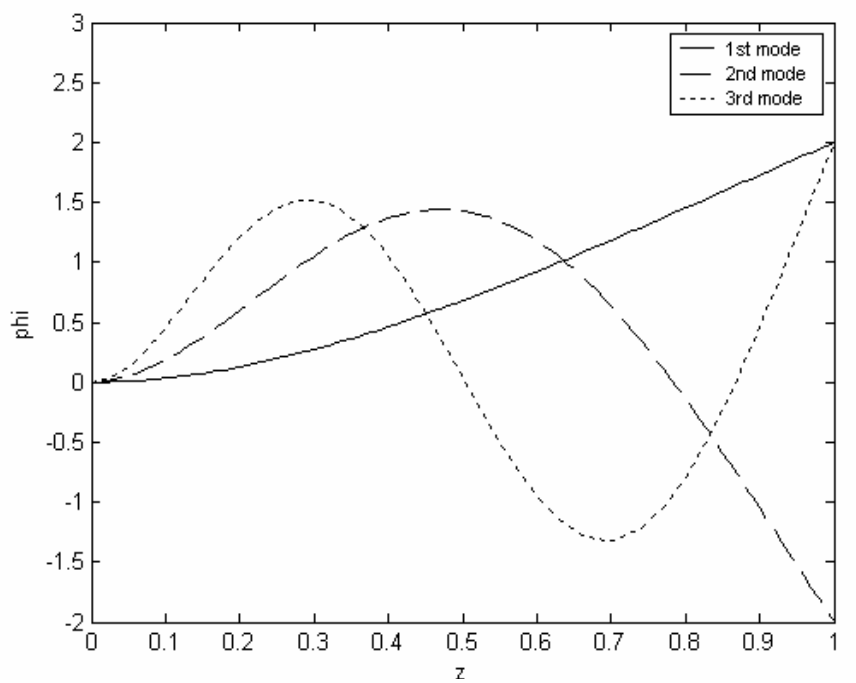

Figure (5-1). The first three mode shapes of clam-free link.

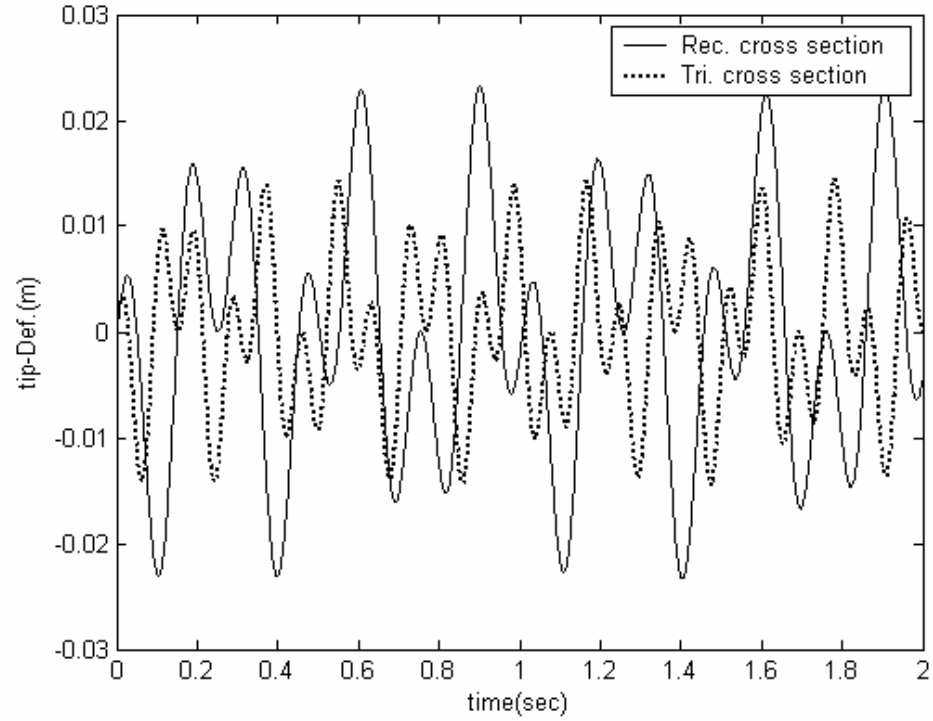

Figure (5-2a). Tip-deflection of flexible link for case 1, (Al), two modes.

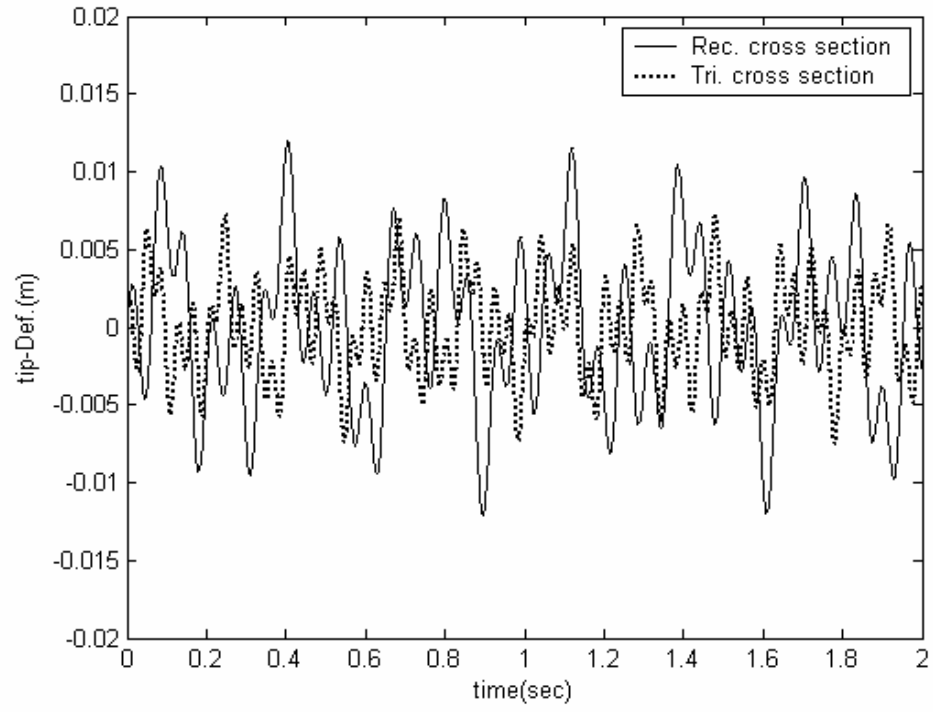

Figure (5-2b). Tip-deflection of flexible link for case 1, (Al), three modes.

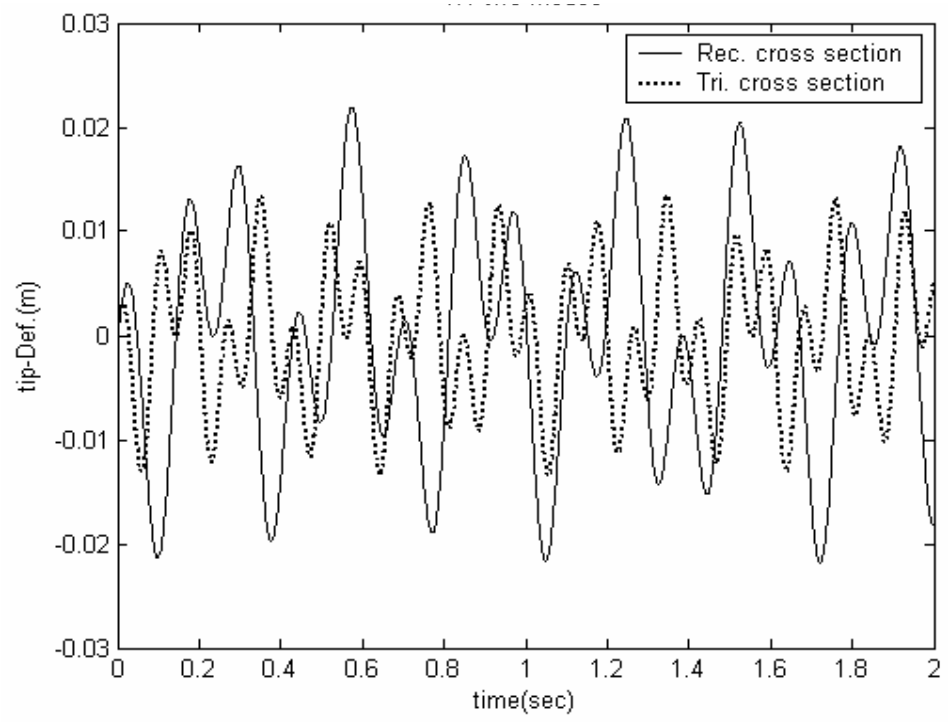

Figure (5-3a). Tip-deflection of flexible link for case 1, (Ti), two modes.

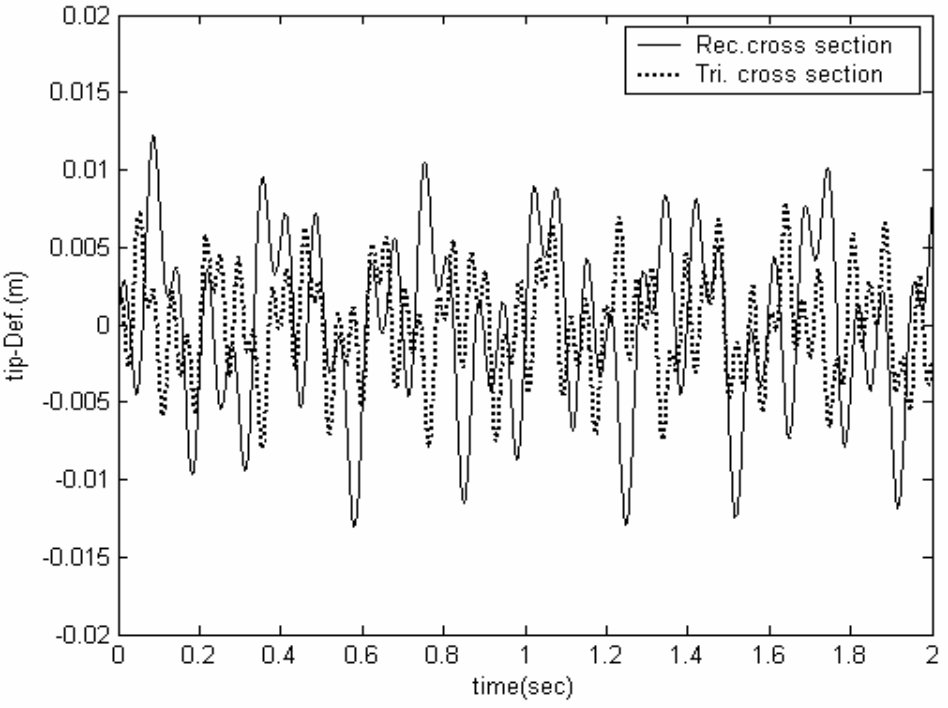

Figure (5-3b). Tip-deflection of flexible link for case 1, (Ti), three modes.

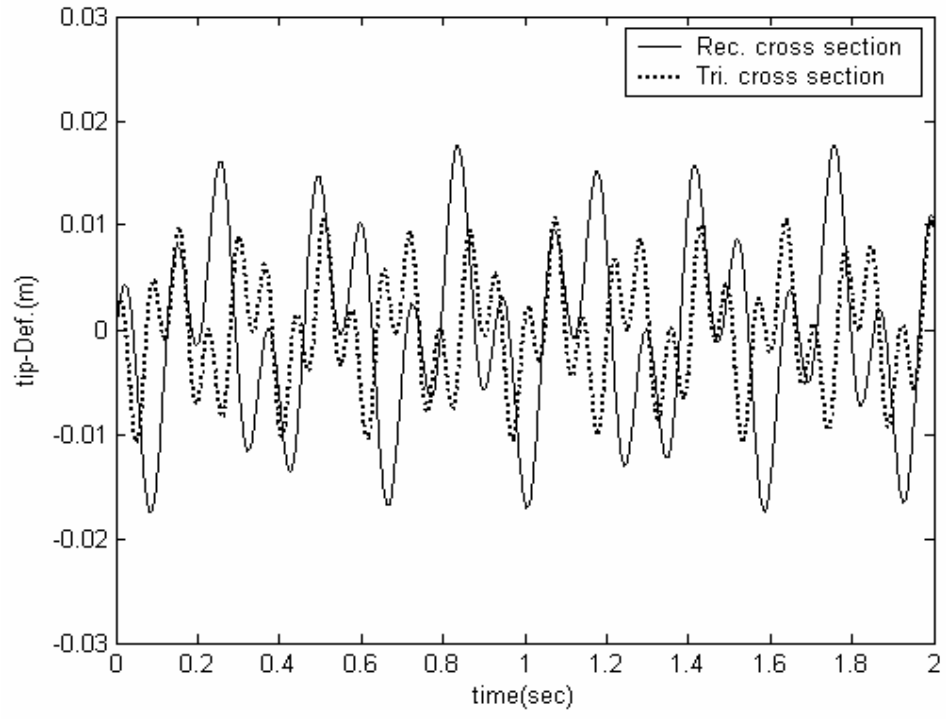

Figure (5-4a). Tip-deflection of flexible link for case 1, (steel), two modes.

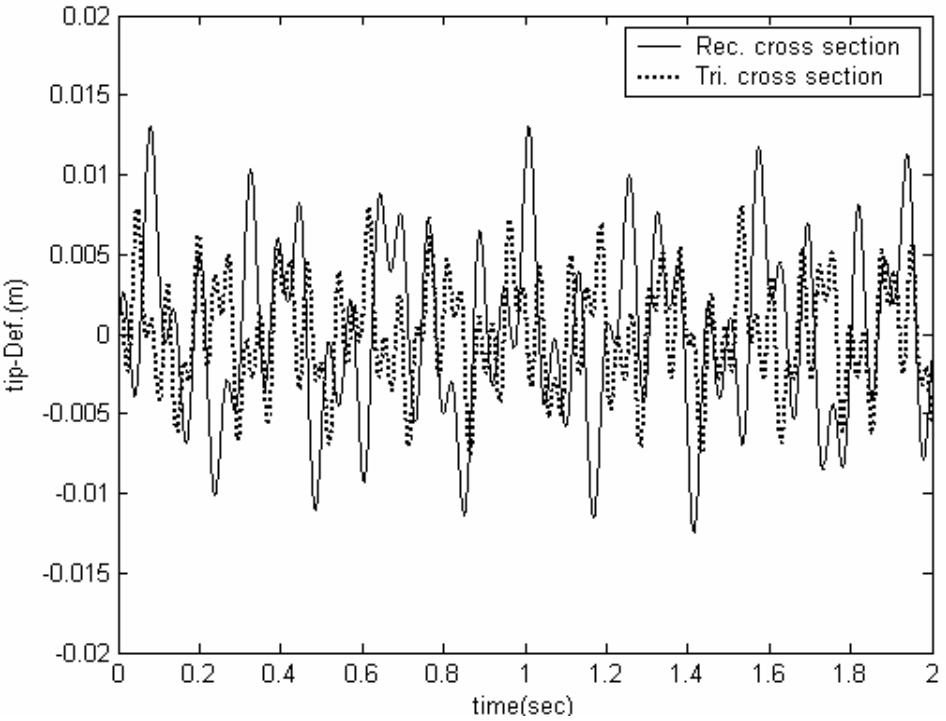

Figure (5-4b). Tip-deflection of flexible link for case 1, (steel), three modes.

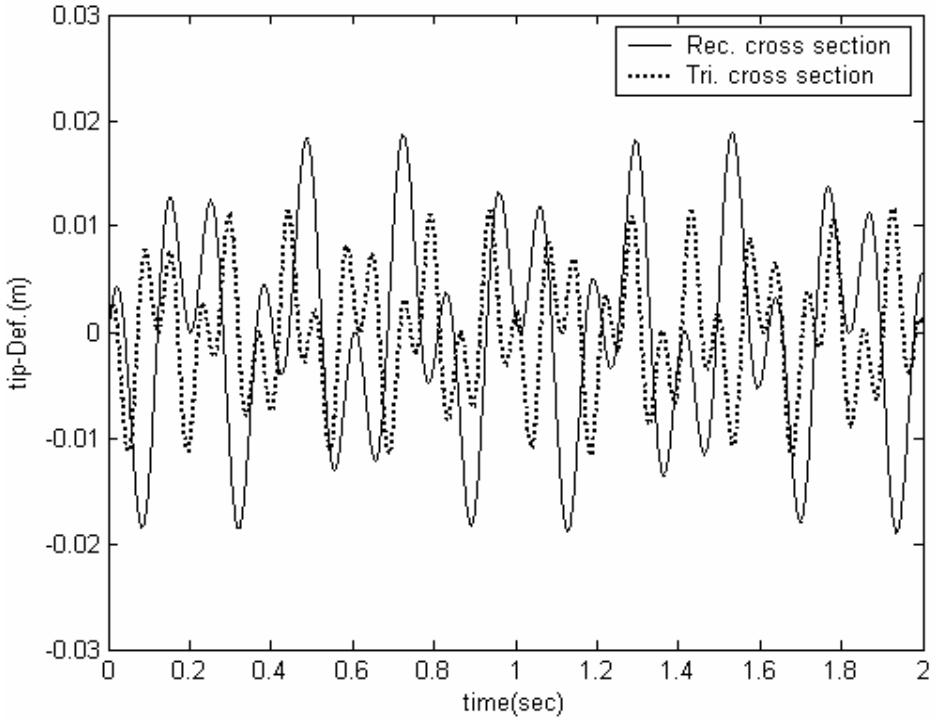

Figure (5-5a). Tip-deflection of flexible link for case 2, (Al), two modes.

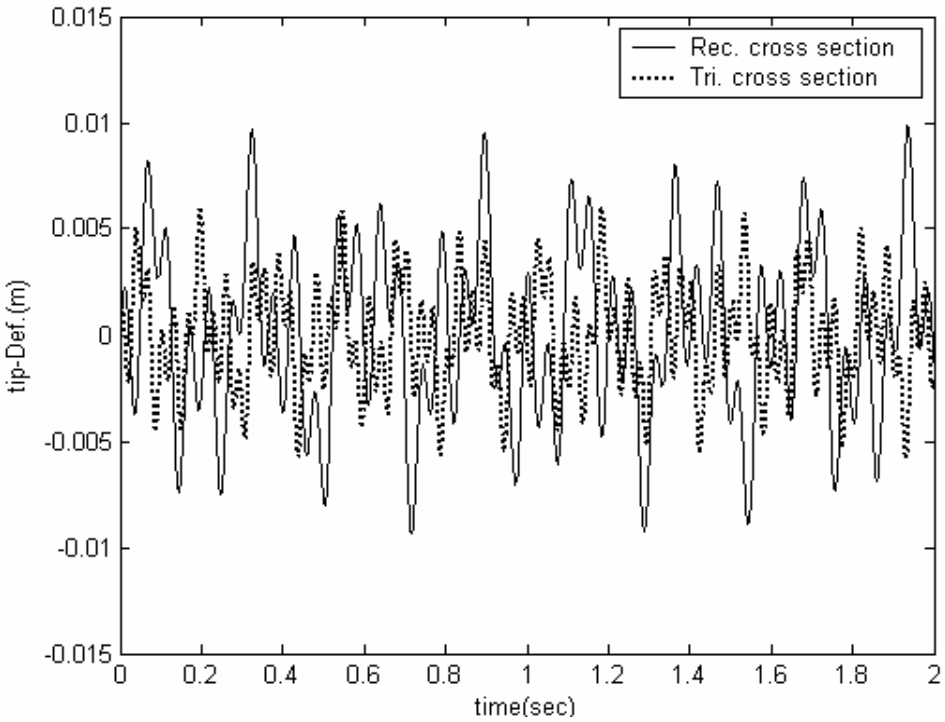

Figure (5-5b). Tip-deflection of flexible link for case 2, (Al), three modes.

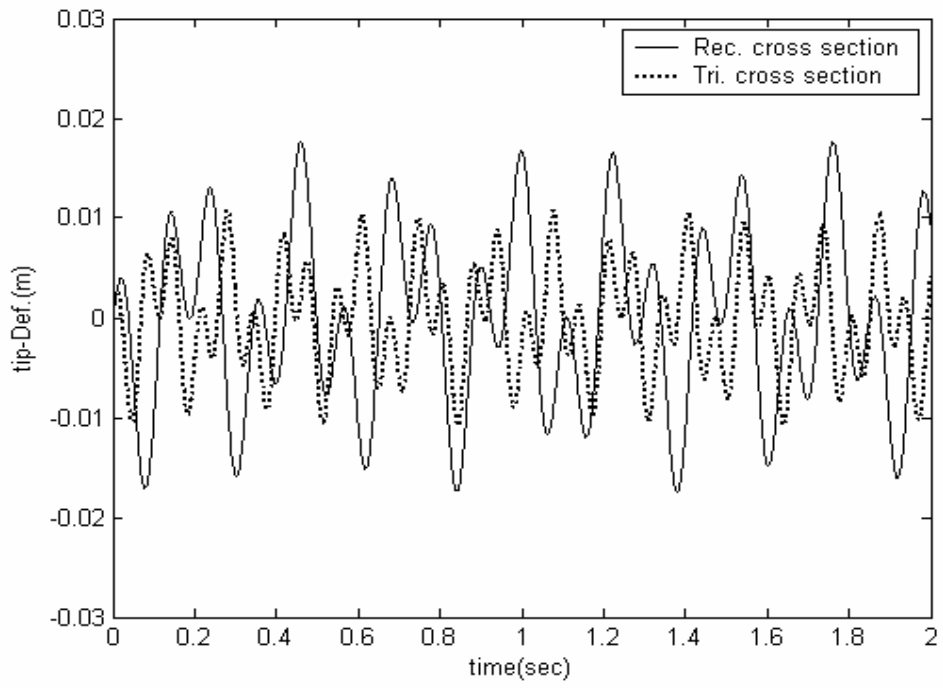

Figure (5-6a). Tip-deflection of flexible link for case 2, (Ti), two modes.

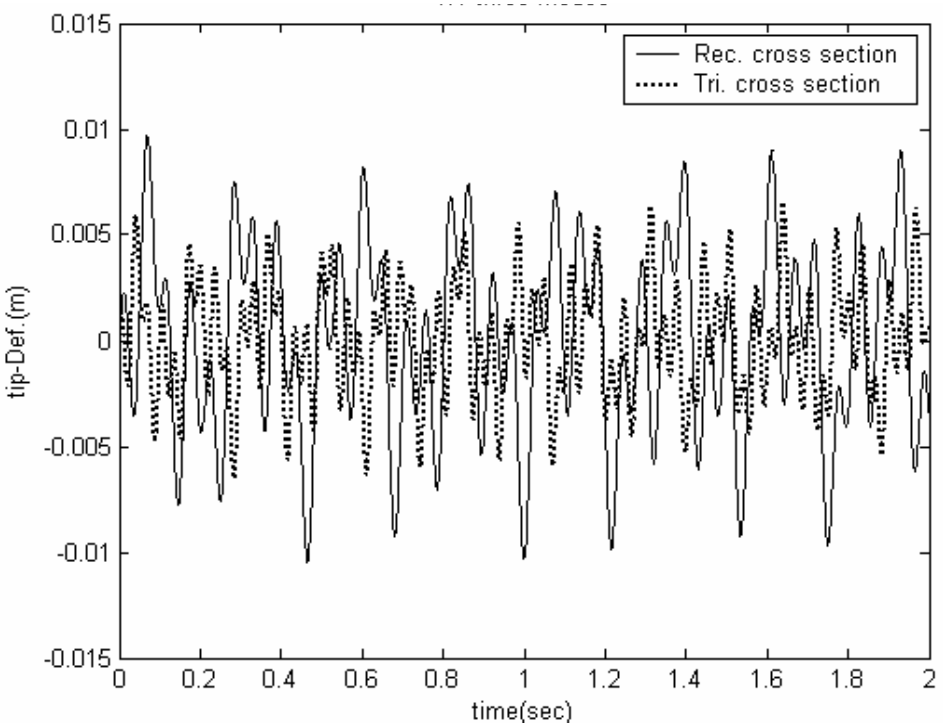

Figure (5-6b). Tip-deflection of flexible link for case 2, (Ti), three modes.

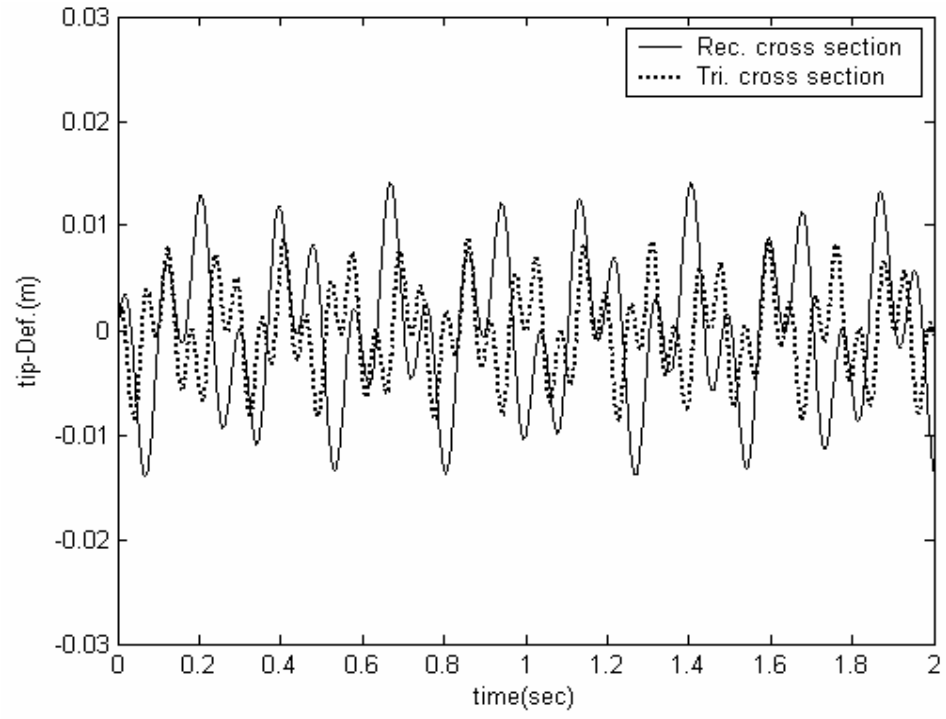

Figure (5-7a). Tip-deflection of flexible link for case 2, (steel), two modes.

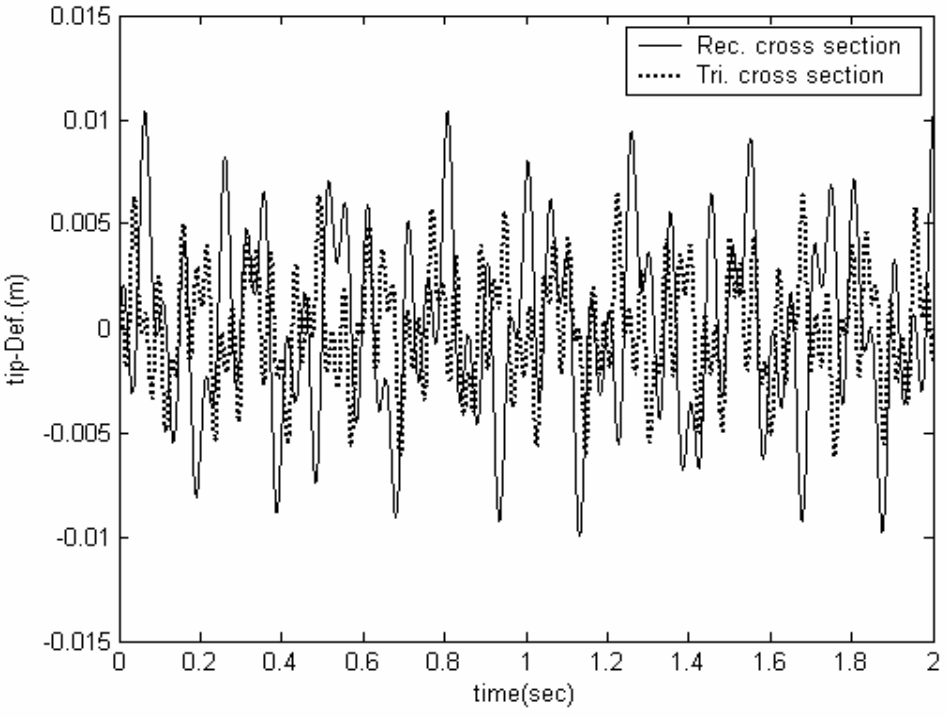

Figure (5-7b). Tip-deflection of flexible link for case 2, (steel), three modes.

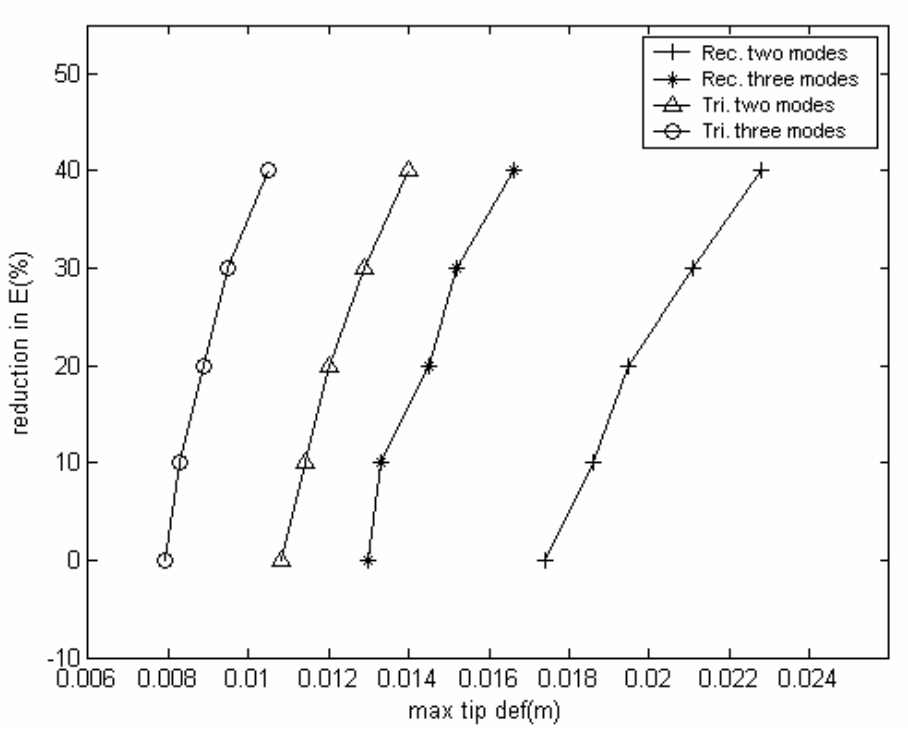

Figure (5-8a). Effect of reduction in (E) on the Max. Tip-deflection (steel, clam-free, case 1)

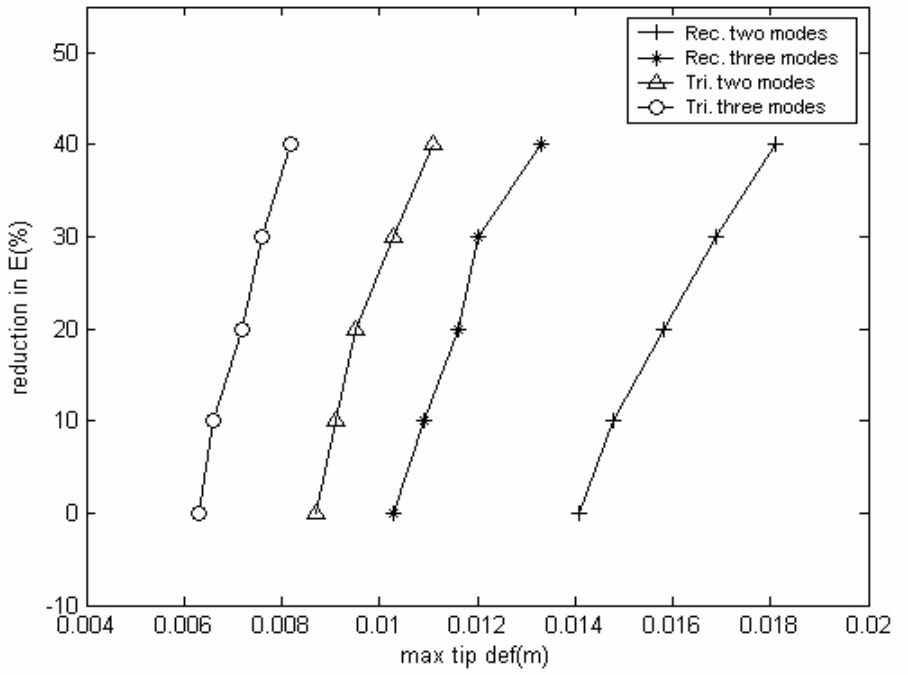

Figure (5-8b). Effect of reduction in (E) on the Max. Tip-deflection (steel, clam-free, case 2)

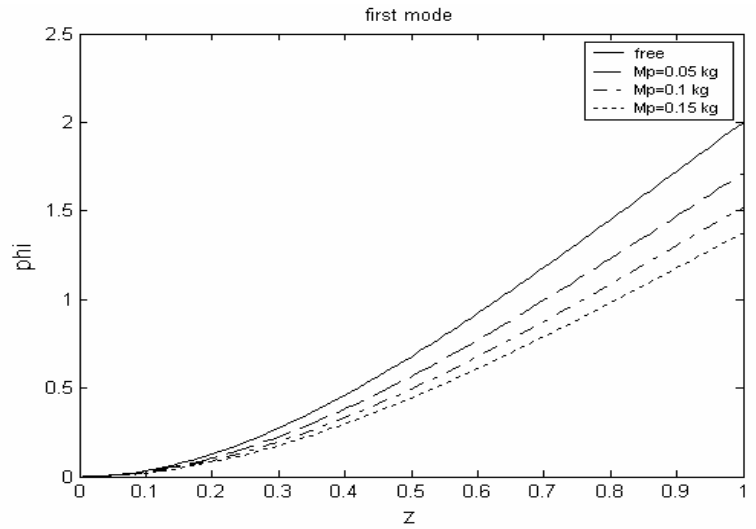

Figure (5-9). Variation first flexible mode with payload.

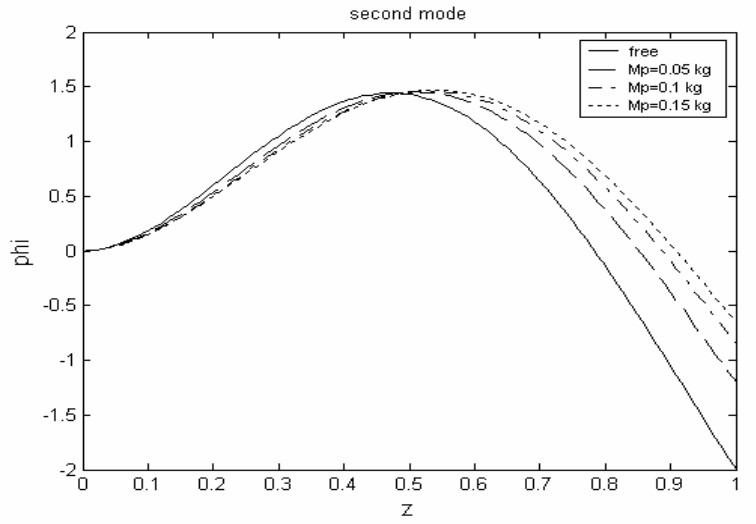

Figure (5-10). Variation second flexible mode with payload.

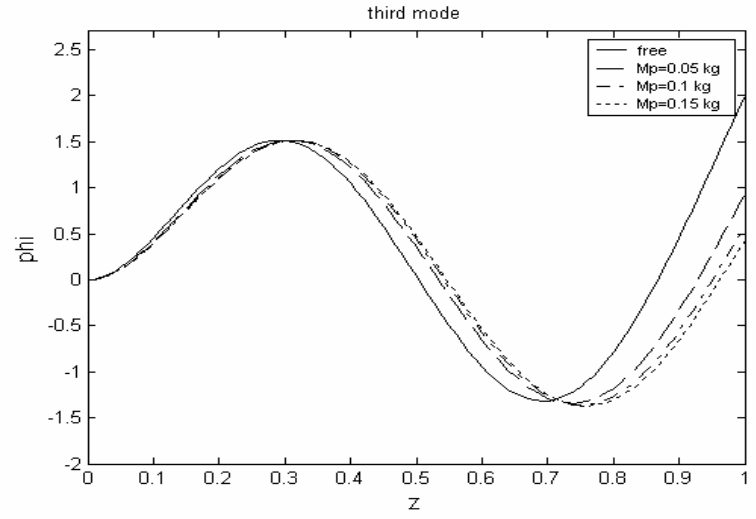

Figure (5-11). Variation third flexible mode with payload.

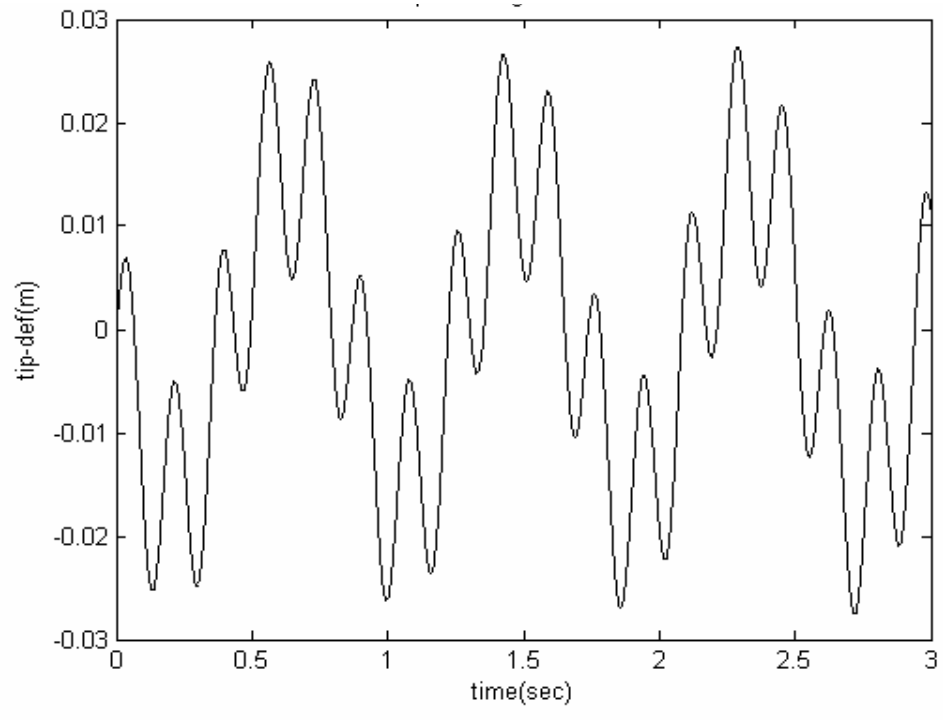

Figure (5-12a). Tip-deflection of flexible link with payload ($m_p = 0.05\,kg$), two modes.

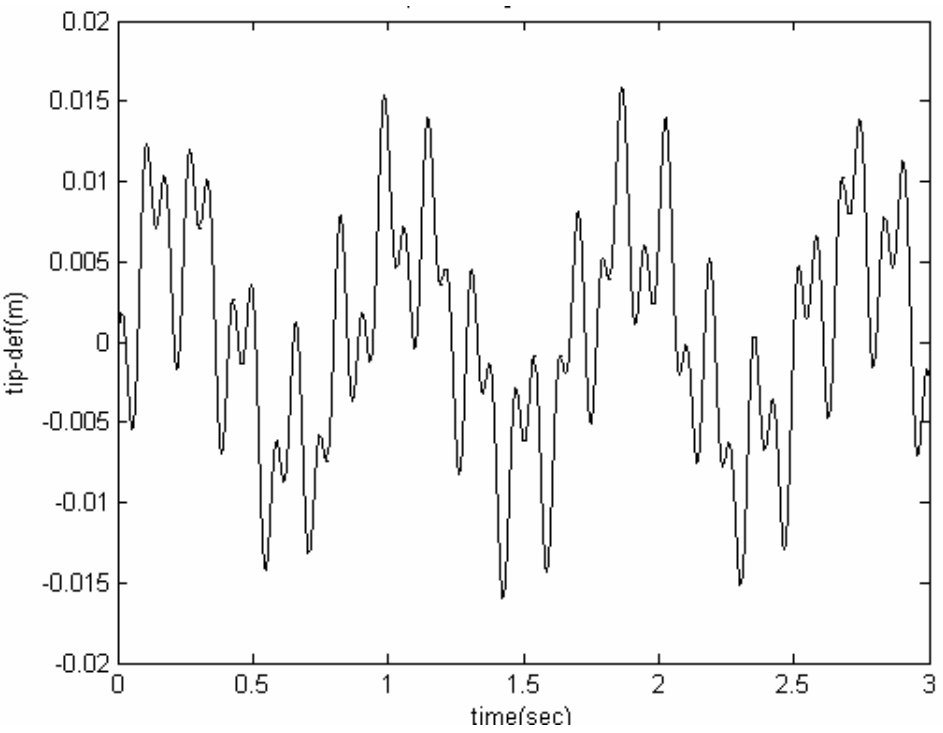

Figure (5-12b). Tip-deflection of flexible link with payload ($m_p = 0.05\,kg$), three modes.

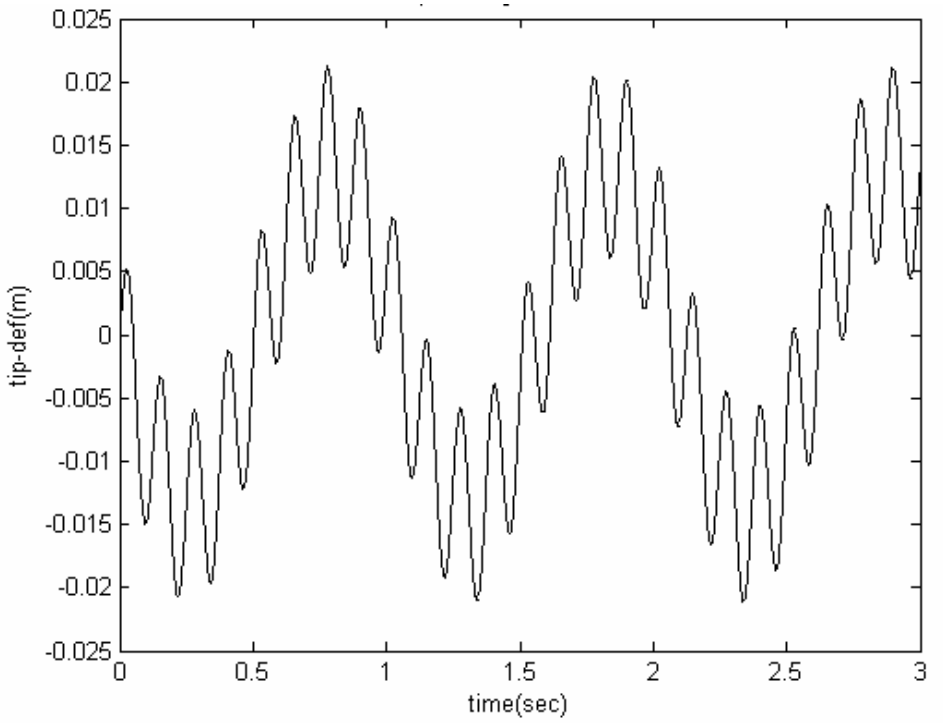

Figure (5-13a). Tip-deflection of flexible link with payload ($m_p = 0.1kg$), two modes.

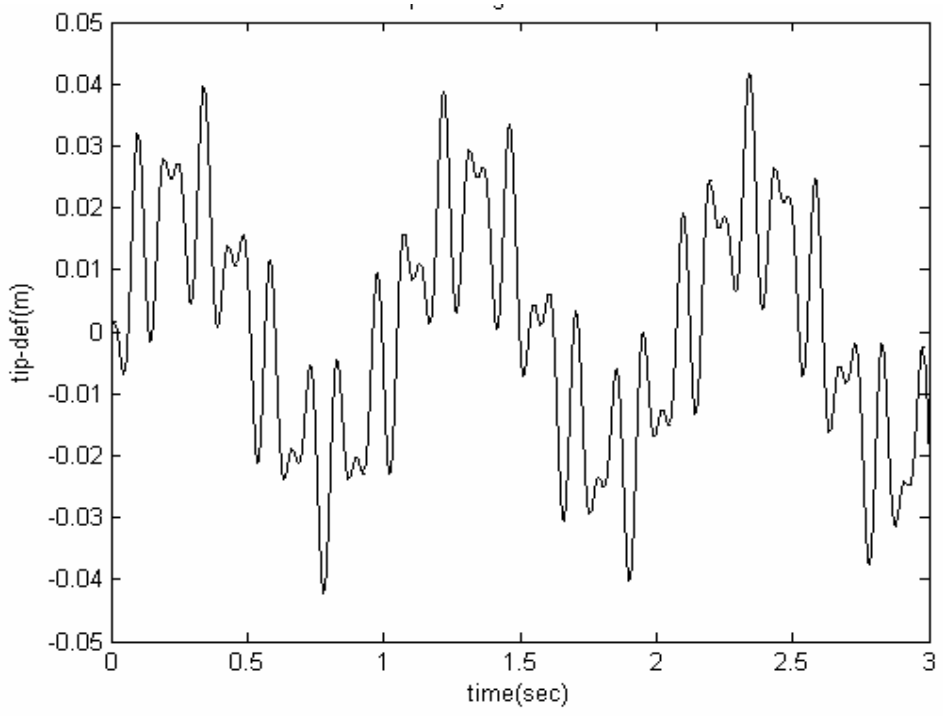

Figure (5-13b). Tip-deflection of flexible link with payload ($m_p = 0.1kg$), three modes.

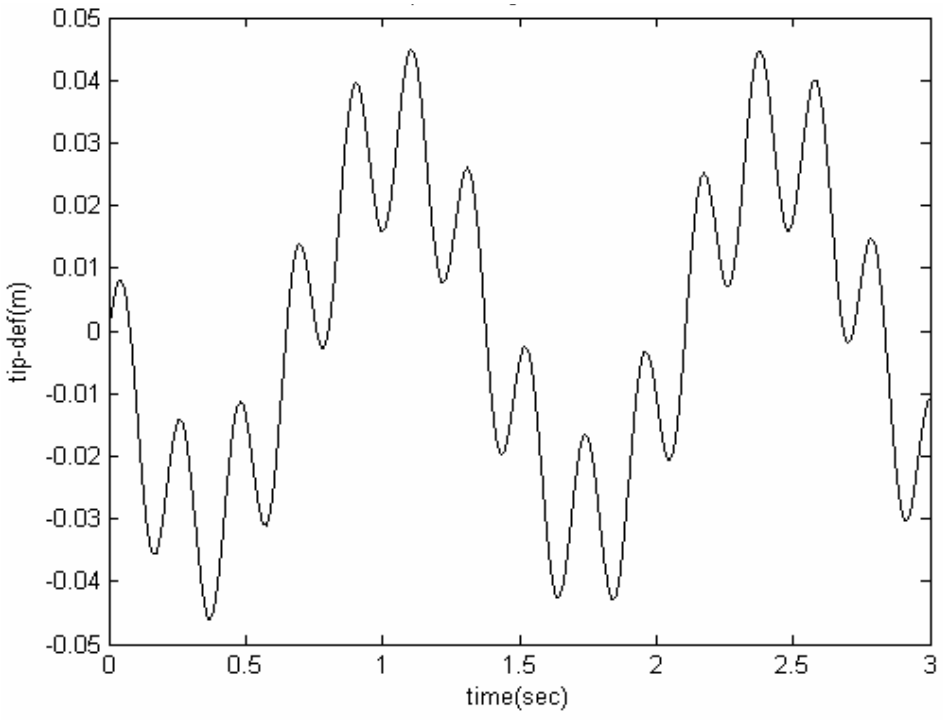

Figure (5-14a). Tip-deflection of flexible link with payload ($m_p = 0.15\,kg$), two modes.

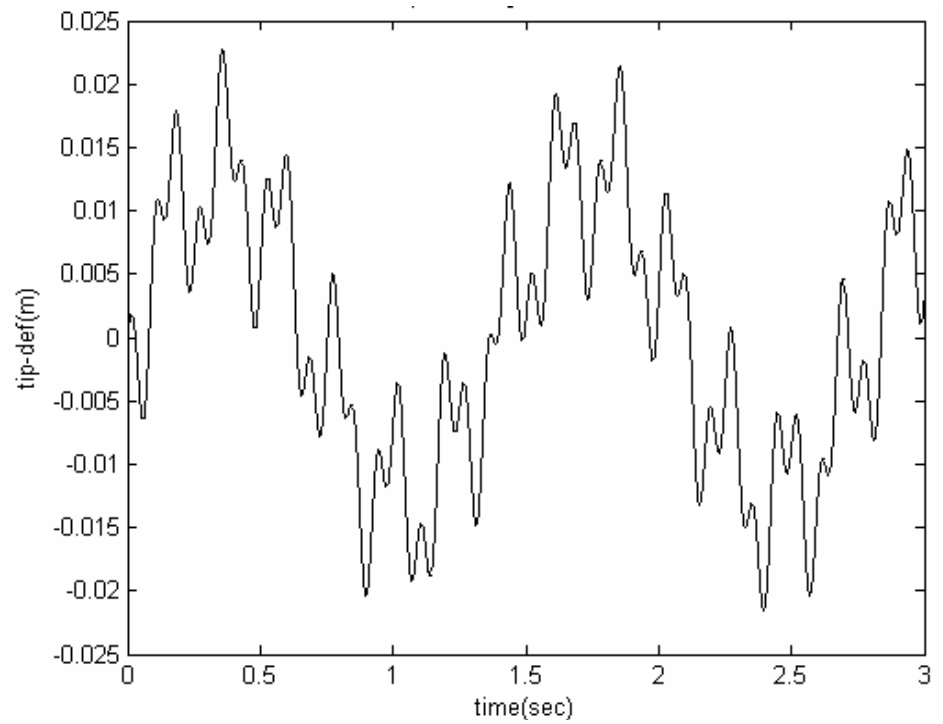

Figure (5-14b). Tip-deflection of flexible link with payload ($m_p = 0.15\,kg$), three modes.

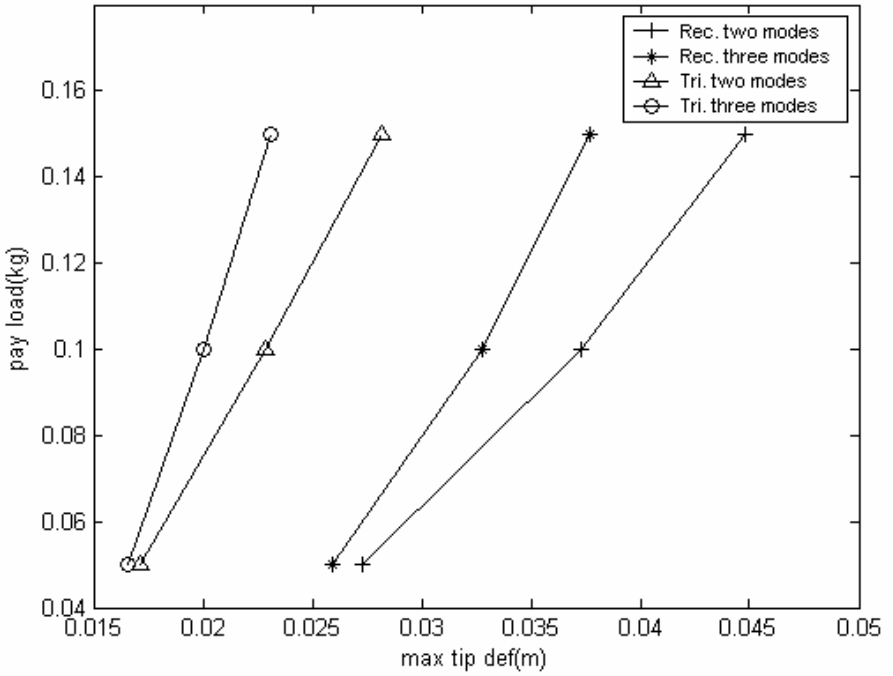

Figure (5-15). Max. tip-deflection versus with payload
For steel link case1&2

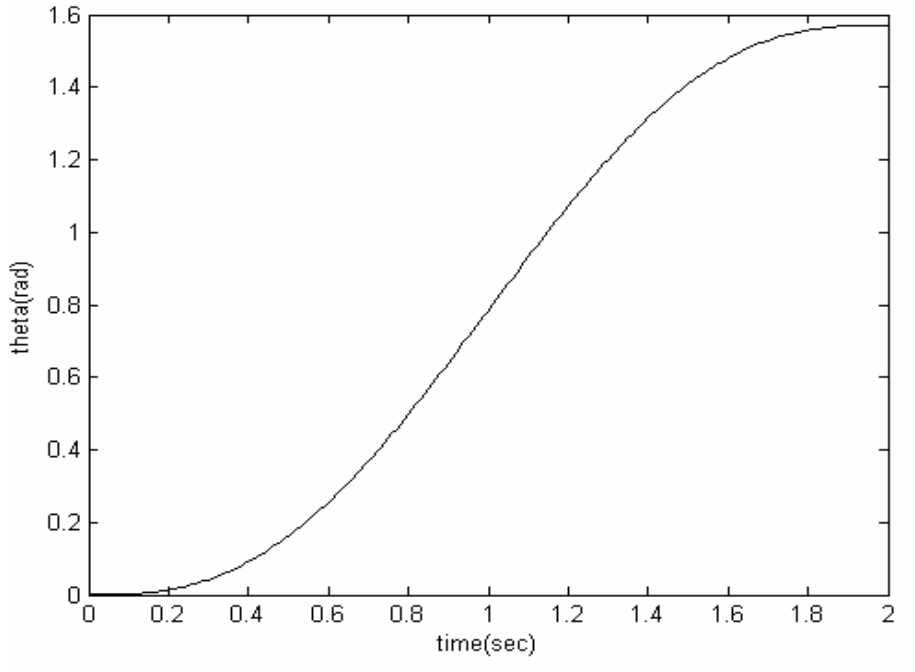

Figure (5-16a). Desired angular position time 2 sec.

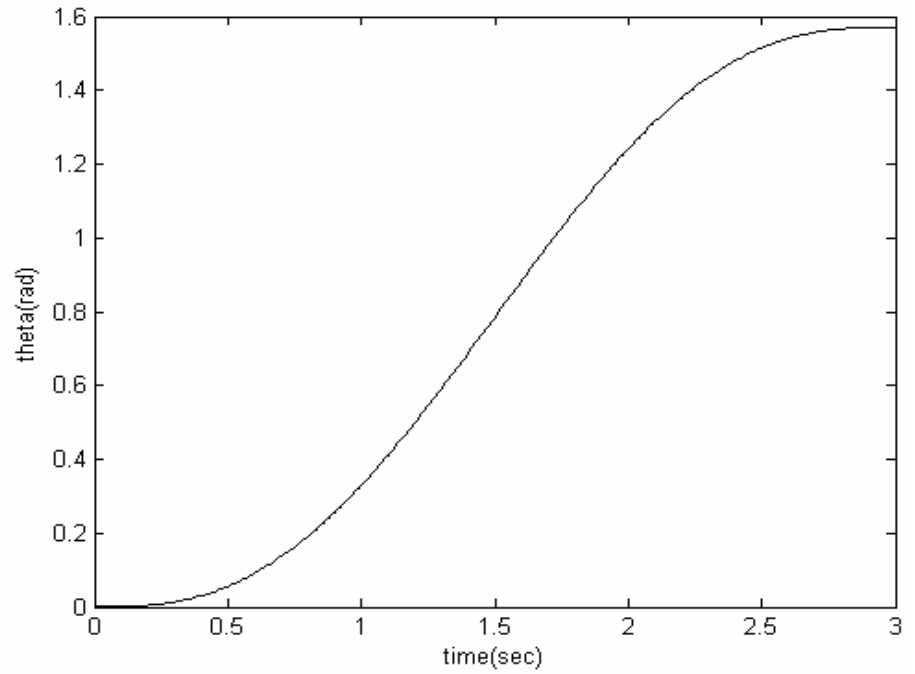

Figure (5-16b). Desired angular position, time 3 sec.

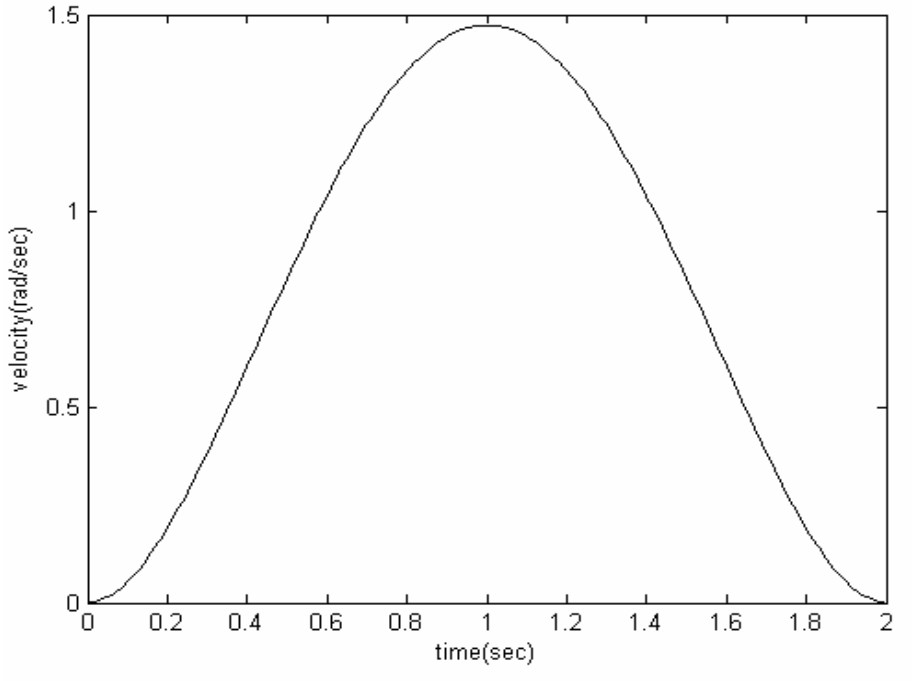

Figure (5-17a). Desired angular velocity, time 2 sec.

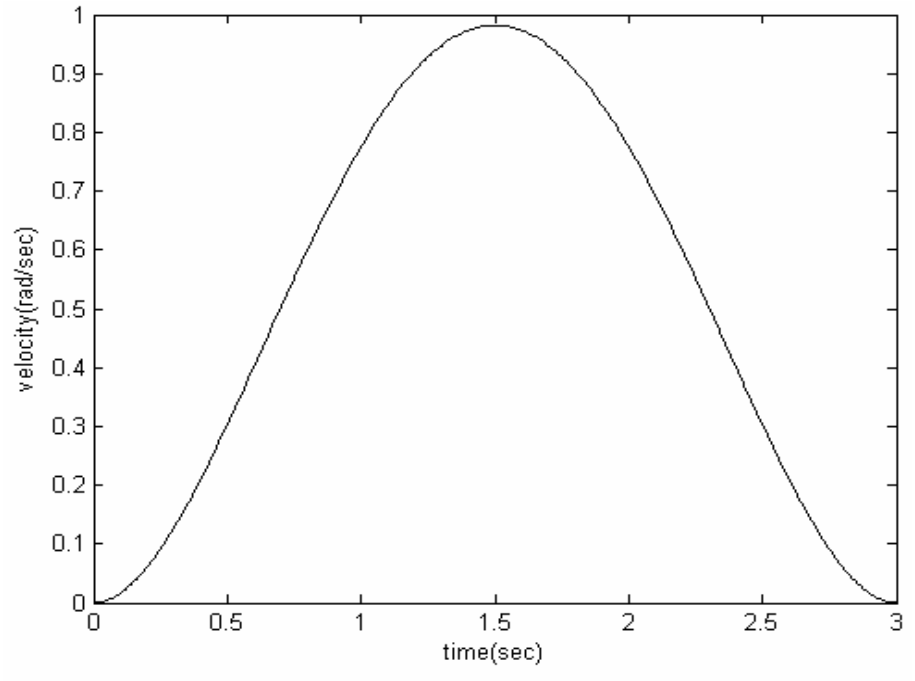

Figure (5-17b). Desired angular velocity, time 3 sec.

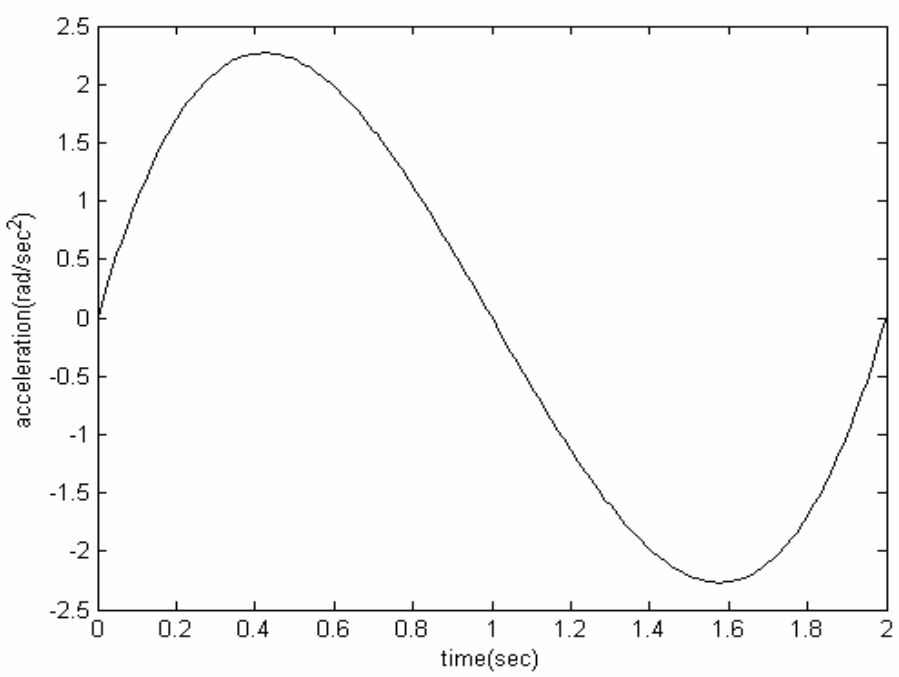

Figure (5-18a). Desired angular acceleration, time 2 sec.

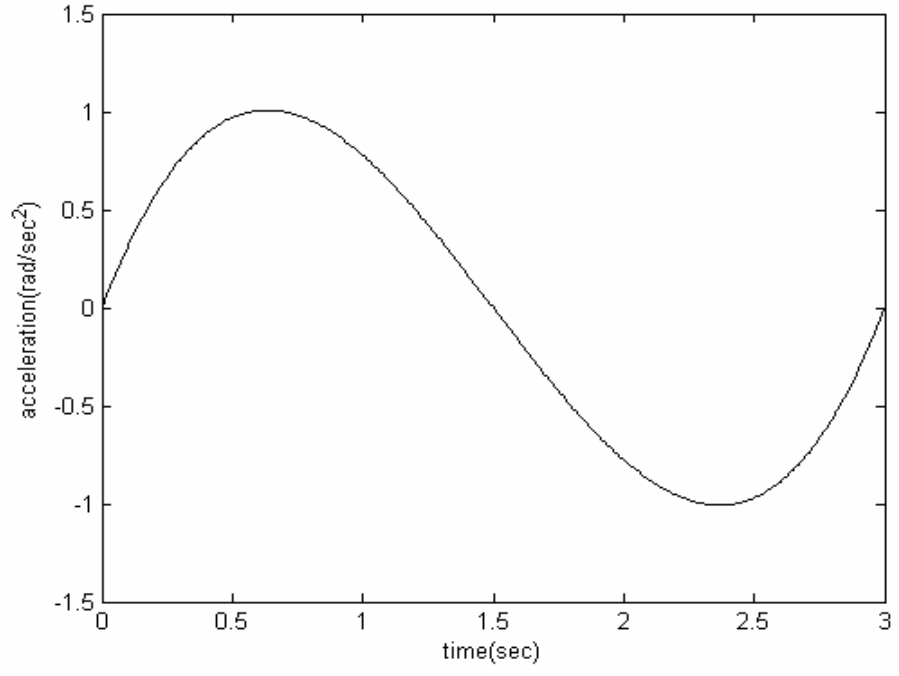

Figure (5-18b). Desired angular acceleration, time 3 sec.

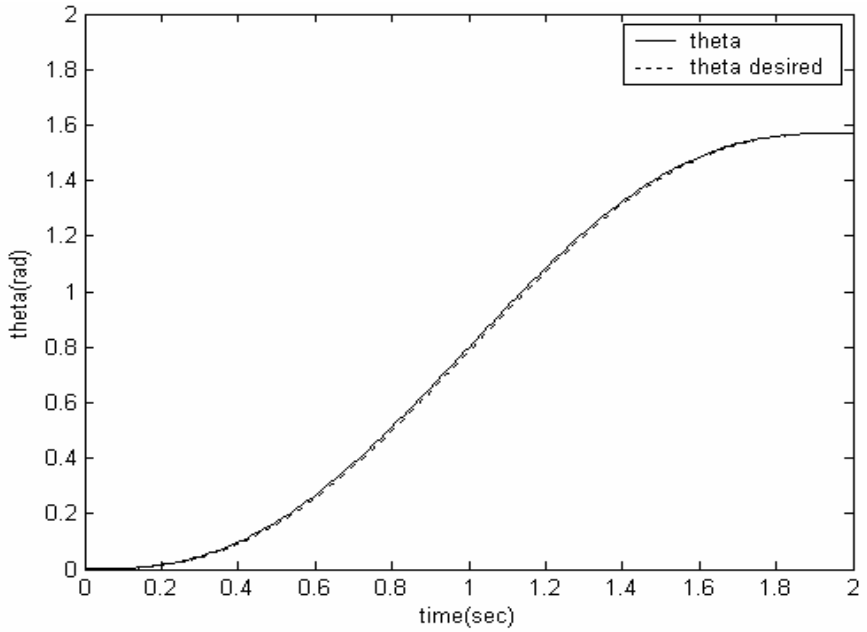

Figure (5-19a). Applying (PD) controller on one link flexible, case 1 (Al) material, angular position θ (desired and simulated), two modes.

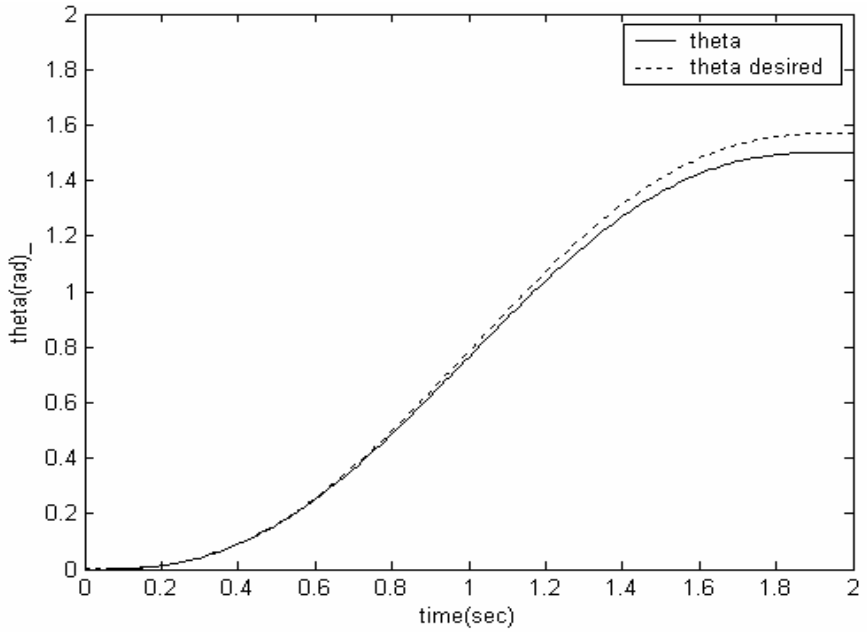

Figure (5-19b). Applying (PD) controller on one link flexible, case 1 (Al) material, angular position θ (desired and simulated), three modes.

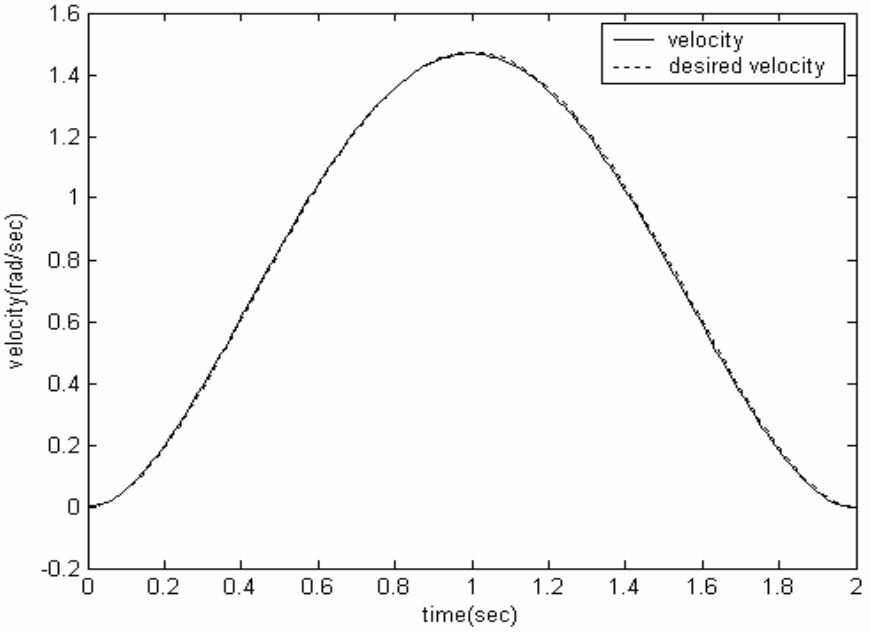

Figure (5-20a). Applying (PD) controller on one link flexible, case 1 (Al) material, angular velocity $\dot{\theta}$ (desired and simulated), two modes.

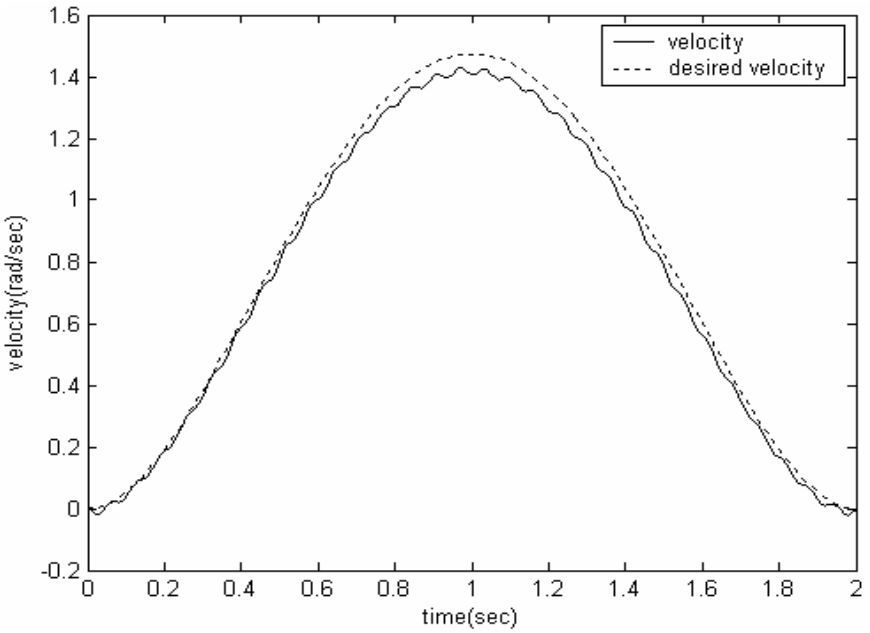

Figure (5-20b). Applying (PD) controller on one link flexible, case 1 (Al) material, angular velocity $\dot{\theta}$ (desired and simulated), three modes.

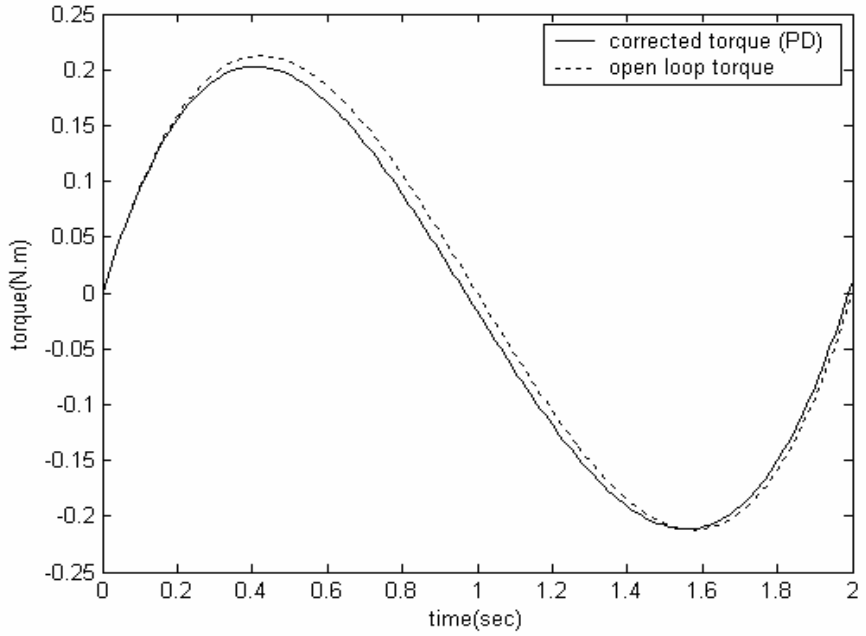

Figure (5-21a). Applying (PD) controller on one link flexible, case 1 (Al) material, torque input τ (desired and simulated), two

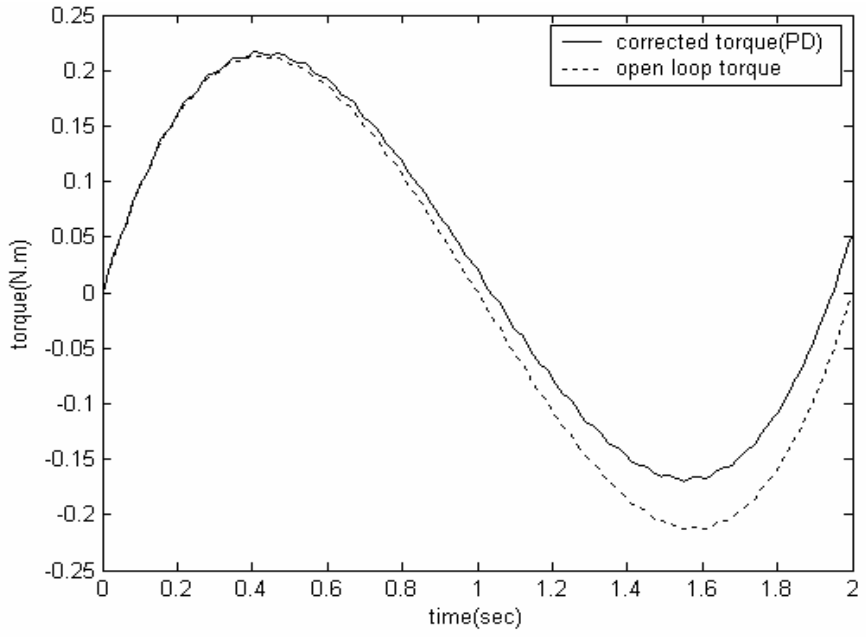

Figure (5-21b). Applying (PD) controller on one link flexible, case 1 (Al) material, torque input τ (desired and simulated), three modes.

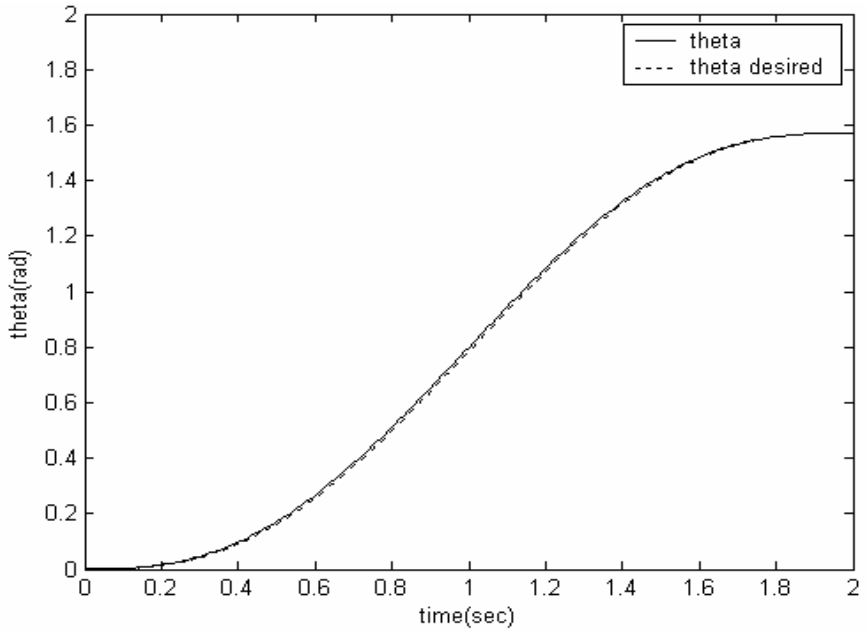

Figure (5-22a). Applying (PD) controller on one link flexible, case 1 (Ti) material, angular position θ (desired and simulated), two modes.

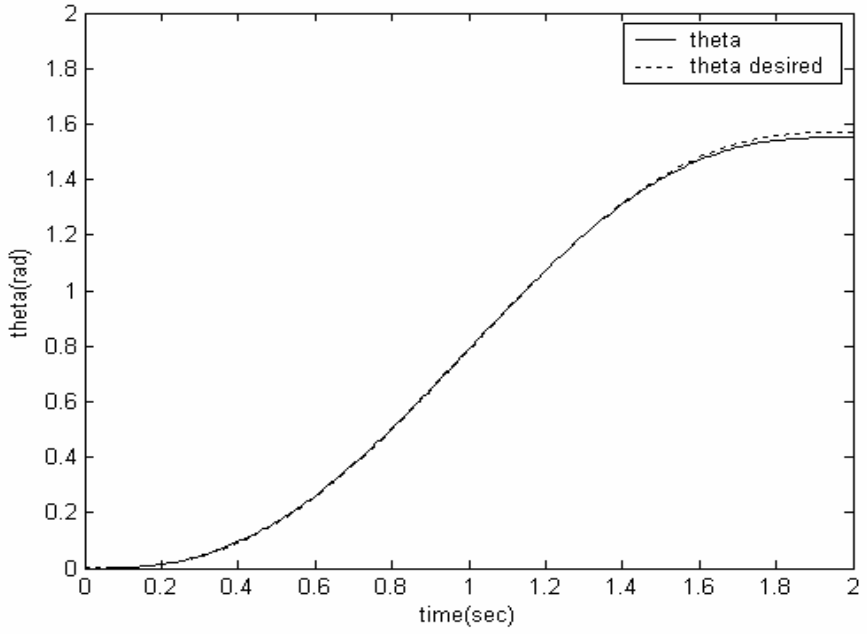

Figure (5-22b). Applying (PD) controller on one link flexible, case 1 (Ti) material, angular position θ (desired and simulated), three modes.

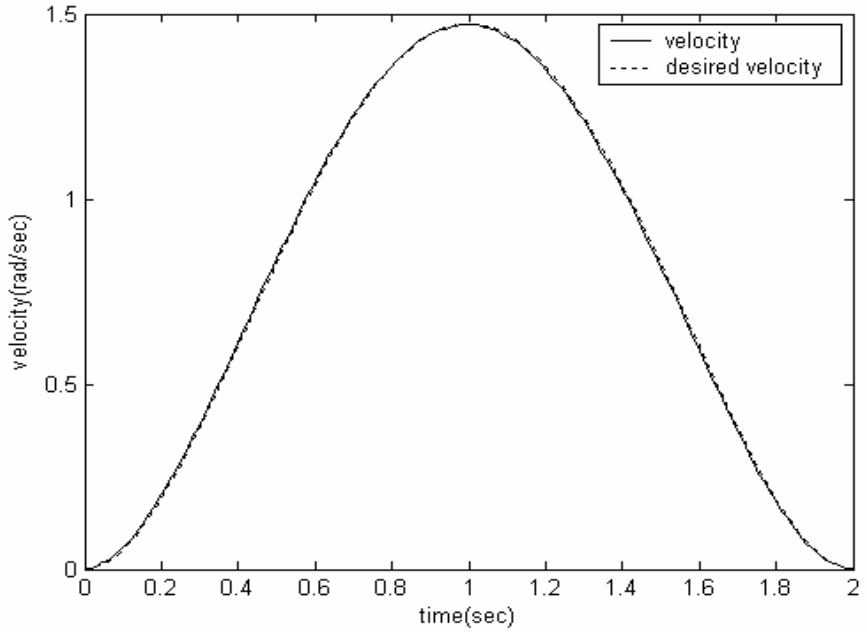

Figure (5-23a). Applying (PD) controller on one link flexible, case 1 (Ti) material, angular velocity $\dot{\theta}$ (desired and simulated), two modes.

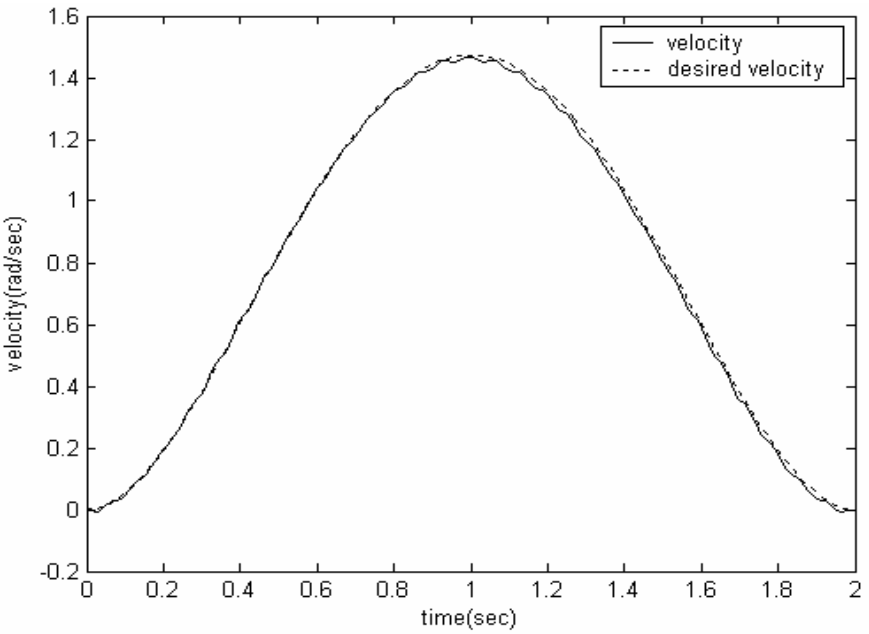

Figure (5-23b). Applying (PD) controller on one link flexible, case 1 (Ti) material, angular velocity $\dot{\theta}$ (desired and simulated), three

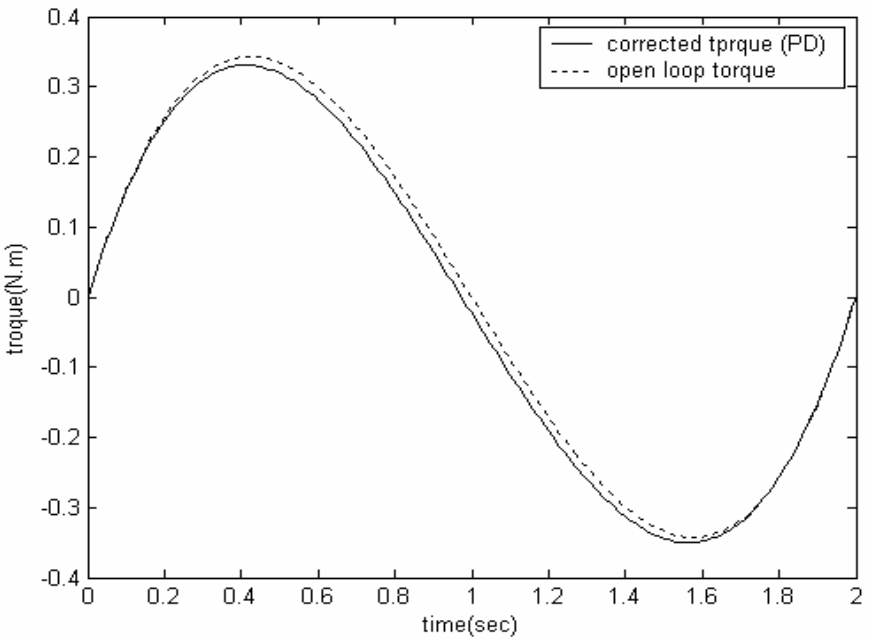

Figure (5-24a). Applying (PD) controller on one link flexible, case 1 (Ti) material, torque input τ (desired and simulated), with two modes.

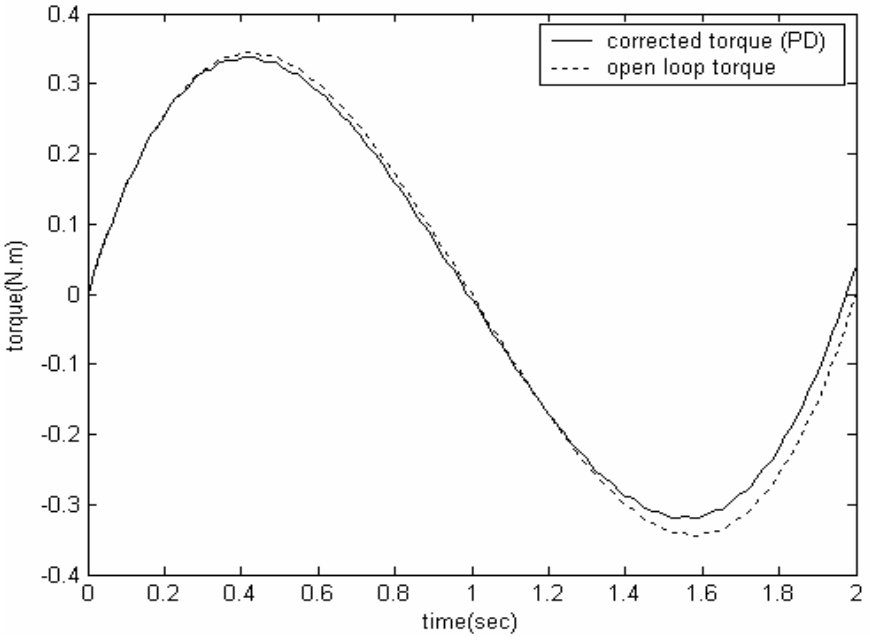

Figure (5-24b). Applying (PD) controller on one link flexible, case 1 (Ti) material, torque input τ (desired and simulated), three modes.

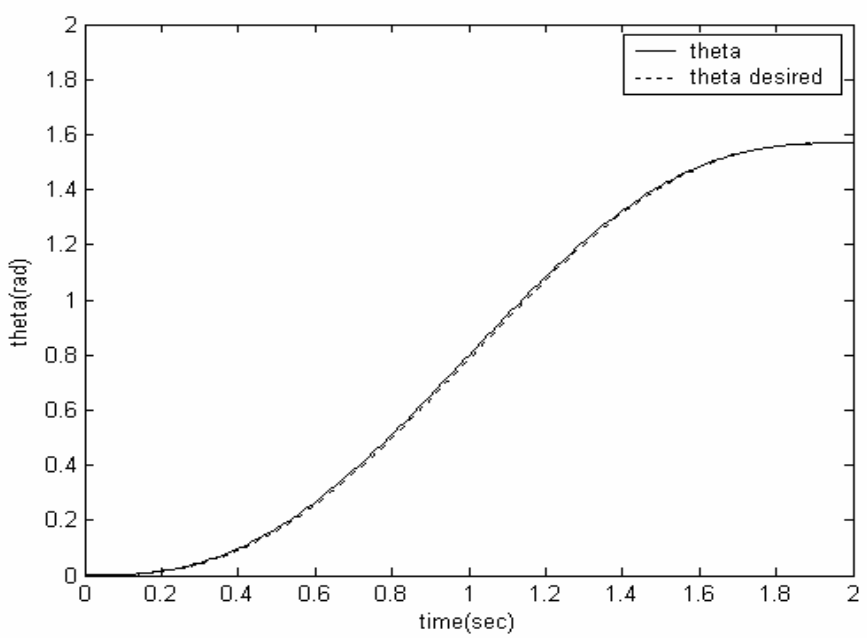

Figure (5-25a). Applying (PD) controller on one link flexible, case 1 (steel) material, angular position θ (desired and simulated), two modes.

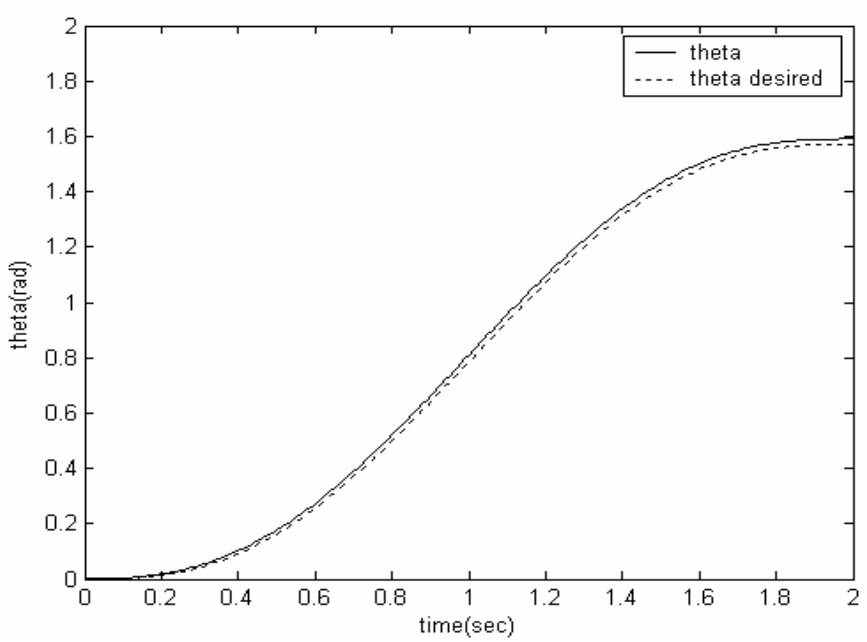

Figure (5-25b). Applying (PD) controller on one link flexible, case 1 (steel) material, angular position θ (desired and simulated), three modes.

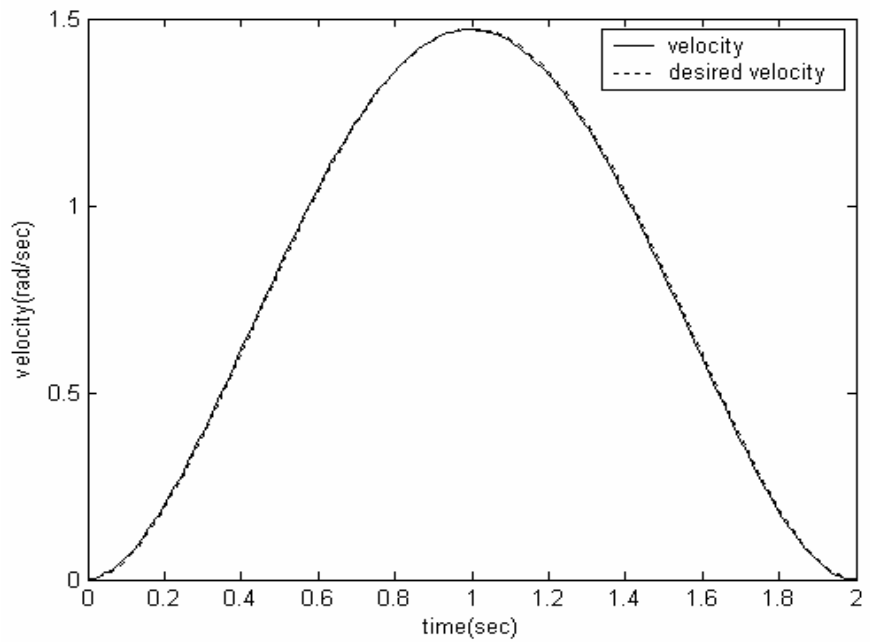

Figure (5-26a). Applying (PD) controller on one link flexible, case 1 (steel) material, angular velocity $\dot{\theta}$ (desired and simulated), two modes.

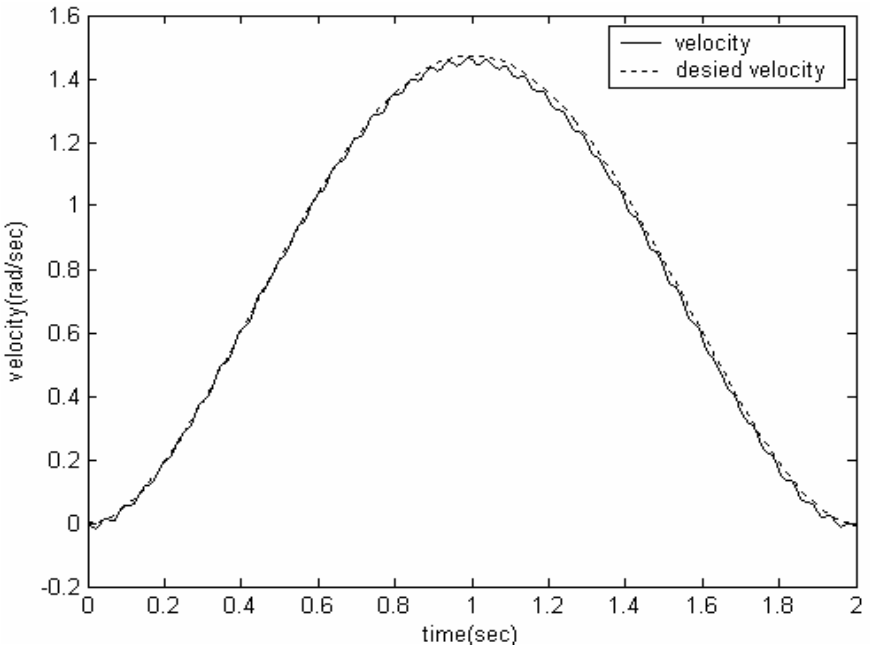

Figure (5-26b). Applying (PD) controller on one link flexible, case 1 (steel) material, angular velocity $\dot{\theta}$ (desired and simulated), three modes.

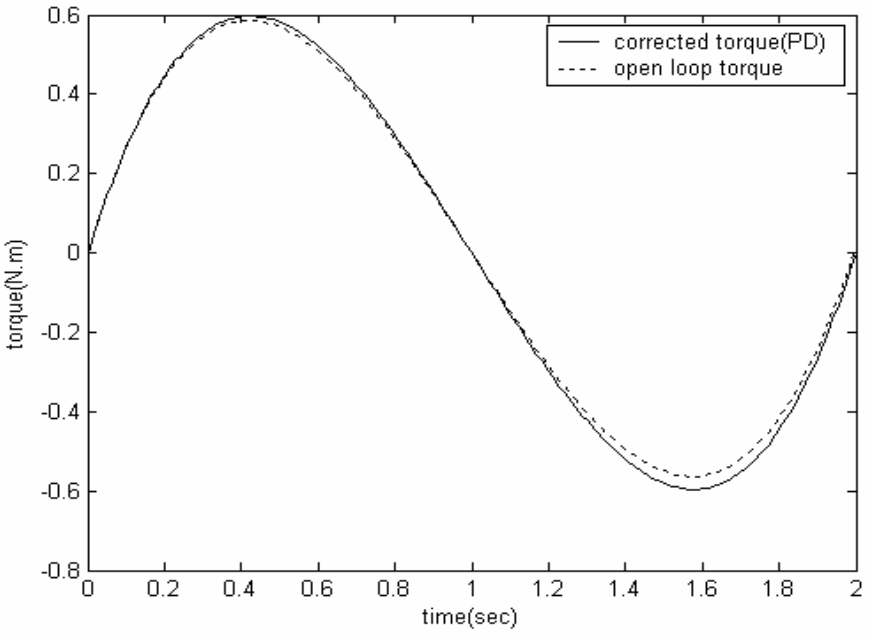

Figure (5-27a). Applying (PD) controller on one link flexible, case 1 (steel) material, torque input τ (desired and simulated), two modes.

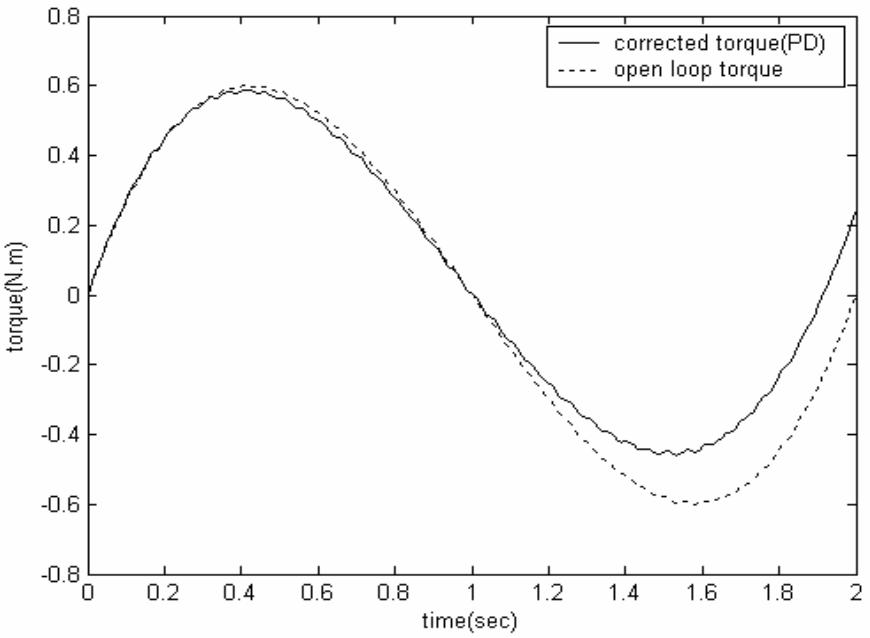

Figure (5-27b). Applying (PD) controller on one link flexible, case 1 (steel) material, torque input τ (desired and simulated), three modes.

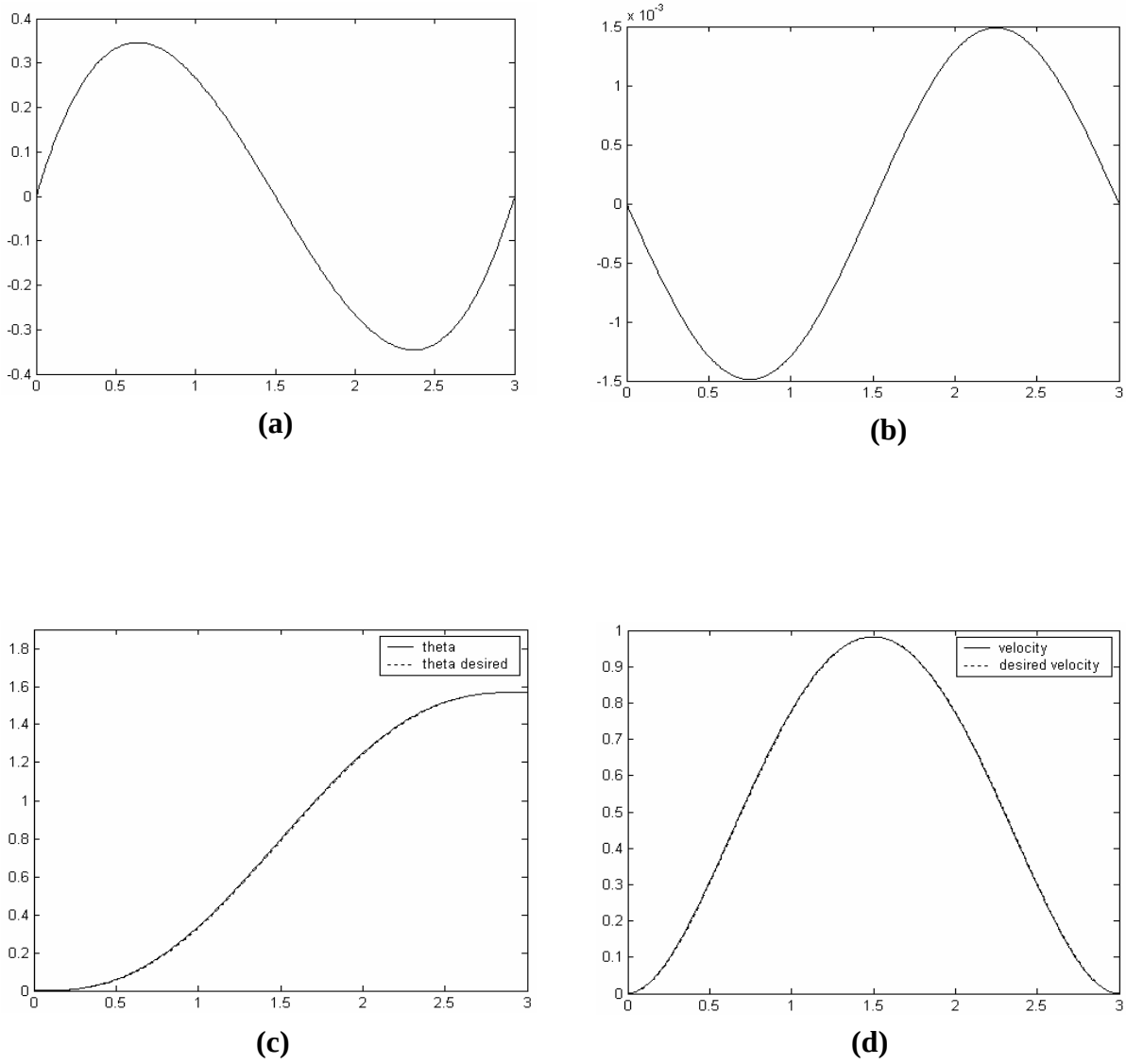

Figure (5-28). Simulation results for single flexible link, case 3, $m_p = 0.05\,kg$ **,using** (PD) **controller(horizontal axis time(sec)):(a) input torque(N.m) ,(b)joint error(rad),(c) simulated and desired trajectory(rad) , (d) simulated and desired velocity(rad/sec).**

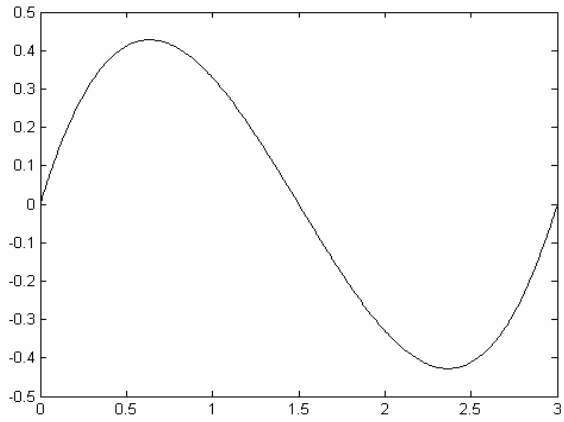

(a)

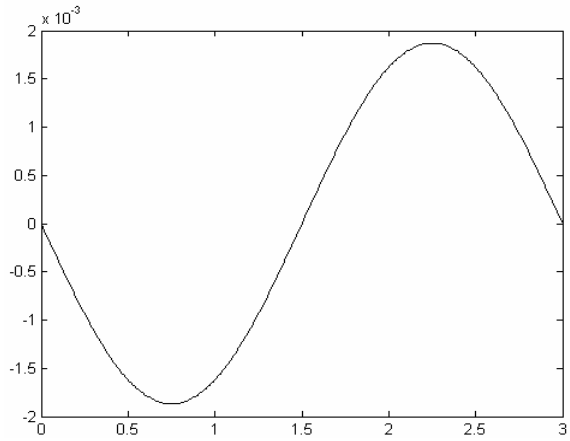

(b)

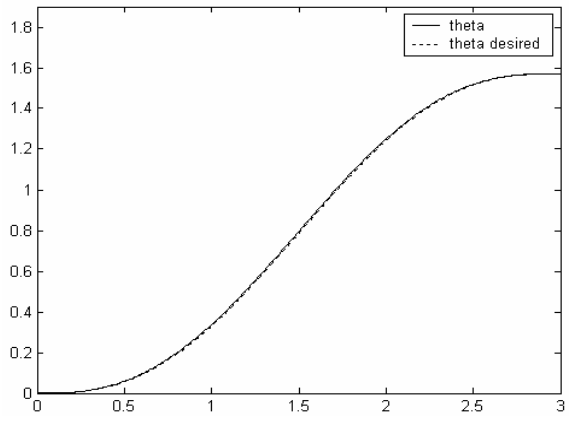

(d)

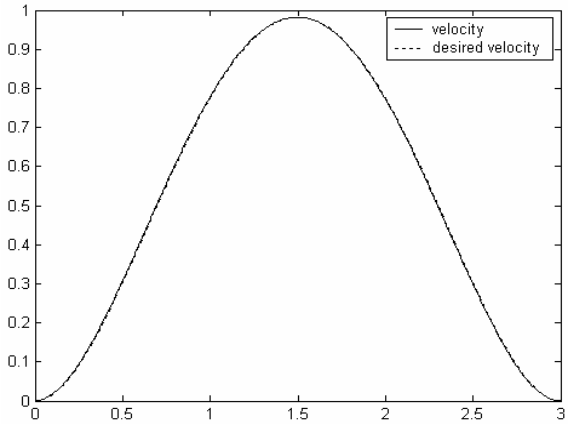

(c)

Figure (5-29). Simulation results for single flexible link, case 3, $m_p = 0.1kg$ **,using** (PD) **controller(horizontal axis time(sec)):(a) input torque(N.m) ,(b)joint error(rad),(c) simulated and desired trajectory(rad) , (d) simulated and desired velocity(rad/sec).**

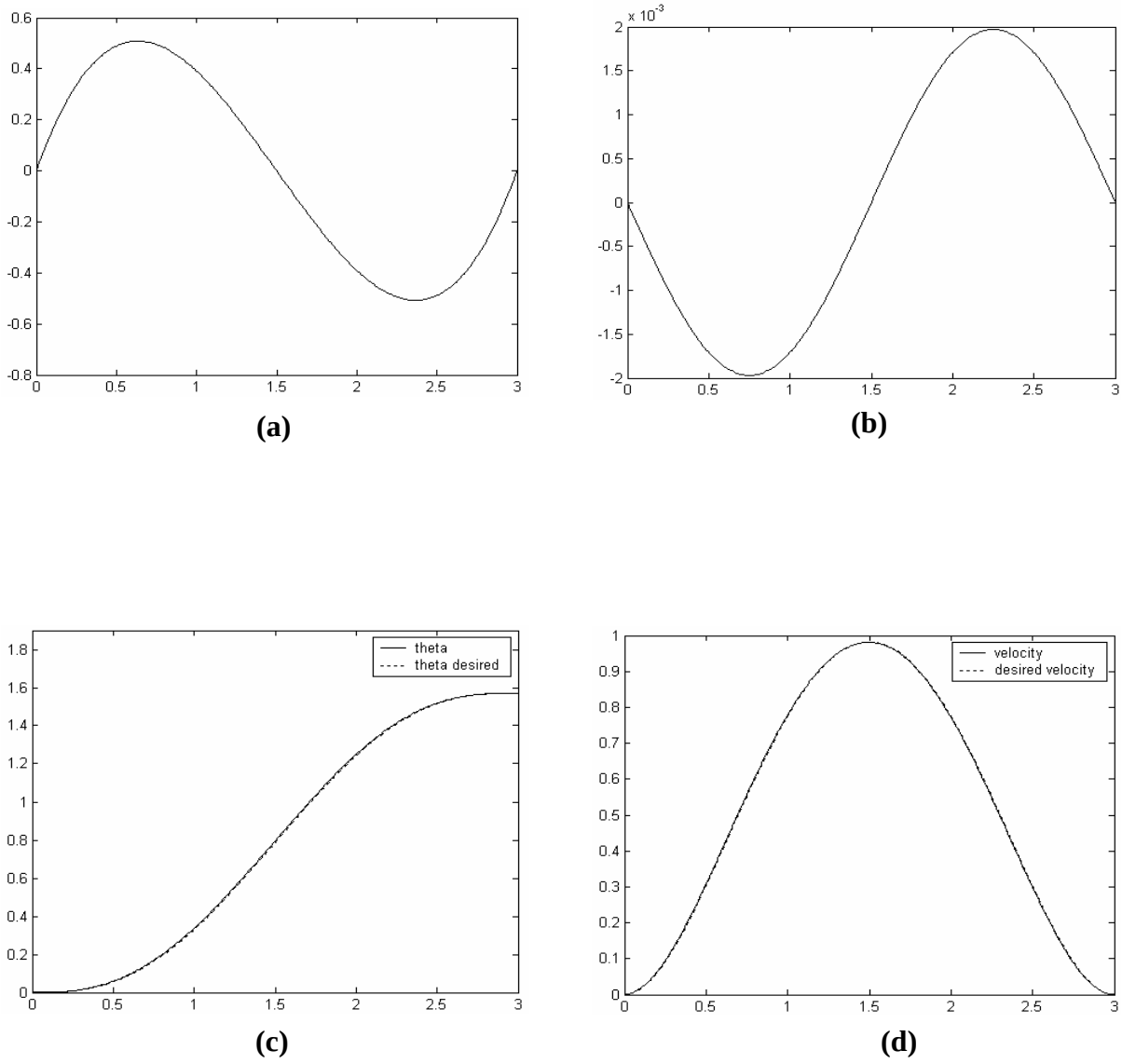

Figure (5-30). Simulation results for single flexible link, case 3, $m_p = 0.15\,kg$ **,using** (PD) **controller(horizontal axis time(sec)):(a) input torque(N.m) ,(b)joint error(rad),(c) simulated and desired trajectory(rad) , (d) simulated and desired velocity(rad/sec).**

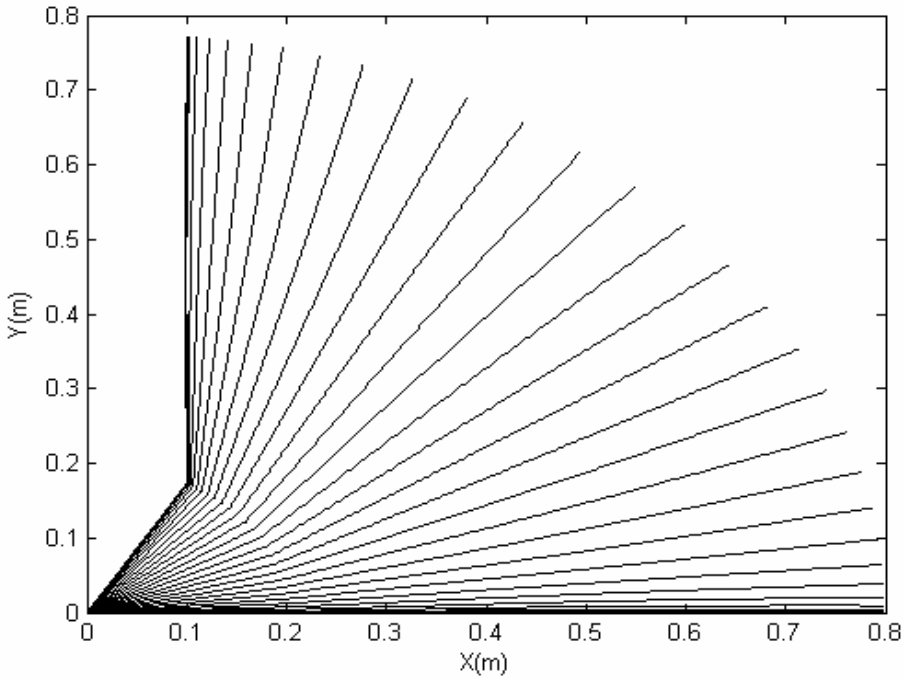

Figure (5-31a) (rigid-flexible) robot motion for conditions:
$\theta_{1f} = 60^{\circ}, \theta_{2f} = 30^{\circ}.$

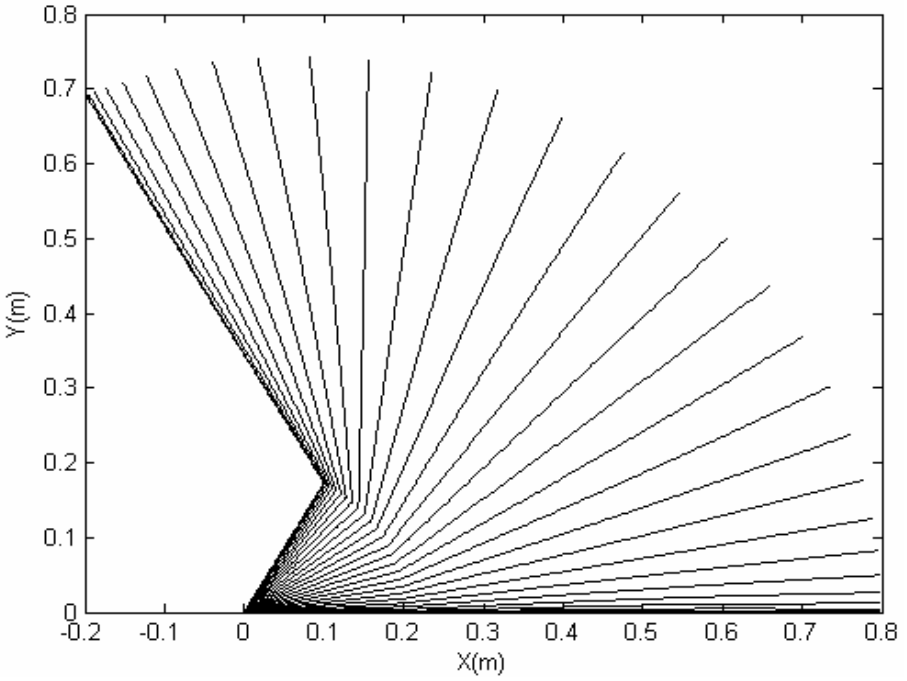

Figure (5-31b) (rigid-flexible) robot motion for conditions:
$\theta_{1f} = 60^{\circ}, \theta_{2f} = 60^{\circ}.$

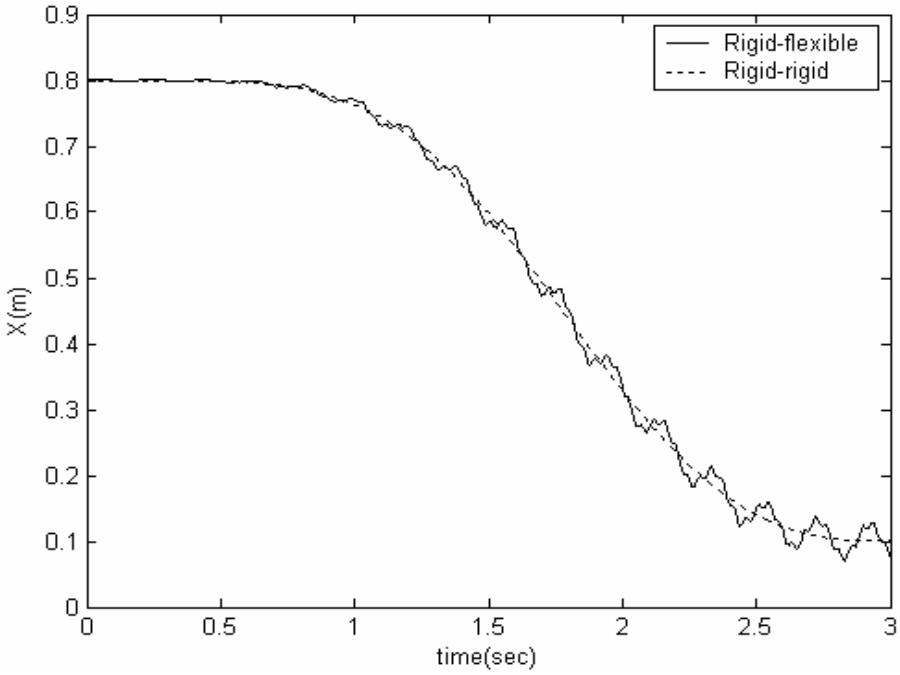

Figure (5-32). Effect of flexibility on the X-component of the end-effector position, $\theta_{1f} = 60^\circ$, $\theta_{2f} = 30^\circ$.

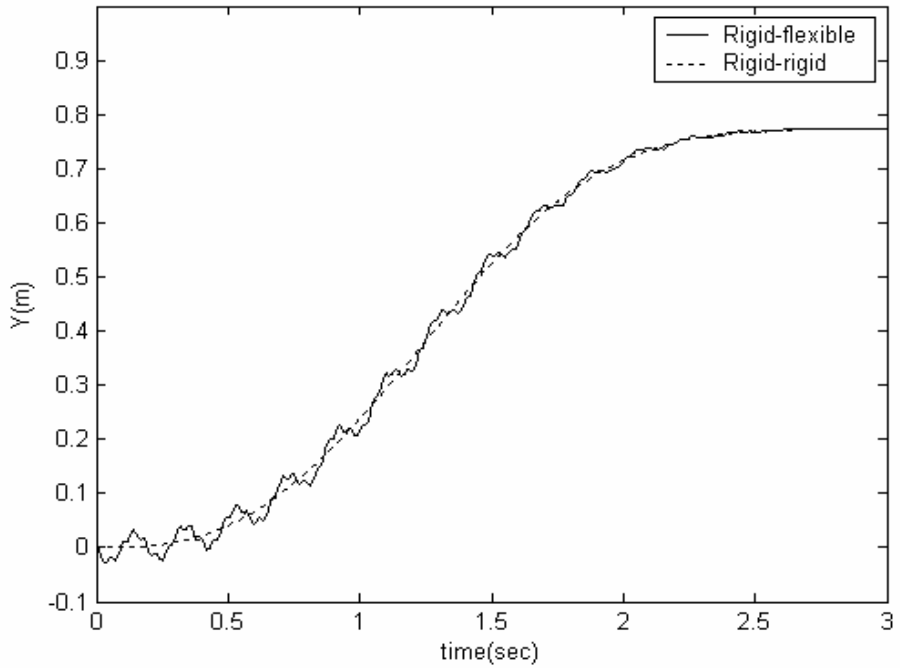

Figure (5-33). Effect of flexibility on the Y-component of the end-effector position, $\theta_{1f} = 60^\circ$, $\theta_{2f} = 30^\circ$.

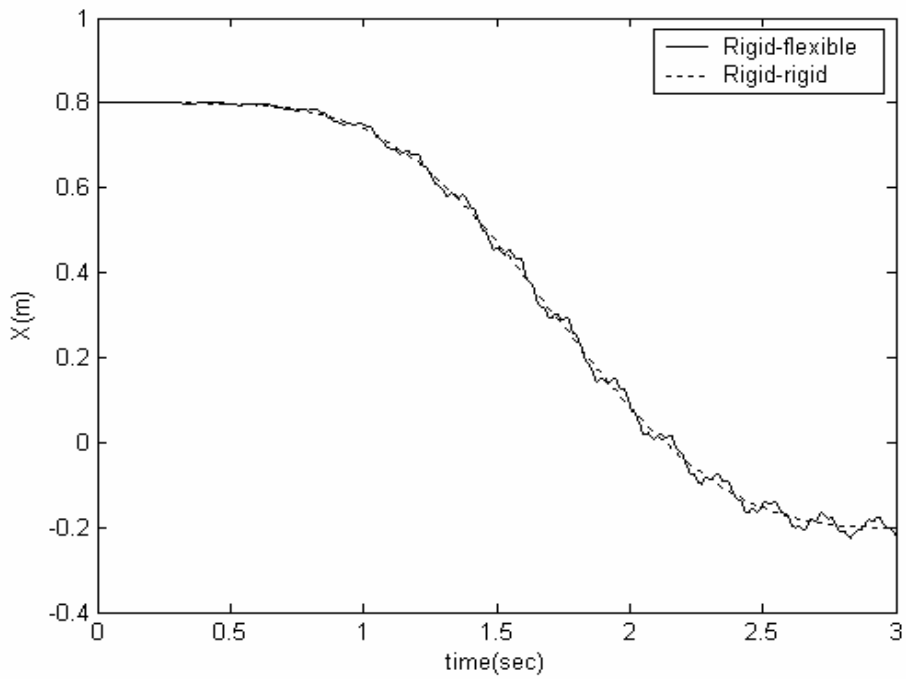

Figure (5-34). Effect of flexibility on the X-component of the end-effector position, $\theta_{1f} = 60^{\circ}, \theta_{2f} = 60^{\circ}$.

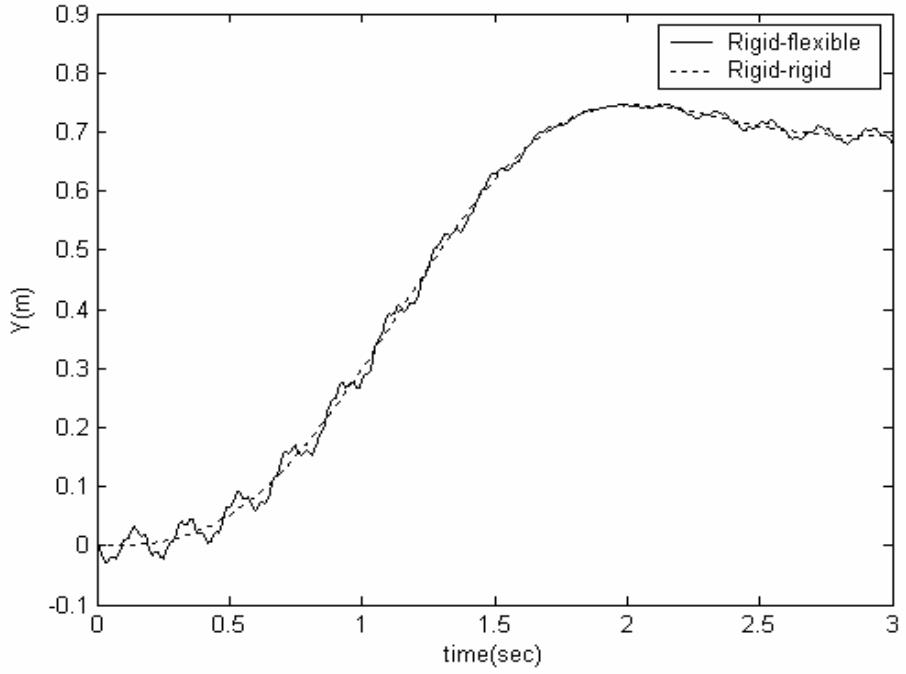

Figure (5-35). Effect of flexibility on the X-component of the end-effector position, $\theta_{1f} = 60^{\circ}, \theta_{2f} = 60^{\circ}$.

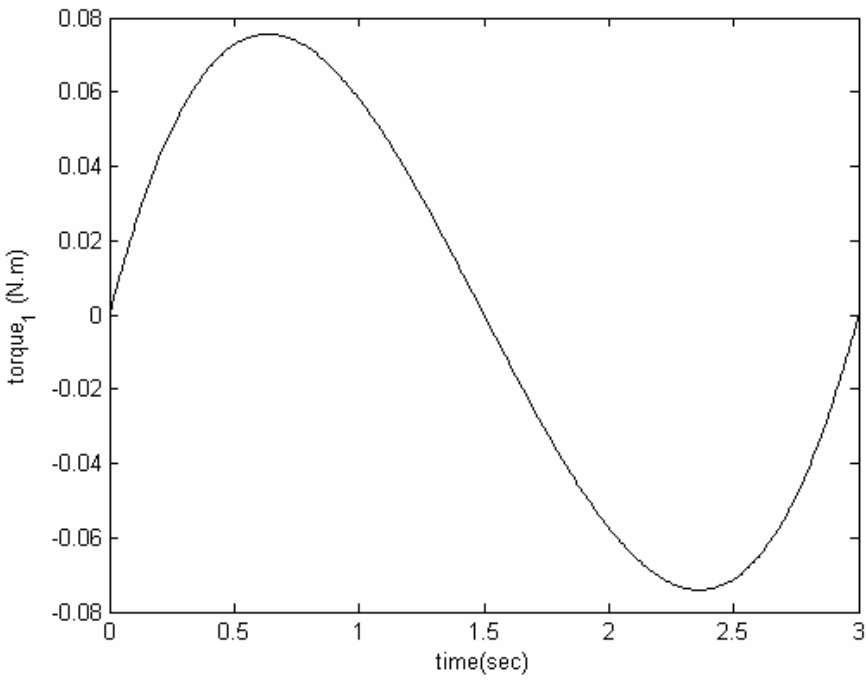

Figure (5-36a). Simulation results for (rigid-flexible) robot: first torque input τ_1, for $\theta_{1f} = 60^\circ$, $\theta_{2f} = 30^\circ$, clam-free flexible

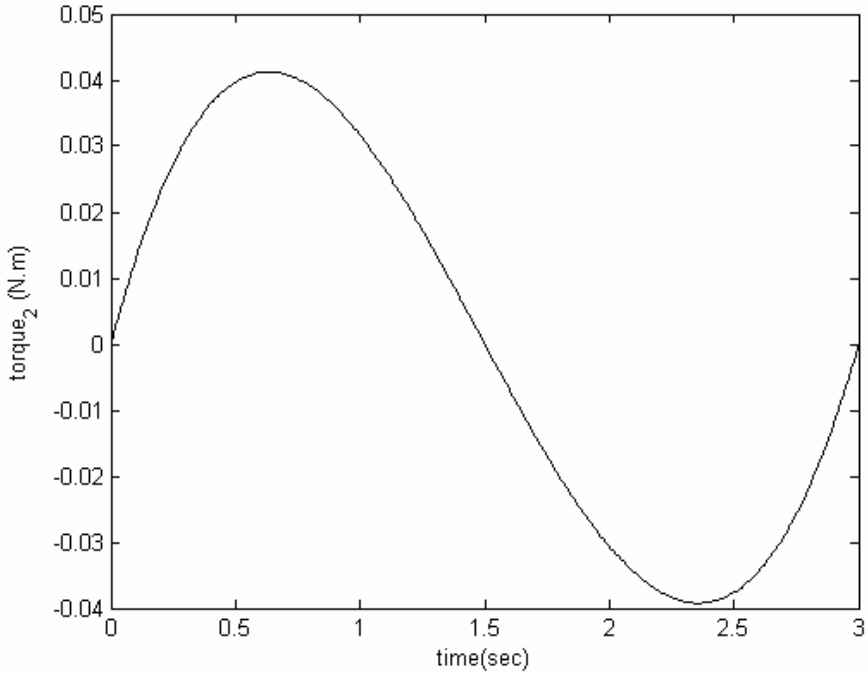

Figure (5-36b). Simulation results for (rigid-flexible) robot, second torque input τ_2, for $\theta_{1f} = 60^\circ$, $\theta_{2f} = 30^\circ$, clam-free flexible

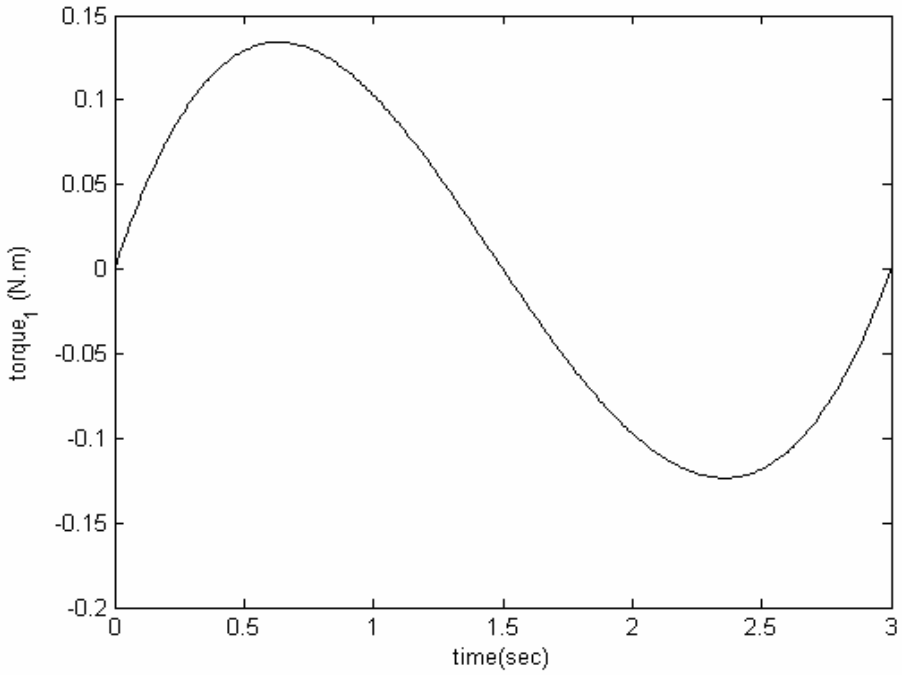

Figure (5-37a). Simulation results for (rigid-flexible) robot: first torque input τ_1, for $\theta_{1f} = 60^\circ$, $\theta_{2f} = 60^\circ$, clam-free flexible link.

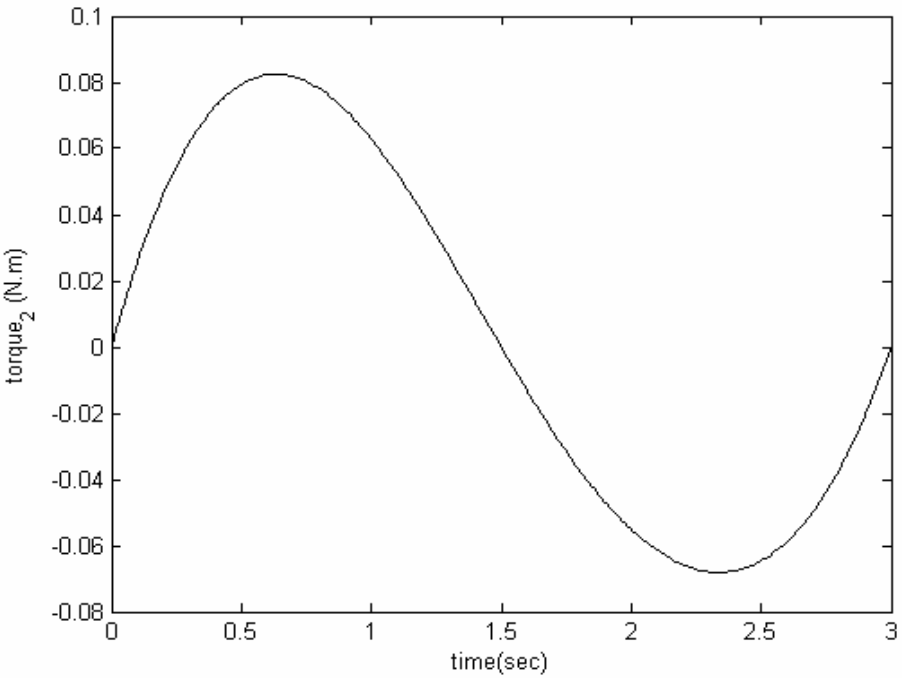

Figure (5-37b). Simulation results for (rigid-flexible) robot: second torque input τ_2, for $\theta_{1f} = 60^\circ$, $\theta_{2f} = 60^\circ$, clam-free flexible link.

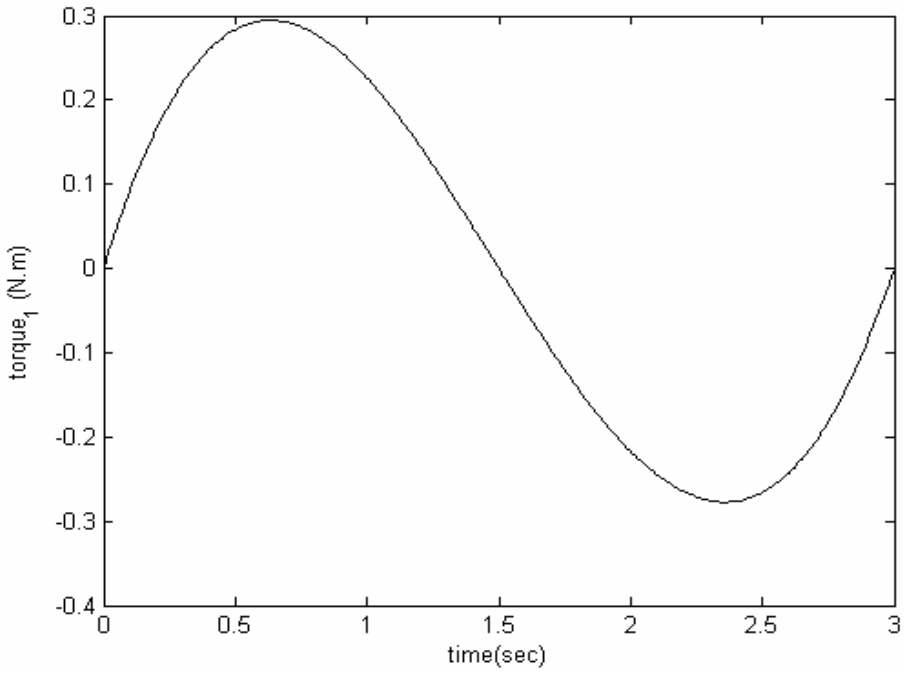

Figure (5-38a). Simulation results for (rigid-flexible) robot (a) first torque input τ_1, for $\theta_{1f} = 60^\circ$, $\theta_{2f} = 60^\circ$, clam-mass flexible link.

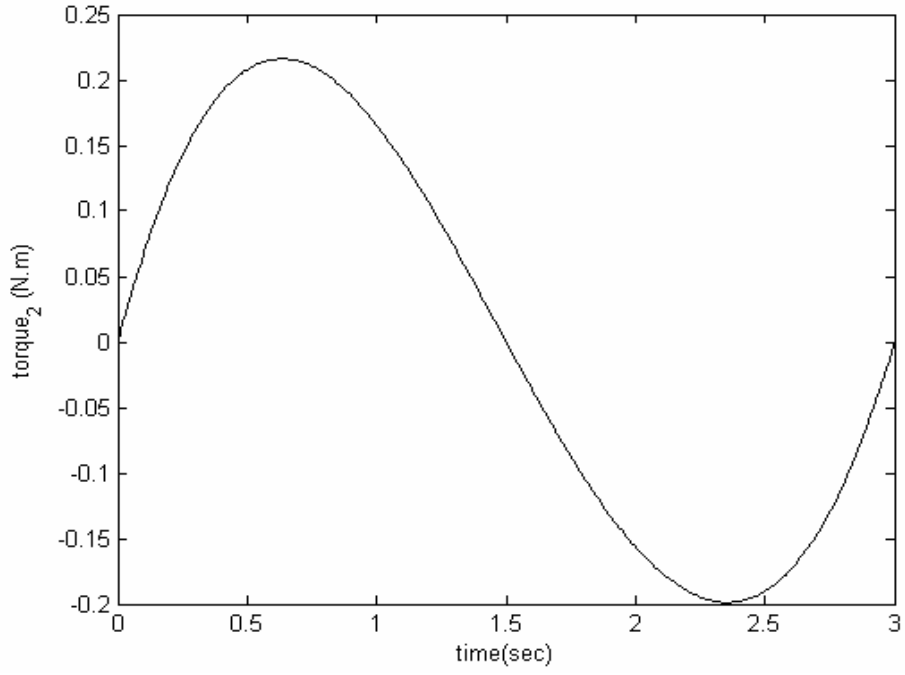

Figure (5-38b). Simulation results for (rigid-flexible) robot: second torque input τ_2, for $\theta_{1f} = 60^\circ$, $\theta_{2f} = 60^\circ$, clam-mass flexible link.

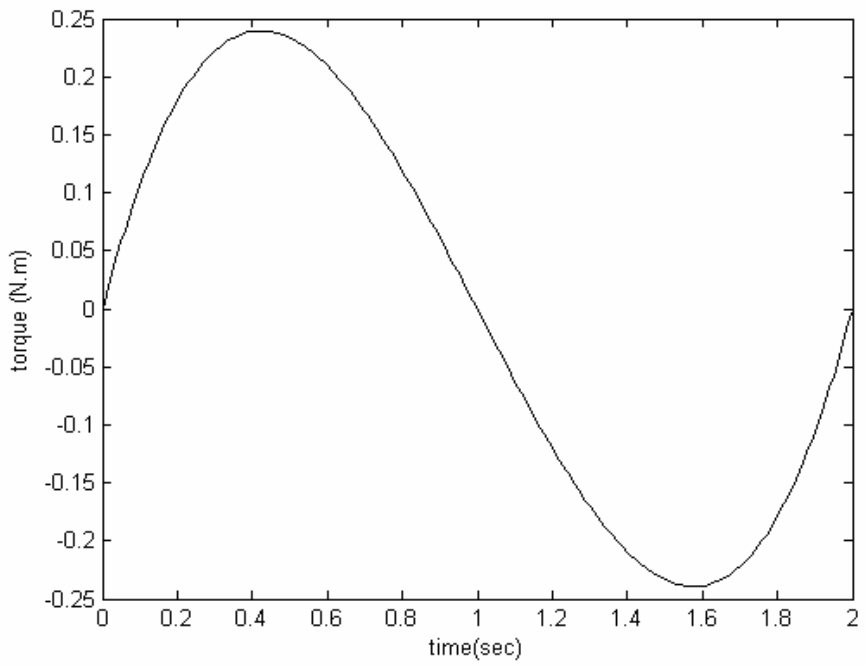

Figure (5-39). Open loop inversion control for a point along the clam-free arm (torque input).

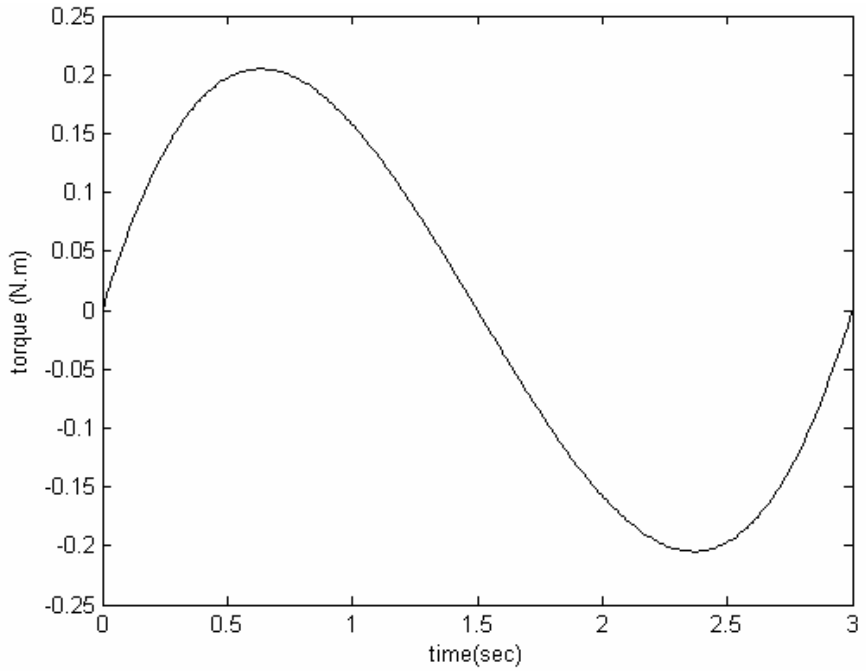

Figure (5-40). Open loop inversion control for a point along the clam-mass arm (torque input).

6

Chapter Six

Conclusions and Future Work

CONCLUSIONS AND SUGGESTIONS FOR FUTURE WORK

6.1. Conclusions

An efficient assumed mode/lagrangian approach for dynamic modeling of lightweight robots with flexible link has been developed, and by using this dynamic model inversion based controller have been designed for tracking output trajectories of a one-link flexible arm, and based on the results presented and discussed in chapter five the following main conclusions can be written:

1. The dynamic model derived in this study is highly nonlinear and coupled and it can be used with two or three flexible modes to modeling the flexible robot arm.
2. The B.C.'s was an influent parameters on the dynamic modeling and trajectory control of flexible arm and the results shows changeable behavior of system with different B.C.'s especially with clam-mass boundary conditions.
3. The payload values, the number of flexible modes, modulus of elasticity, and cross section type were chosen in the dynamic modeling and control; have direct effects on tip-deflection and joint error; with different levels of effects.
4. Open loop computation of joint torque plus a *PD* joint trajectory controller yields satisfactory results with a max joint error as (0.002 rad).
5. The development has been carried out for a single flexible-link; it is has been extended to described the dynamic and control analysis for two-link (rigid flexible) robot depending on the joint based approach to the two-link (rigid-flexible) case.

6. The differences between desired and simulated results in the two and three mode cases, is not due to failure of the numerical analysis, but due to the nature of the problem which is noncausal.
7. An alternative strategy has been investigated and shows good results that allows for the trajectory control of range of angular output defined along the link.

5.2 Suggestions for Future Work

Flexible robots are a new type generation of lightweight, heavy payload, and high speed manipulator systems and the dynamic model of these types of robots are not known exactly until now, and the work in control of these systems is very wide range. Much more work is required in this field of robotics, to increase the accuracy of the dynamic model, and robust the control systems. Based on this work the following suggestions can be written:

1. Experimental verification of the models. This is due to the fact that regardless of how precise the mathematical description is, a model should be tested experimentally.
2. Modeling and control, of flexible link and flexible joint robot. This due to the neglecting the flexibility of the joint in this work, which important parameter in the modeling of robot.
3. Modeling of multi-link flexible manipulator to study the effect of the serial flexible link on the operation of the robot.
4. Using inversion control for the End-effector trajectory tracking which is the toughest control problem for flexible robots.
5. Control of flexible robot arm by using sliding mode control.
6. Time optimal control for flexible robot arm.

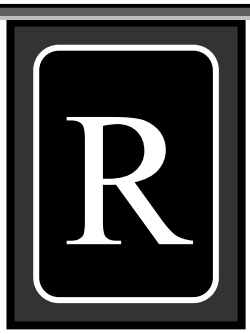

References

[1] Book W. J., "Analysis of Massless Elastic Chains with Servo Controlled Joints," ASME Journal of Dynamic Systems, Measurements, and Control, Vol. 101, pp. 187-192, 1979.

[2] Sunada W., and Dubowsky S., "The Application of Finite Element Methods to the Dynamic Analysis of Flexible Spatial and Co-Planar Linkage Systems," ASME Journal of Mechanical Design, Vol. 103, pp. 643-651, 1981.

[3] Book W. J., "Recursive Lagrangian Dynamics of Flexible Manipulator Arms," International Journal of Robotics Research, Vol. 3, pp. 87-101, 1984.

[4] Usoro P. B., Nadira R., and Mahil S. S., "A Finite Element / lagrangian Approach to Modeling Lightweight Flexible Manipulators," ASME Journal of Dynamic Systems, Measurements, and Control, Vol. 108, pp. 198-205, 1986.

[5] Naganathan G., and Soni A. H., "Nonlinear Modeling of kinematic and Flexibility Effects in Manipulator Design," ASME Journal of Mechanisms, Transmission and Automation in Design, Vol. 110, pp. 243-254, 1988.

[6] Benati M., and Morro A., "Dynamics of Chain of Flexible links," Journal of Dynamic Systems, Measurement, and Control , Vol. 110, pp. 411-415, 1988.

[7] James D. Lee, and Ben-Li Wang, "Dynamic Equations for Two-Link Flexible Robot Arm," Robot Systems Division, National Bureau of Standards, Gaithersburg, journal of computers and structures Vol. 29, No. 3, pp.469-477,1988.

[8] Mehrdad M., "Control and Design of Flexible Links," PhD thesis, Concordia University, The Department of Electrical and Computer Engineering, Montreal, Québec, Canada, 1996.

[9] Mehrdad F., "Dynamic Modeling and Optimal Control of Flexible Manipulators," PhD thesis, Calgary University, Department of Mechanical Engineering, Calgary, Alberta, 1997.

[10] Jean-Claude P., "Recursive modeling of serial flexible manipulators," Journal of Astronautcal sciences, Vol. 46, No. 1, pp. 1-24, 1998.

[11] Victor O., and Gamarra-Rosado, "A planar flexible Robotic manipulator" Division of Mechanical Engineering, College of Engineering UNESP, Guaratingueta, Brazil, Cybernetic, Vol. 29 No. 5/6, pp. 787-796, 2000.

[12] Ali Meghdari, and Farbod Fahimi, " On the First-Order Decoupling of Dynamical Equations of Motion for Elastic Multibody Systems as Applied to a Two-Link Flexible Manipulator," Sharif University of Technology, School of Mechanical Engineering, Tehran, Iran, Printed in the Netherlands, Journal of Multibody System Dynamics Vol. **5,** pp**.** 1–20, 2001.

[13] Somolinos J.A., Feliu V., and Sanchez L., "Design, dynamic modeling and experimental validation of a new three-degree-of-freedom flexible arm," Journal of Mechatronics, Vol. 12, pp. 919–948, 2002.

[14] Mohamed S., Jean-Claude P., Ouassima, A., and Lahcen, S., "Modal analysis of assumed-mode models of a flexible slewing beam," International Journal Modeling, Identification and Control, Vol. 1, No. 4, pp.325-337, 2006.

[15] Cannon R. H., and Schmitz E., " initial Experiments on End-Point Control of a Flexible One- Link Robot," International Journal of Robotics Research, Vol. 3, pp. 49-54, 1984.

[16] Hasting G. G., and Book W. J., "Experiments in the Optimal Control of a Flexible Manipulators," Proceedings of American Control Conference, pp. 828-729, 1985.

[17] Bayo E., "A finite Element Approach to Control the End-Point Motion of a Single-link Flexible Robot," Journal of Robotic Systems, Vol. 4, pp. 63-75, 1987.

[18] Khorrami and Ozguner, "Singular Perturbation Analysis of a Distributed parameter Mode1 of Flexible Manipulators," Proceedings of American control conference, pp. 1704-1709, 1988.

[19] De Luca A., and Siciliano B., "Trajectory Control of Non-Linear One-Link Flexible Arm," International Journal of Control, Vol. 50, No. 5, pp. 1699-1715, 1989.

[20] Aoustin Y., and Chevallereau C., "The singular perturbation control of a two-flexible-link robot," IEEE International Conference on Robotics and Automation, Vol.3, pp. 737-742, 1993.

[21] Aria A., "Force Control of Flexible Manipulators," PhD thesis, Carleton University, Department of Mechanical and Aerospace Engineering, Ottawa, Ontario, Canada, 1997.

[22] Mohammad J. Yazdanpanah, "Control of Flexible-Link Manipulators Using Nonlinear H, Techniques," PhD thesis, Concordia University, Department of Electrical and Computer Engineering, Montréal, Québec, Canada, 1997.

[23] Nurkan Yagiz, Ismail Yuksek, Tamer Kepceler, and Faris Kaya, " Sliding Mode Control of A planar Flexible Single-Arm Robot," 5th Engineering Systems Design and Analysis Conference of ASME, July 10-13, Montreux, Switzerland, 2000.

[24] Reza Olfati-Saber, "Trajectory Tracking for a Flexible One-Link Robot using a Nonlinear Noncollocated Output," Massachusetts Ave. Cambridge, 2002.

[25] Min G., and Jean-Claude P., "A Flexible-Arm as Manipulator Position and Force Detection Unit," Control Engineering Practice, Space Technologies, Canadian Space Agency, Québec, Canada, 2003.

[26] Knani J., "Dynamic Modeling and Trajectory Computer Simulation of Flexible Robotic Mechanisms," Journal of Systems Analysis Modeling Simulation, Vol. 43, No. 4, pp. 397–409, 2003.

[27] De Luca A., "Robots with Flexible Links: Modeling and Control," outlined, Roma University, Department of informatics and systematic (DIS), Roma, 2003.

[28] Tso S.K., Yang T.W., Xu W.L., and Sun Z.Q., "Vibration control for a flexible-link robot arm with deflection feedback," International Journal of Non-Linear Mechanics Vol. 38, pp. 51–62, 2003.

[29] Etxebarria A., Sanz A., and Lizarraga I., "Control of a Lightweight Flexible Robotic Arm Using Sliding Modes," International Journal of Advanced Robotic Systems, Vol. 2, No. 2, pp. 103 - 110, 2005.

[30] Rush D., Robinett Clark D., Richard E., John F., Gordon G., David G., and Dennis S., "FLEXIBLE ROBOT DYNAMICS AND CONTROL," International Federation for System Research, International Series on systems and Engineering, Volume 19, 2002.

[31] Dean G. Duffy "ADVANCED ENGINEERING MATHMATICS," New York: CRC Press, 1998.

[32] Meirovitch L., "ANLYTICAL METHODS IN VIBRATIONS," New York: Macmillan, 1967.

[33] William T., Thomson, "THEORY OF VIBRATION WITH APPLICATION," New Jersey, 1972.

[34] Chin H. Chang, "Mechanics of Elastic Structures with Inclined Members," Lecture Notes in Applied and Computational Mechanics, Springer: Berlin Heidelberg, 2005.

[35] Atef A. Ata, and Habib Johar, "Dynamic simulation of task constrained of a rigid-flexible manipulator," International Journal of Advanced Robotic Systems, Vol. 1 No. 2, pp. 61 - 66, 2004.

[36] Mathworks Inc., "Dynamic System Simulation for MatLab (Writing S-Function) Version 4," United States, 2000.

[37] Jaan K., "NUMERICAL METHODS IN ENGINEERING WITH MATLAB," Cambridge university press.

[38] Richard C. D., and Robert H. B., "MODERN CONTROL SYSTEM," Addison-Wesley, United States, 1998.

[39] John J. G., "INTRODUCTION TO ROBOTICS," Addison-Wesley, United States, 1989.

[40] Peter I. Corke, "robotics Toolbox for Use with Matlab," Release 6, 2002.

Appendix

Data of Links for All Cases

A.1. Case 1

The link in this case is under clam-free B.C.'s the area, and the length of link is the same for all type of material $area = 50\,mm^2$, $l = 1m$ and the moment of inertia is show below the table:

Cross section			Rectangular	triangular
Material	M. of E.	Mass per unit length (kg/m)	(50*1)mm^2	(50*2)mm^2
Steel	E=195	0.3925	EI=0.8125	EI=2.1667
Al	E=75	0.1376	EI=0.3125	EI=0.8333
Ti	E=110	0.2243	EI=0.45833	EI=1.2222

Table (A-1) case 1 link parameters.

For all rectangular cross section links h,b are the height and width respectively and for triangular h,b are the height and the base respectively and the moment of inertia of the link is: $I_{Rec.} = \frac{b\,h^3}{12}$, $I_{Tri.} = \frac{b\,h^3}{36}$.

The natural frequencies which was calculated from the dynamic model of the case 1, shown below:

Cross section	Rectangular			Triangular		
material	Al	Ti	Steel	Al	Ti	steel
ω_1	18.797	19.2488	20.6352	30.6941	31.3939	33.6975
ω_2	43.7377	46.5079	54.53	71.4215	75.7782	89.0602
ω_3	96.665	94.2891	101.0558	157.8506	153.888	165.065

Table (A-2) case 1 natural frequencies.

The natural frequencies in this case and in all cases were calculated by using equations (3.48) and (3.49).

A.2. Case 2

The link in this case is also under clam-free B.C.'s the area, and the length of link is the same for all type of material $area = 50\,mm^2$, $l = 1m$ and the moment of inertia is show below the table:

Cross section			Rectangular	triangular
Material	M. of E.	Mass per unit length (kg/m)	(40*1.25)mm^2	(40*2.5)mm^2
Steel	E=195	0.3925	EI=1.2695	EI=3.3854
Al	E=75	0.1376	EI=0.4883	EI=1.3021
Ti	E=110	0.2243	EI=0.7161	EI=1.9097

Table (A-3) case 2 link parameters.

And the natural frequencies obtained from the dynamic model of the case 2 shown below:

Cross section	Rectangular			Triangular		
material	Al	Ti	Steel	Al	Ti	steel
ω_1	23.4016	24.0313	25.7936	38.2139	39.2429	42.1215
ω_2	54.4193	58.0058	68.1612	88.864	94.7237	111.3089
ω_3	120.8849	117.796	126.3173	197.4006	192.362	206.28

Table (A-4) case 2 natural frequencies.

A.3.Case3 (clam-mass)

In this case the link data is shown in table below:

Parameter		Value	unit
Beam material		Steel	
Mass per unit length	ρ	0.3925	(kg/m)
Modulus of elasticity	E	195×10^9	(N/m^2)
Length	l	1	m
Cross section area	a	1×50	mm
Hub moment of inertia	J_h	0.002	$(kg.m^2)$

Table (A-5) case 3 link parameters.

The payload is changed form$(0.05-0.15)kg$, and the Eigen modes which are calculated from the transcendental characteristic equation are:

$m_p(kg)$	0.05	0.1	0.15
λ_1	1.69	1.571	1.483
λ_2	4.354	4.222	4.153
λ_3	7.403	7.278	7.221

Table (A-6) case 3 eigen modes.

And the natural frequencies obtained from the dynamic model of the case 3 shown below:

$m_p(kg)$	0.05	0.1	0.15
ω_1	7.4125	5.999	4.5012
ω_2	36.4207	32.388	29.7629
ω_3	78.2514	77.4339	75.2633

Table (A-7) case 3 natural frequencies.

A.4. Case 4 (two-link (rigid-flexible) manipulator)

In this case the data of these two links is shown in table below:

Parameter link 1		Value	unit
Beam material		Steel	
Density	ρ_1^*	7980	$\left(kg/m^3\right)$
Modulus of elasticity	E	190×10^9	$\left(N/m^2\right)$
Length	l_1	0.2	m
Cross section area	a_1	13×30	mm^2
Hub moment of inertia	J_{h_1}	0.02	$\left(kg.m^2\right)$
Parameter link 2		Value	unit
Beam material		Steel	

Length	l_2	0.6	m
Cross section area	a_2	1.25×40	mm^2
Hub moment of inertia	J_{h_2}	0.002	$\left(kg.m^2\right)$
Payload	m_p	0.25	kg

Table (A-8) case 4 two links parameters.

B

Appendix

Computer Programming

This appendix contains the ***M.files*** for ***MatLab 6.5*** program which was used in the working up this research the all files are used successfully and the all results presented in chapter 5 are obtained using these files.

B.1. Solving the transcendental characteristics equation

```
%       example
a=0;b=10;dx=0.01;
nroots=0;
while 1
   [x1,x2]=rootsearch(@fex4_3,a,b,dx);% function introduced below
   if isnan(x1)
      break
   else
      a=x2;
      x=bisect(@fex4_3,x1,x2,1);
      if ~isnan(x)
         nroots=nroots+1;
         root(nroots)=x;
      end
   end
end
root
```

……

```
function [x1,x2]=rootsearch(func,a,b,dx)
x1=a;    f1=feval(func,x1);
x2=a+dx; f2=feval(func,x2);
while f1*f2>0.0
   if x1 >= b
      x1=NaN;x2=NaN;return
   end
   x1=x2;    f1=f2;
   x2=x1+dx; f2=feval(func,x2);
end
```

……

```
function root =bisect(func,x1,x2,filter,tol)
%function was presented by [ ]
if nargin <5;tol=1.0e4*eps;end
if nargin <4; filter=0;end
f1=feval(func,x1);
if f1==0.0;root=x2;return;end
```

```
f2=feval(func,x2);
if f2==0.0;root=x2;return;end
if f1*f2>0;
   error('root is not bracketed in (x1,x2)')
end
n=ceil(log(abs(x2-x1)/tol)/log(2.0));
for i=1:n
   x3=0.5*(x1+x2);
   f3=feval(func,x3);
   if(filter==1)&(abs(f3)>abs(f1))...
         &(abs(f3)>abs(f2))
      root=NaN;return
   end
   if f3==0.0
      root=x3;return
   end
   if f2*f3 < 0.0
      x1=x3;f1=f3;
   else
      x2=x3;f2=f3;
   end
end
root=(x1+x2)/2
```

```
function y=fex4_3(x)
y=1+cos(x)*cosh(x);
```

B.2. MatLab New Functions

1- Function ϕ

```
function p=phi(la,l,x)
%function phi find the mode shape of the S.F.L.
% la is the eigen frequency of the link,l is the length, x is the position.
%if the uer did not enter x,the function create analytical form of mode shape.
if(nargin==3)
   p=cosh(la.*x/l)-cos(la.*x/l)-
((cos(la)+cosh(la))/(sin(la)+sinh(la)))*(sinh(la.*x/l)-sin(la.*x/l));
elseif(nargin==2)
   x=sym('x');p=cosh(la.*x/l)-cos(la.*x/l)-
((cos(la)+cosh(la))/(sin(la)+sinh(la)))*(sinh(la.*x/l)-sin(la.*x/l));
else
   error('not enough input argument')
end
```

```
function p=phi1(b,z)
```

```
%function phi find the mode shape for normalized position of the S.F.L.
% b is the eigen modes vector , z is the value of normalized position
%if the user did not enter z, the function create analytical form of mode shape.
if(nargin==2)
   p=((cosh(b*z)-cos(b*z))-(((cos(b)+cosh(b))/(sinh(b)+sin(b)))*(sinh(b*z)-
sin(b*z))));
elseif(nargin==1)
   z=sym('z');
   p=((cosh(b*z)-cos(b*z))-(((cos(b)+cosh(b))/(sinh(b)+sin(b))) *(sinh(b*z)-
sin(b*z))));
else
   error('not enough input argument')
end
```

2- Function δ

```
function d=delta(C1,C2,w,t)
%function delta find the time sol.of B.E.Eq.
%where C1,C2 is the constants from delta=C1*sin(w*t)+C2*cos(w*t),
%w is the natural frequency,t is the time.

if (nargin==4)
   d=C1*sin(w*t)+C2*cos(w*t);
elseif(nargin==3)
   t=sym('t');d=C1*sin(w*t)+C2*cos(w*t);
else
   error('not enough input argument')
end
```

3- Function W

```
function y=W(b,C1,C2,w,n,z,t)
%function W find the link deflection.
% b,w,z,and t is the parameters of phi and delta.
% y= sum(phi_i*delta_i)
%b:eigen frequency; w:natural frequency; z=(x/l)=(0:1)
% n must be integer,which represent degrees of freedom.
% b and w must enters as avecters.
if(nargin==7)
   yo=0;for i=1:n
   y=yo+(phi1(b(i),z).*delta(C1,C2,w(i),t));
   yo=y;
end
elseif(nargin==6)
    yo=0;for i=1:n
   y=yo+(phi1(la(i),z)*delta(C1,C2,w(i)));
   yo=y;
```

```
end
else
   error('not enough input argument')
end
```

……

B.3. Modeling

Find the natural frequency of the model

```
M=[……]; %  M mass matrix
k=[……] ; % k stiffness matrix
mi=inv(M);
mi(1,:)=[];mi(:,1)=[];
w_2=mi*k;
w=sqrt(eig(w_2))
```

……

Find tip-deflection of the link using the above new equations

```
w=[……];b=[……..];a=1;
 %w: natural frequency vector, b: eigen modes vector
if n==2
       C1=0.3/((w(1)*phi1(b(1),1))+(w(2)*phi1(b(2),1)));C2=0;n=2;z=1;
       t=0:0.01:2;
       def=W(b,C1,C2,w(1:2),n,z,t);
       plot(t,def,'k');
       xlabel('time(sec)');ylabel('tip-def(m)');%title('Mp=0.3 kg-two modes');
       a=a+1;
 else n==3
C1=0.3/((w(1)*phi1(b(1),1))+(w(2)*phi1(b(2),1))+(w(3)*phi1(b(3),1)));
       C2=0;n=3;z=1;t=0:0.01;2;
       def=W(b,C1,C2,w(1:3),n,z,t);
       plot(t,def,'k');
       xlabel('time(sec)');ylabel('tip-def(m)');title('Mp=0.3 kg-three modes');
       a=a+1;
end
```

……

B.4. Control

Find desired flexible modes

```
%enter inertia,stifness,and damping matrecies
M=[……..]; % mass matrix
K=[……..];% stiffness matrix
%****************************************
%enter time vector,generate desired rigid coordinates
ro=0.3925;time=[0:0.01:2]';[q,qd,qdd]=jtraj(0,pi/2,time);n=1;
%****************************************
```

```
%enter flexible coordinate
t=[0:0.01:2]';
d1=C1*cos(w1*t)+C2*sin(w1*t);d_d1= w1(-C1*sin(w1*t)+C2*cos(w1*t));
d2=C1*cos(w2*t)+C2*sin(w2*t);d_d1= w2(-C1*sin(w2*t)+C2*cos(w2*t));
d3=C1*cos(w3*t)+C2*sin(w3*t);d_d1= w3(-C1*sin(w3*t)+C2*cos(w3*t));
delta=[d1 d2 d3]';
d_delta=[d_d1 d_d2 d_d3]';
%*****************************************
%find elastic accelerations
for i=1:201
IMdd(1:3,1:3)=inv(M(2:4,2:4));
d2_delta(:,n)=-IMdd*(qdd(i).*M(2:4,1)+K*delta(:,i));
n=n+1;
end
%*****************************************
%find desired elastic coordinates
a=1;
for i=1:3
   b=2;d_dd0=d_delta(:,1);d_ddo=d_dd0(i);d_dd(:,1)=d_dd0(:);
   dd0=[0 0 0]';ddo=dd0(i);dd(:,1)=0;
   for j=2:length(t)
      d_dd(a,b)=(d2_delta(i,j)*(t(j)-t(j-1)));%+(d_ddo-(d2_delta(i,j-1)*t(j-1)));
      dd(a,b)=(d_dd(i,j)*(t(j)-t(j-1)));%+(ddo-(d_dd(i,j-1)*t(j-1)));
      %d_ddo=d_dd(a,b);ddo=dd(a,b);
      b=b+1;
   end
   a=a+1;
end
```

……

Find torque input

```
time=[0:0.01:2]';[q,qd,qdd]=jtraj(0,pi/2,time);n=1;
for t=0:0.01:2
%*************************************
IMdd(1:3,1:3)=inv(M(2:4,2:4));

tau(n)=((M(1,1)+(M(1,2:4)*IMdd*M(1,2:4)'))*qdd(n)) –
                                    (0.01*(M(1,2:4)*IMdd)*(K*dd(:,n)));
n=n+1;
end
```

……

Simulation

```
n=2;dt=0.01;r=1;s=1;
time=0:0.01:2;x=1;
theta1=0;theta0=0;
```

```
%*************************************
IMdd(1:3,1:3)=inv(M(2:4,2:4));
ms=(M(1,1)+M(1,2:4)*IMdd*M(2:4,1));
%*************************************
theta(1)=0;
for i=2:length(time)
   theta(n)=(((tau(i)+((M(1,2:4)*IMdd)*(K*dd(:,i))))/ms)*(dt^2))+2*theta1-
theta0;
   theta1=theta(n);
   theta0=theta(n-1);
   n=n+1;
end
thetao=0;
for k=1:length(time)
   d_theta(x)=(theta(k)-thetao)/dt;
   thetao=theta(k);
   x=x+1;
end
```

PD controller

```
t=2;dt=0.01;r=1;s=1;
time=0:0.01:2;x=1;p=1;
theta1=0;theta0=0;kp=…..;kv=…..;
%*************************************
IMdd(1:3,1:3)=inv(M(2:4,2:4));
ms=(M(1,1)+M(1,2:4)*IMdd*M(2:4,1));
%*************************************
er=q-theta';d_er=qd-d_theta';
for m=1:length(time)
  tau1(p)=tau(m)+(M(1,1)-
                    M(1,2:4)*IMdd*M(2:4,1))*((kp*er(m))+(kv*d_er(m)));
   p=p+1;
end
%*************************************
theta(1)=0;
for o=2:length(time)
theta(t)=(((tau1(o)+((M(1,2:4)*IMdd)*(K(1:3,1:3)*dd(:,o))))/ms)*(dt^2))+2*the
ta1-theta0;
   theta1=theta(t);
   theta0=theta(t-1);
   t=t+1;
end
```

الخلاصة

في هذه الرسالة تم دراسة موضوعين الاول هو التحليل الرياضي (النمذجة) ، السيطرة على مسار الحركة: لذراع مرنة مفردة ، و لذراعين الاول غير قابل للتشوه(اثناء الحركة) والثاني مرن.في البداية تم ايجاد معادلات الحركة باستخدام طريقة (الانماط الافتراضية/ وطريقة لاكرانج) للحركة بمستوي واحد ، وظهر من خلال التحليل ان معادلات الحركة تكون غير خطية ومتداخلة الى حد كبير.ثم بعد ذلك تم استخدام معادلات الحركة الناتجة من التحليل باستخدام طريقة التحليل المعكوس لحل مشكلة السيطرة على الذراع المرنة. ان الطريقة المقترحة للسيطرة بواسطتها تم ايجاد العزم اللازم لحركة نقطة نهاية الذراع على طول مسار محدد . المسيطر المفترض من النوع (PD) وهو يستخدم لزيادة فعالية نظام السيطرة ، ولاكسابه مقدرة على تعديل الحركة عند التعرض للمتغيرات في النظام . اوضح العمل على طريقة التحليل الرياضي المعكوس ان هذه الطريقة فعالة ويمكن استخدامها مع انظمة السيطرة المغلقة وذلك لتقليل دور الشارة الراجعة.

جمهورية العراق
وزارة التعليم العالي والبحث العلمي
جامعة بابل
كلية الهندسة

النمذجة والسيطرة لذراع الأنسان الآلي المرنة بمستوي واحد

رسالة

مقدمة إلى كلية الهندسة في جامعة بابل وهي جزء من متطلبات نيل

درجة ماجستير علوم في الهندسة الميكانيكية

(مكانيك تطبيقي)

أعدت من قبل

مصطفى تركي حسين الخفاجي

بكالوريوس علوم في الهندسة الميكانيكية

١٤٢٨ هـ 2007 م